Thermodynamic and kinetic characterisation of antibody / hapten pairs and optimisation of an immunoassay of fluorescence in homogeneous phase

Thermodynamische und kinetische Charakterisierung von Antikörper / Hapten Paaren und Optimierung von einem Fluoreszenzimmunoassay in homogener Phase

DISSERTATION

der Fakultät für Chemie und Pharmazie

der Eberhard-Karls-Universität Tübingen

zur Erlangung des Grades eines Doktors

des Naturwissenschaften

2001

vorgelegt von

Ingrid Coille

UNIVERSITE LOUIS PASTEUR – STRASBOURG I

FACULTE DES SCIENCES DE LA VIE

THESE

Présentée pour obtenir le titre de

DOCTEUR DE L'UNIVERSITE LOUIS PASTEUR

en SCIENCES DE LA VIE ET DE LA SANTE

par

Ingrid COILLE

Thermodynamic and kinetic characterisation of antibody / hapten pairs and optimisation of an immunoassay of fluorescence in homogeneous phase.

Caractérisation thermodynamique et cinétique de systèmes anticorps / haptène et optimisation d´un immunoessai de fluorescence en phase homogène.

Soutenue le 14 Septembre 2001 devant la Commision d´Examen :

Mr. M.H.V. VAN REGENMORTEL	Examinateur
Mr. OBERHAMMER	Examinateur
Mr. Y. MELY	Rapporteur interne
Mr. J.POLSTER	Rapporteur externe
Mr. J. HOEBEKE	Co-Directeur de these
Mr. G. GAUGLITZ	Directeur de thèse

Tag der mündlichen Prüfung: 14. September 2001

Dekan: Prof. Dr. H. Probst

Erster Berichterstatter: Prof. Dr. G. Gauglitz

Zweiter Berichterstatter: Dr. J. Hoebeke

1. Introduction and Motivation

1.1. INTRODUCTION TO THE THEME

In 1933, Cook et al. wrote a publication about "the first compound of known chemical constitution found to have a definite oestrus-exciting activity". This discovery was a big step in the clinical domain. An endocrine disruptor (ED), such as the substance discovered by Cook, is defined as "an exogeneous substance that causes adverse health effects in an intact organism, or its progeny, subsequent to changes in endocrine function". Other compounds which do not show obvious effects in intact animals, but "that possess properties that might be expected to lead to endocrine disruption in an intact organism" are defined as "potential endocrine disruptors" (PED) (Phillips and Harrison, 1999).

Since the beginning of the 90ties publications about compounds with estrogenic activity are numerous and the preoccupation with the effects on wildlife and humans is growing. Guillette et al. (1995) observed a population of demasculinised alligators in Lake Apopka, Florida, as a consequence of a contamination with p-p'-DDE, a product of the degradation of DDT. Sumpter reported in 1995 a feminisation of the fish in effluent from sewage treatment work, and he discovered in 1998 that a mixture of natural and synthetic estrogens, natural plant sterol and synthetic alkylphenols were responsible of this effect (Matthiessen and Sumpter, 1998). The decline of the population of the bald eagles in the Great Lake area, USA, was associated with the exposure to polyhalogenated aromatic compounds (Colborn, 1991). Concerning the human diethylbestrol (DES) is well-known to cause cell carcinoma of the vagina (Degen and Bolt 2000). The phthalate esters and butyl benzyl phthalate used in the plastic industry, the polychlorinates biphenyl (PCB) and β-hexachlorocyclohexane, an insecticide lindane residue, are linked with breast cancer (Rollerova et Urbancikova. 1999). Several abnormalities of the reproduction system where observed, e.g. reduction in sperm count and quality and increase of the testicular and prostate cancers, but the link with the EDs could not be proven (Phillips and Harrison, 1999).

Estrogens are a family of steroid hormones that regulate and sustain female sexual development and reproductive function. The mechanisms of interactions are varied and complex. The interaction of the EDs with the estrogen receptors was studied first, but there are also other possibilities through the complex regulation mechanism of the hormone system. The EDs can influence the levels of circulating hormones, as well as modulate expression of the estrogen receptor or even affect the level of protein transporting lipid soluble hormones in blood (Phillips and Harrison, 1999).

The biological activity depends on the mechanism of action and is not systematically correlated with the binding affinity. Two stereo-isomers may have totally different binding properties and therefore different biological effects. Endocrine disruptors can act as agonist or antagonist (Degen et al., 1999). However, it is not easy to define which substance is an endocrine disruptor. Indeed, effects are related to dose and potency of the substance, moreover the risk depends on the sex and the age of the subject, as well as on the existence of different receptors (Degen and Bolt, 2000 and Witorsch, 2000).

The potency of the substances, defined as the amount needed to produce a certain response, various according to the method used to define it, but basically the natural estrogens 17-β-estradiol, estrone and estriol and the synthetic estrogens diethylstilbestrol (DES) and ethinylestradiol are the most potent (Witorsch, 2000 and Soto et al., 1995). Other xenoestrogens show a much smaller estrogenicity.

Such endocrine disruptors belong to various classes of substances which can be divided into four categories. The first class, with the highest estrogenicity effect, groups together the **natural hormones**: estrone, estradiol, estriol. The second class represents the **synthetic hormones**, such as ethinylestradiol and diethylstilbestrol (DES), principally used in pharmaceutical and medicinal applications. The third class represents the **naturally occurring compounds** with estrogenic activity: phytoestrogens (Santti et al., 1998) (coumestans, isoflavonoids) and mycoestrogens. The fourth and last class encompasses all other industrial **chemicals**, principally pesticides, detergents, plasticizers, heavy metals (Rollerova and Urbancikova, 1999). Another name for the unnatural estrogens is xenoestrogens, from the Greek xenos, which means guest, stranger, foreigner.

Because of the varied nature of EDs, the sources of these substances are numerous. Natural and synthetic hormones can be found in wastewater treatment plants. Phytoestrogens are found in plants, soya contains genistein and daidzein for example (Degen and Bolt, 2000). Bisphenol A is a compound used to manufacture a type of plastic, the polycarbonate (Feldman, 1997). Numerous pesticides, such as DDT or PCB, are also known as endocrine disruptors (Levi, 1999). The number of chemicals considered as xenoestrogens is so large (insecticides, fungicides, plasticizers, rubber additives, disinfectant, etc.) that it is difficult to list them (Rollerova and Urbancikova, 1999). The degradation of the xenoestrogens in wastewater treatment plants can lead to more potent substances. At the end of all these sources, the food is the most important source for human exposure to endocrine disruptors of all kinds. The exposure, with food and water, is estimated at several µg/day (Degen and Bolt 2000, Rollerova and Urbancikova, 1999).

As yet, there are no laws concerning endocrine disrupting compounds and industry rejects that e.g. restrict the permitted concentration in water. But the European Community was aware, and on 20th December 1999 the European Commission adopted a communication on a community strategy for endocrine disruptors. The objectives are to identify the problem of endocrine disruption, its causes and consequences and to define an appropriate policy action on the basis of the precautionary principle. (Commission of European Communities, 1999).

Since there are no actual regulations concerning EDs, there is also no standard method for identification and quantification of these substances. Numerous research groups are working on this issue. The identification of potential endocrine disruptors can be realized by in vitro tests, which are well adapted to clarify the mechanism of action. But in vivo tests are also required since the definition of EDs includes the notion of effects in intact animals. A simple common in vitro assay uses the estrogen receptor as ligand, instead of antibodies in immunoassays. An adaptation of an ELISA resulted in the Enzyme Linked Receptor Assay (ELRA) (Seifert, Haindl et al. 1999). Similarly, the radio immunoassay could by way of adaptation turned into a Radio-Receptor Assay (RRA) (Arts et al., 1989). These methods are also coupled with chromatographic methods (Oosterkamp et al. 1996, Seifert, Brenner-Weiss et al., 1999) to identify the compounds in a mixture that are responsible for estrogenic

activity. If the in vitro tests do not use direct binding to the estrogen receptor, they are generally based on proliferation of cells, gene activation or toxicological approaches. A well-known in vitro test based on the proliferation of the MCF-7 breast cancer cells in presence of estrogenic substances, is the so called E-screen assay (Soto et al., 1995, Körner et al. 1999). A yeast-based screen for estrogenic activity developed by Routledge and Sumpter is based on gene transcription (1996). The techniques for detection of estrogenicity are well reviewed by Korach and McLachlan (1995) and compared in a study by Andersen et al. (1999).

Indeed, in vitro but also in vivo tests are necessary to define the real potency of potential endocrine disruptors. Daidzein and p-tert-octylphenol present an equipotency in in vitro tests, but by in vivo tests it can be shown that p-tert-octylphenol has an estrogenic potency ten times higher than daidzein (Bolt et al. 1998).

In vivo tests are based on the detection of a biomarker. A biomarker is a physiological or pharmacological measure that is used to predict a toxic event in an animal. Vitellogenin is a protein from birds and amphibia that is the precursor of the protein phosvitin and lipovitellin when stimulated by female sex hormones. Vitellogenin is proven to be a biomarker for the presence of endocrine disruptors (Sumpter and Jobling, 1995 and Hansen et al., 1998). The most sensitive assay used to quantify vitellogenin is the ELISA (Sherry et al., 1999, Christiansen et al., 1998). RIA (Borst et al. 2000 and Routledge et al., 1998) and single radial immunodiffusion (SRID) (Fujii et al., 1998 and Koya et al., 1997) are also well developed. Chromatographic methods, such as HPLC (Yamanaka et al., 1998) are rarely used.

Since the effects of the EDs are related to the potency but also to the dose of substances, quantification of the EDs and PEDs is necessary. The methods developed to quantify estrogens and xenoestrogens are principally based either on chromatography or on immunoassays. Liquid Chromatography (LC) coupled with Mass Spectroscopy (MS) was established for example by Pedersen et al. (1999); Lopez de Alda and Barcelo coupled LC with Diode Array Detection (2001); High Pressure Liquid Chromatography (HPLC) as well as GC-MS were used by Schmid and Fruhauf (1998) and Wang et al. (1994); fluorescence detection in a HPLC method was employed recently by Snyder et al. (1999).

Contrary to chromatography methods, Enzyme-Linked Immunosorbent Assay (ELISA) and immunoassays in general have relatively low limits of detection without pre-concentration of the sample. One of the difficulties in the establishment of an immunoassay is to have available an antibody with high affinity, if possible monoclonal in order to be able to produce systematically exactly the same results. One example of a commercially available ELISA for the detection of estradiol gives a limit of detection of 0.05 µg/l (Riedel-de Haën). Chromatographic methods and immunoassays were often compared or combined in scientific literature. ELISA was compared with GC coupled with tandem MS-MS (Huang and Sedlak, 2001). Snyder et al. (1999) compared a Radio-Immuno-Assay (RIA) with a HPLC method. Combinations of LC or Capillary Electrophoresis (CE) with immunoassay combining the separation of different compounds from a mixture with a sensitive quantification are reviewed by Shahdeo and Karnes (1998). A more uncommon method to separate a mixture and to detect each compound was realised with the combination of a Molecular Imprinted Polymer (MIP) with fluorescence detection (Rachkov et al., 2000) and with the use of cyclodextrin (Narita et al., 2000).

The immunoassays, used for the quantification of EDs or biomarkers, can be classified in different ways. One possibility is to differentiate the competitive from the non-competitive assays. In competitive assays analytes compete with labelled analytes for a limited number of antibody binding sites. This is in contrast to non-competitive immunoassays where an excess of antibody is used and only antibodies that are bound to antigens are detected (Price and Newman, 1997). Competitive assays are quite easy and fast to perform since they do not require any separation steps. Consequently, they can be easily automated and miniaturised. Furthermore, only small quantities of substances are necessary, making them, in contrast to non-competitive sandwich-assays (i.e ELISA), cost-effective. However, competitive assays cause always higher limits of detection (LOD) than non-competitive assays which are performed using an excess of reagent (Jackson and Ekins, 1986). Nevertheless, the LODs of competitive assays can be optimised by choosing an appropriate system: analyte/antibody/labelled analyte derivative. In competitive assays, analyte and analyte derivatives compete for binding to the antibody. The two competitive reactions are defined by two affinity constants. The ratio of the two affinity constants of the antibody to its analyte and to

the employed labelled analyte derivative determines the assay performance. Therefore the affinity constants are of high importance to optimise the LOD of the competitive assay.

1.2.   GOAL AND STRUCTURE OF THE STUDY

A part of this study consisted of the characterisation of different systems of antibodies and analytes and analyte derivatives. A monoclonal anti-estradiol antibody was fully characterised by surface plasmon resonance (SPR): the active concentration as well as the kinetic rate constants and affinity constants of the antibody to several cross-reactive estrogenic compounds were determined. The kinetic measurements at several temperatures allowed to obtain thermodynamic constants, which helped to define the nature of the interactions.

A competitive immunoassay based on energy transfer was developed and characterised by Schobel (1999). In order to accelerate the optimisation of the assay, we wanted to know if it was possible to predict, before the labelling, which pair antibody/analyte derivative gives the best results (limit of detection) with the competitive fluorescence immunoassay. Here the ratio of the affinity constants of the antibody to the analyte and to the analyte derivative were used. SPR was also used to characterise three polyclonal anti-estrone, anti-estradiol and "anti-total-estrogen" antibodies. As for the monoclonal antibody, the average of active concentration of each polyclonal antibody was measured, as well as the kinetic constants and the affinity constants for several analyte (estrone, estradiol and ethinylestradiol) and analyte derivatives. Moreover, the affinity constants of the labelled antibodies were measured in order to ensure that the labelling does not influence the affinity constants. The affinity constants were determined in parallel with another method: Reflectometric Interference Spectroscopy (RIfS). The affinity constants determined with both methods were compared.

Simulations of the homogeneous fluorescence immunoassay were calculated, under simplified conditions, to show the influence of several critical parameters of the assay: affinity constants of the antibody for the analyte and the competitive analyte derivative as well as the concentration of the analyte derivative.

The different possibilities of calibration of estrone and estradiol were measured with the fluorescence immunoassay and then compared to the expected results according to the affinity constants previously determined and to the simulations.

Within the framework of the European project SANDRINE (ENV4 – CT98 – 0801), the fluorescence immunoassay was applied to determine the concentration of spiked analytes in synthetic wastewater. A simple preparation of the samples and a method of correction of the signal in wastewater were required.

The second objective concerning the fluorescence immunoassay was the miniaturisation of the immunoassay, principally in order to reduce the costs of the assay. The immunoassay had to be transferred progressively to a nanotiterplate (NTP), where the total volume of each measurement was 70 nl. The pre-incubated mixture of antibody, analyte and analyte derivative was first transferred to the NTP. Direct pipetting of each compound onto the NTP showed problems of unspecific adsorption at the surface of the NTP. Coating the NTP with an appropriate protein solution prevented the unspecific adsorption. The sample was pipetted sequentially onto the NTP and the concentration of antibody was reduced to improve the performance of the assay.

The final objective was the application of the fluorescence immunoassay to the vitellogenin of rainbow trout, the biomarker of the presence of endocrine disruptors. This part was also included in the SANDRINE project. The traditional assay was not successful, neither was the assay with a new fluorophore. A fluorescence immunoassay with phase separation (PSFIA) was established to test the binding capacity of each labelled compound.

2. Theory

2.1. ANTIBODY/ANTIGEN INTERACTIONS

2.1.1. Structure of antibody and forces of interactions

2.1.1.1.   Immunological system

The immune system of vertebrates has evolved to protect the organism from foreign bodies and infections by viruses, bacteria and other micro-organisms. The first step in this defence is to differentiate "self" from "non-self". Once the danger has been localised and recognised, the immune system undertakes the necessary actions against the foreign body to eliminate it. The acquired immune system can be separated into two groups: the cellular immune response and the humoral immune response.

The cellular immune response leads to the production of cytotoxic T lymphocytes which kill the infected cells. The humoral immune response leads to the production of antibodies, belonging to the immunoglobulin protein classes (Igs). Both immune responses have an "immunologic memory", which improves the defence from repeated attacks.

The immunoglobulins are glycoproteins, produced by plasma cells, which derive from B lymphocytes. Each lymphocyte has its specificity to one antigen. The B lymphocytes have receptors on their membrane which can bind to this foreign molecule. These receptors are the antibodies themselves. The binding activates the lymphocytes which proliferate and differentiate to produce the antibodies with one specificity to one antigen (Gemsa et al., 1991, and Liddell and Weeks, 1996).

Mammals generate five types of immunoglobulin: IgA, IgD, IgE, IgG and IgM. These five isotypes are present in the serum and in various organs at different concentrations. The different types of Igs are produced according to the mode of immunisation.

- IgA represents 15 % of the total Igs in plasma, it is very heterogeneous with monomer, dimer and polymer forms, and it is not easily purified from plasma.

- IgD is not of analytical interest since it is present in trace amounts in plasma.

- IgE plays an important role in allergies but it is only present in extremely small concentration in plasma, between 0.5 and 0.002 %.

- IgM is a pentamer Ig, decavalent, with a molecular mass of 970 kDa. Due to their low specificity and high cross-reactivity, they are rather poor analytical reagents. Moreover, only 7 % of Igs in plasma are IgM.

- IgG represents 75 % of the Igs in plasma and it corresponds to "the analytical antibody in immunochemistry" (Lottspeich and Zorbas, 1998).

2.1.1.2.   Properties and structure of IgG

IgG is the smallest antibody of the Ig classes, with a molecular mass of 150 kDa. IgG is easy to produce and to extract from blood serum.

IgGs are very suitable for analytics also because of their stability: they are very soluble in aqueous solutions, they remain active at high salt concentrations and over a large pH range, between 4 and 9.5. Moreover, they may be stored at –20°C to –80°C at high concentrations almost without deterioration. They may also be denatured reversibly. This property is very useful for the isolation and the purification of IgG. With several chemical groups on its surface it tends itself to be easily functionalised with markers, like dyes, enzymes, radioactive labels, etc. (Lottspeich and Zorbas, 1998).

IgGs are comprised of four chains of polypeptides: two identical light chains (L) and two identical heavy chains (H) linked together by disulfide bonds (S), salt bridges, Van der Waals forces and hydrogen bonds. Each light chain consists of approximately 220 amino acids, while each heavy chain contains around 440 amino acids. The four chains are composed of a variable region (V_L and V_H), and one or three constant regions for the light and the heavy chain (C_L and C_H1, C_H2 and C_H3) respectively. C_H1 and C_H2 are not directly in contact: they are linked through the hinge. The flexibility of the antibody is due to the hinge. The variable region of the light chain (V_L) (approximately 110 amino acids) is near to the amino-terminal (NH_3^+), and the

constant region (C_L) is at the other side, near to the carboxyl-terminal (COO⁻). The variable regions of the heavy chain and the light chain form the binding sites of the antibody.
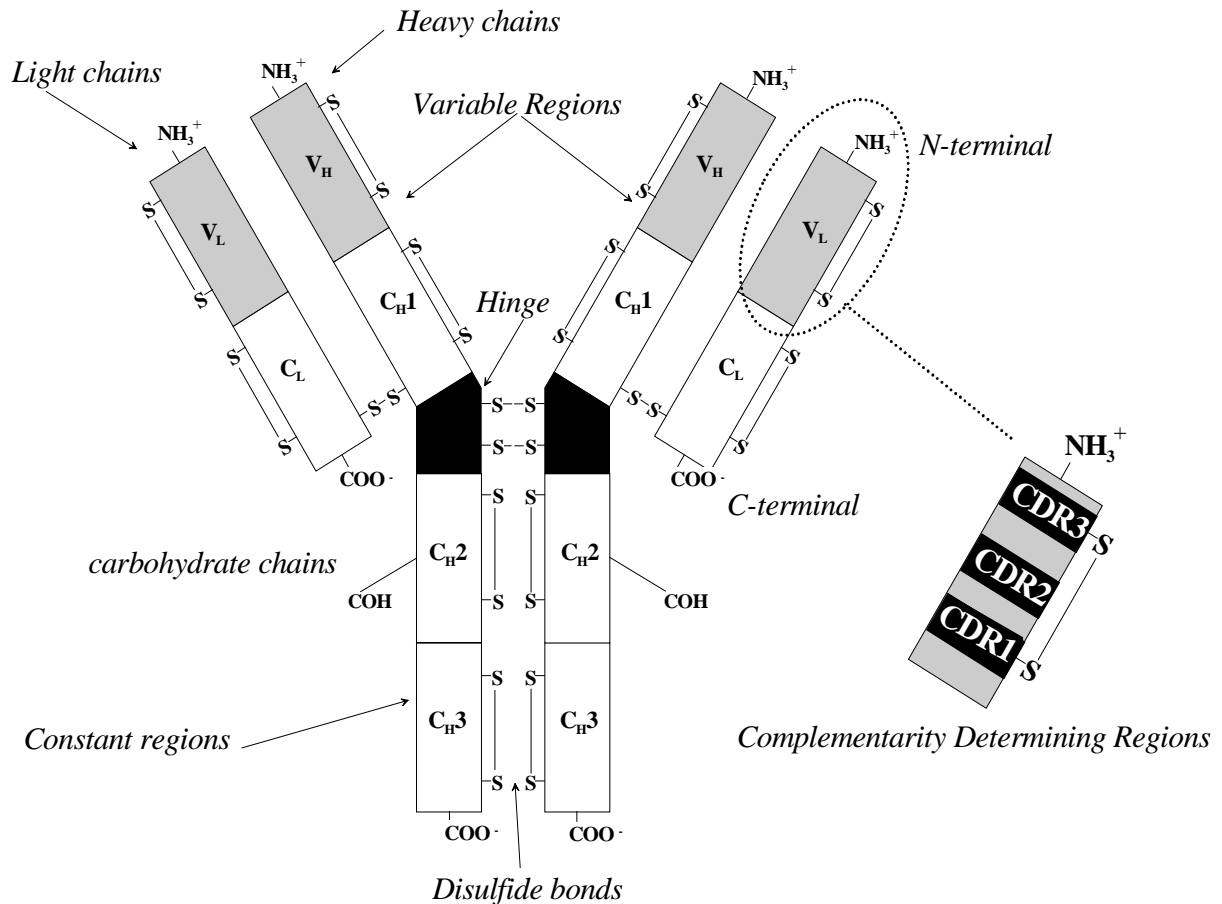
Fig. 1: Structure of an IgG

In fact, only parts of the variable regions bind the antigen. Each variable region presents three hypervariable regions, called "Complementarity Determining Regions" or CDR1, CDR2 and CDR3. These represent 15 to 20 % of the variable region. The rest of the variable regions is called framework (FW) (Laune, 1998). The group of amino acids most important for binding the antigen is called paratope. The corresponding binding sites on the antigen form the epitope.

Inside the IgG class four isotypes are distinguished: $IgG_{1, 2, 3}$ and $_4$. In humans the four different subclasses of IgG can be differentiated by the size of their hinge region and the position and number of disulfide bonds. They can also be distinguished by function (Belmont University, WEB site).

Antibodies are analytically defined by their affinity for the immunogen and by their cross reactivity to other substances.

2.1.1.3.   Production of antibodies

Every foreign molecule for the body can induce an immune response if the molecule is big enough. Molecules inducing an immune response are called immunogens. Small molecules, called haptens, have to be coupled to a protein, such as bovine serum albumin (BSA), to produce Igs. This procedure is used to produce antibodies for an analytical goal. Because the acquired immune system has an immunological memory the immunisation phases are repeated several times in order to have IgG with high affinity.

Because each lymphocyte synthesises its own antibody with one affinity to the antigen, the population of produced antibodies is heterogeneous. Such a mixture of antibodies is defined as polyclonal. In order to produce one IgG defined by one affinity to the antigen, the antibodies have to come from one B lymphocyte. This can be done by cloning the selected B cell. This is realised by the fusion of the immunised B lymphocyte with myeloma cells. The produced hybrid cells possess the properties of secreting one antibody like the selected B-cell as well as the long lifetime of the myeloma cells. These hybridoma cells can produce high quantities of monoclonal antibody when grown at high density in culture medium or in ascitic fluids (Liddell and Weeks, 1996).

2.1.1.4.   Forces of interactions IgG/antigen

Macroscopic scale interactions in aqueous medium between antigen and antibody or in a general way between hydrophilic substances, are repulsive. But an antigen and its antibody can nevertheless bind together thanks to the specific interactions between them. This specific attraction needs to overcome the macroscopic repulsion over a distance of at least 3 nm.

The forces responsible for the repulsion at long range and the attraction at microscopic range are the same. The forces are made of a sum of weak interactions: hydrophobic interactions, electrostatic and Van der Waals forces. In this case, hydrogen bonding is considered a minor force. This force is too weak to produce an effect at long range. At close distance hydrogen bonding requires a precise bond angle and an exact bond distance, making it very improbable (Van Oss, 1995).

- The tendency of non-polar or partly non-polar molecules to attract each other in aqueous medium defines the hydrophobic interaction. The force is mostly represented by the Lewis acid-base interactions: electron-Donor and electron-Acceptor interactions. The hydrophobic attraction is due to the free energy of cohesion of water due to intermolecular hydrogen bonding. For apolar compounds the electron-Acceptor surface tension parameter and the electron-Donor surface tension, which contribute to the free energy of interaction, are zero. That is why almost only the water is responsible of the attraction.

- The presence of ionised sites with opposed charge on the epitope and on the paratope can create electrostatic forces, termed the Coulomb force. Typically the groups COO^- and NH_3^+ are engaged in this type of interaction.

- The Van der Waals forces correspond to interactions between dipole/dipole (Keesom interaction), dipole/induced-dipole and induced-dipole/induced-dipole (London interaction). A dipole shows the tendency to align another dipole into a favourable arrangement. This orientation is energetically more advantageous. A dipole has also the property to polarise a neighbouring molecule which is not necessarily polar. A second molecule becomes polarised by the first dipole. The third and last possibility concerns the non-polar molecules. They are considered instantaneous dipoles. The direction of the polarisation for the molecules varies but the variations follow each other so much so that the attractive effect is not zero (Atkins, 1999).

- In a simplified way, the binding reaction can be detailed in two steps: Firstly, the primary attraction at long distance and the expulsion of the water from the binding site. Secondly, the precise bonding between epitope and paratope. The principal forces in the attraction at long distance which overcome the macroscopic repulsion are mainly hydrophobic and electrostatic. The Van der Waals forces are at this step negligible. After the expulsion of the water from the binding site, the Van der Waals bonds are the strongest. This is when the distance between the epitope and the paratope is the smallest. The best fit between the two surfaces is the most important factor in achieving the maximum bond strength (Van Oss, 1995).

The strength of the interaction can be further characterised by the affinity constant and by thermodynamic terms, which quantify the force of the interactions.

2.1.2. Equilibrium and kinetics of a reaction

2.1.2.1.   Equilibrium

IgG reacts with the antigen (*Ag*) and forms a complex *IgG-Ag*.

$$IgG \; + \; Ag \; \underset{K_D}{\overset{K_A}{\rightleftharpoons}} \; IgG - Ag \tag{1}$$
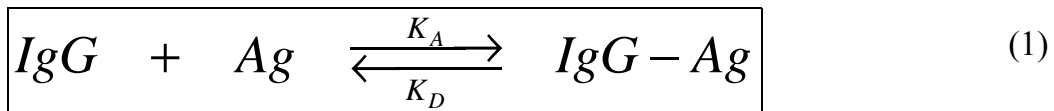
The equilibrium is dependent on the concentrations of the three compounds, symbolised in the following equations in brackets. These concentrations are linked together to define two constants, called affinity constant (K_A) and dissociation constant (K_D). These two constants are the inverse of each other.

$$K_A = \frac{[IgG - Ag]}{[IgG] \cdot [Ag]} = \frac{1}{K_D} \tag{2}$$

2.1.2.2.   Kinetics

The affinity constant does not completely characterise the reaction. No information about the velocity of the reaction, the time necessary to reach the equilibrium, is given. This information is given by the association and dissociation-rate constants k_{ass} and k_{diss} respectively.

$$\frac{d[IgG - Ag]}{dt} = k_{ass} \cdot [IgG] \cdot [Ag] \tag{3}$$

$$\frac{d[IgG - Ag]}{dt} = -k_{diss} \cdot [IgG - Ag] \tag{4}$$

These two equations define the increase in concentration of the complex over time and the decrease in concentration of the complex over time respectively.

K_{ass} is typically in a range from 10^2 to 10^7 M$^-$1·s^{-1}, whereas k_{diss} varies in a range from 10^{-5} to 10^{-2} s^{-1} (BIACORE, 1991).

Near the equilibrium, the rate of formation is defined as the sum of the association and dissociation rates and it is equal to zero. From this a new equation is deduced:

$$\frac{d[IgG-Ag]}{dt} = k_{ass} \cdot [IgG] \cdot [Ag] - k_{diss} \cdot [IgG-Ag] = 0 \qquad (5)$$

After rearrangement it is possible to define the affinity constant with the association and dissociation rate constants:

$$\frac{k_{ass}}{k_{diss}} = \frac{[IgG-Ag]}{[IgG] \cdot [Ag]} = K_A \qquad (6)$$

2.1.2.3. Thermodynamics

The affinity constant is under certain conditions easily linked to the standard Gibbs free energy change of the interaction (ΔG^0):

$$\Delta G^0 = -R \cdot T \cdot \ln K_A \qquad (7)$$

In this equation, R is the molar gas constant (1.98 cal·deg^{-1}·mol^{-1} or 8.31 J·K^{-1}·mol^{-1}) and T is the absolute temperature (K). A negative ΔG^0 indicates the spontaneity of the reaction (Arnaud, 1991).

The standard Gibbs free energy change is defined in the Gibbs-Helmholtz's equation (8), by the standard enthalpy change (ΔH^0) and the standard entropy change (ΔS^0). The variation of enthalpy represents the heat of the reaction, whereas the variation of entropy expresses the disorder produced by the reaction. In a graphical representation of ΔG^0 as a function of the temperature the slope of the linear regression delivers ΔS^0 and the intercept gives ΔH^0.

$$\Delta G^0 = \Delta H^0 - T \cdot \Delta S^0 \qquad (8)$$

The kinetic rates are linked to the variation of internal energy (or activation energy) of association and dissociation (ΔE_{ass} and ΔE_{diss}) in the Arrhenius's equation (9) (Atkins, 1999).

$$ln\, k_{ass} = \frac{-\Delta E_{ass}}{R \cdot T} + \text{constant} \qquad (9)$$

$$\boxed{ln\,k_{diss} = \frac{-\Delta E_{diss}}{R\cdot T} + \text{constant}}$$
(10)

The variation of internal energy represents the heat exchanged between the system and the outside. The slopes of the linear regressions of the equations (9) and (10) are proportional to the ΔE. The activation energy is the energy required to bring the reactants to a transition state, called activated complex. The activated complex is at a higher energy level than the reactants themselves. In a simplified way it can be considered as the energy required for the system to overcome the repulsive forces.
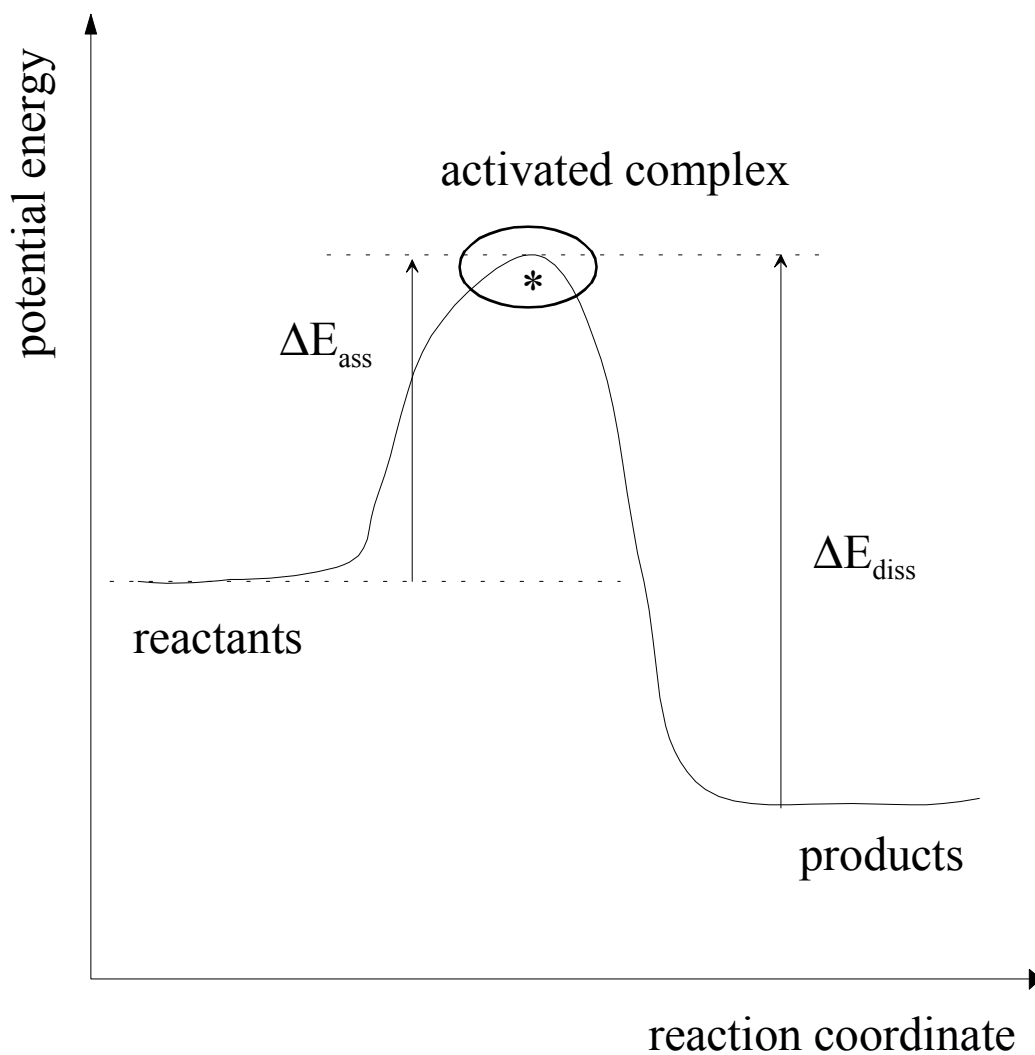
Fig. 2: Reaction profile. The activated complex is represented by the region near the potential maximum. ΔE_{ass} and ΔE_{diss} are the activation energy of association and dissociation respectively.

The relation between the variations of internal energy of association and dissociation gives the variation of enthalpy:

$$\Delta E_{ass} - \Delta E_{diss} = \Delta H^0 \qquad (11)$$

The kinetic rates are also dependant on the variations of enthalpy and entropy of the association and dissociation of the activated complex. The additional asterisk * in the standard notation symbolises the activated complex (see Fig. 2).

$$ln\left(\frac{k_{ass}}{T}\right) = \ln\left(\frac{k}{h}\right) + \frac{\Delta S_{ass}^*}{R} - \frac{\Delta H_{ass}^*}{R \cdot T} \qquad (12)$$

$$ln\left(\frac{k_{diss}}{T}\right) = \ln\left(\frac{k}{h}\right) + \frac{\Delta S_{diss}^*}{R} - \frac{\Delta H_{diss}^*}{R \cdot T} \qquad (13)$$

The constants k and h are the Boltzmann and the Planck constants and are equal to $1.3806 \cdot 10^{-23}$ J·K^{-1} and to $6.6262 \cdot 10^{-34}$ J·s respectively.

Finally, the enthalpy change and entropy change of the reaction are calculated with the values of the activated complex.

$$\Delta H_{ass}^* - \Delta H_{diss}^* = \Delta H^0 \qquad (14)$$

$$\Delta S_{ass}^* - \Delta S_{diss}^* = \Delta S^0 \qquad (15)$$

Possibilities to calculate the variation of enthalpy and entropy by graphical representation and linear regression allow to calculate an average of the values (Glasstone, 1960).

2.1.3. Methods of detection

2.1.3.1. Detection at equilibrium

A variety of methods are available for measuring the affinity of biomolecular interactions: both direct methods, such as calorimetry and spectroscopy, and indirect methods, such as ELISA or Radio-Immuno-Assay (RIA) (Karlsson and Roos, 1997).

- In calorimetry, the heat of the reaction is measured (Taquet et al., 1998). The number of binding sites, the affinity constant, and the change in enthalpy and entropy are deduced from the measurements. Kinetic measurements are not possible. The disadvantage is that both compounds have to be present in quite high concentrations (μM) and the affinity must be high ($>10^8$ M). The system is titrated, but it can be done in less than one hour.

- Absorption and fluorescence spectroscopy allow to follow a binding reaction kinetically (Garnier et al., 1998). However, only the association rate constant is accessible. The direct fluorescence or the fluorescence of the labelled antibody or antigen can be followed (Krishna et al., 1998). Fluorescence polarisation and correlation can also be used with low molecular mass haptens, where the binding with heavy IgG changes drastically the polarisation and the diffusion properties (Dorn et al., 1998).

- ELISA is a competitive immunoassay with separation of the bound and unbound compounds. Because of the separation step, it allows to measure crude antibody in body fluids. As with calorimetry, kinetic measurements are impossible (Zeck et al., 1999).

2.1.3.2.   <u>On-line detection of binding</u>

Spectroscopy can be used for some kinetic measurements but dissociation rate constants are inaccessible. The best methods for kinetic measurements are methods that detect on-line changes in optical parameters at a sensor surface: Surface Plasmon Resonance (SPR), Resonant Mirror, Reflectometric Interference Spectroscopy (RIfS) and a combination of waveguiding film material with a diffraction grating on a glass surface (Karlsson and Roos, 1997, and Nice and Catimel, 1999).

2.2.   SURFACE PLASMON RESONANCE: SPR

A plasma oscillation in a metal is a collective longitudinal excitation of the electron gas. A plasmons is defined as a quantum of a plasma oscillation. Surface plasmons can be excited by reflection of photons at a metallic film (Kittel, 1986).

2.2.1. Dispersion relation

The plasmons spread on the surface of the metal film with their own dispersion according to the angular frequency (ω), the light speed (c), and the dielectric constants of the metal (ε_1) and of the environmental medium (ε_2) (Raether 1988).

$$k_x = \frac{\omega}{c} \cdot \left(\frac{\varepsilon_1 \cdot \varepsilon_2}{\varepsilon_1 + \varepsilon_2} \right)^{1/2} \qquad (16)$$

Concerning the light the dispersion relation in vacuum is:

$$\omega = k \cdot c \qquad (17)$$

The component of the wave vector in the x direction, k_x, is then defined by:

$$k_x = k \cdot \sin \Phi \qquad (18)$$

where Φ symbolises the angle of incidence.

Fig. 3 shows the dispersion of the light and the dispersion of the surface plasmons. The energy/momentum relation of the light is situated left from the dashed straight line (in the hatched area), according to the angle of incidence. The light in the air cannot excite surface plasmons since the relation of dispersion of the light and of the surface plasmons do not cross.
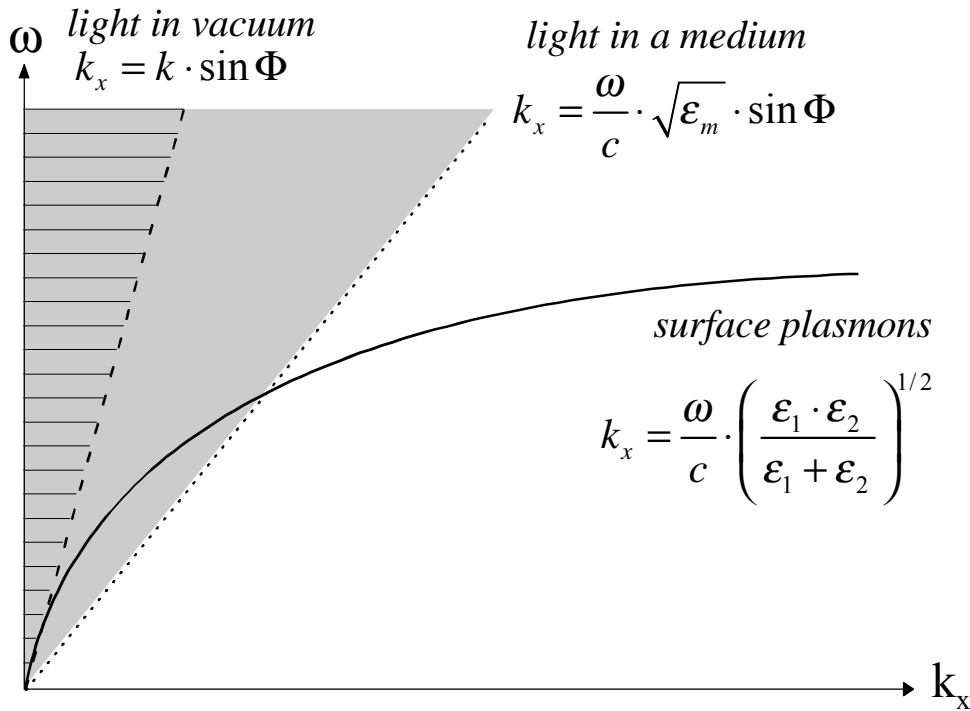
Fig. 3: Relation of dispersion (energy/momentum) for the light in vacuum and in a medium and for surface plasmons at the metal/air interface.

An increase of the momentum of the light is required and is obtained by the introduction of a medium with a high index of refraction (n_1). This medium can be, for example, a prism. The enhancement of the refractive index by the introduction of the medium increases the dielectric constant ($\varepsilon_m > 1$) and, therefore, the dispersion of the light in the x direction.

The dispersion of light in a medium is equal to:

$$\boxed{\omega = \frac{k \cdot c}{\sqrt{\varepsilon_m}}} \tag{19}$$

The component of the wave vector in the x direction is then (Raether, 1988):

$$\boxed{k_x = \frac{\omega}{c} \cdot \sqrt{\varepsilon_m} \cdot \sin \Phi} \tag{20}$$

However the surface plasmons cannot be directly produced from the light because the medium changes also the dispersion relation of the surface plasmons. The relations of dispersion of light and surface plasmons at the interface prism/metal still do not cross.

Nevertheless, it is possible with the prism to work under conditions of total reflection of the light, if the angle of incidence (Φ) is higher than the critical angle (Φ_c) (Göpel et al, 1992)

$$\Phi_c = \arcsin\left(\frac{n_1}{n_0}\right) \qquad (21)$$

n_1 and n_0 being respectively the refractive indices of the metal and prism. Under total reflection the light produces an evanescent field in the medium with the lower refraction index, the metal film. This evanescent field (E) decreases exponentially in the metal layer (z).

$$E(z) = E_0 \cdot \exp\left(\frac{-z}{d_p}\right) \qquad (22)$$

E_0 is the electrical field at the interface and d_p is the distance at which E_0 decreases by a factor 1/e of its value. d_p is also defined with

$$d_p = \frac{\lambda}{\left[2 \cdot \pi \cdot n_1 \cdot \left(\sin^2 \Phi - \sin^2 \Phi_c\right)^{1/2}\right]} \qquad (23)$$

n_1 being the refractive index of the metal (Göpel et al, 1992). The evanescent field possesses the dispersion relation of the light in the prism. Therefore, with an appropriate layer thickness of metal, the evanescent field can induce surface plasmons at the interface metal/sample.

2.2.2. Configuration of the system

There are two possibilities of excitation by light while staying under conditions of total reflection. Either the angle of incidence is kept constant and the wavelength of the light varies or the wavelength is kept constant and the angle of incidence varies. Since the employed device works with a constant wavelength and variable angle of incidence the latter possibility will be detailed. The experimental scheme is shown in Fig. 4 (Raether, 1988).

excitation light

reflected light

air

prism

n

n_0

k_x

k

Φ Φ

metal
n_1

surface plasmon

evanescent field

n_2 sample
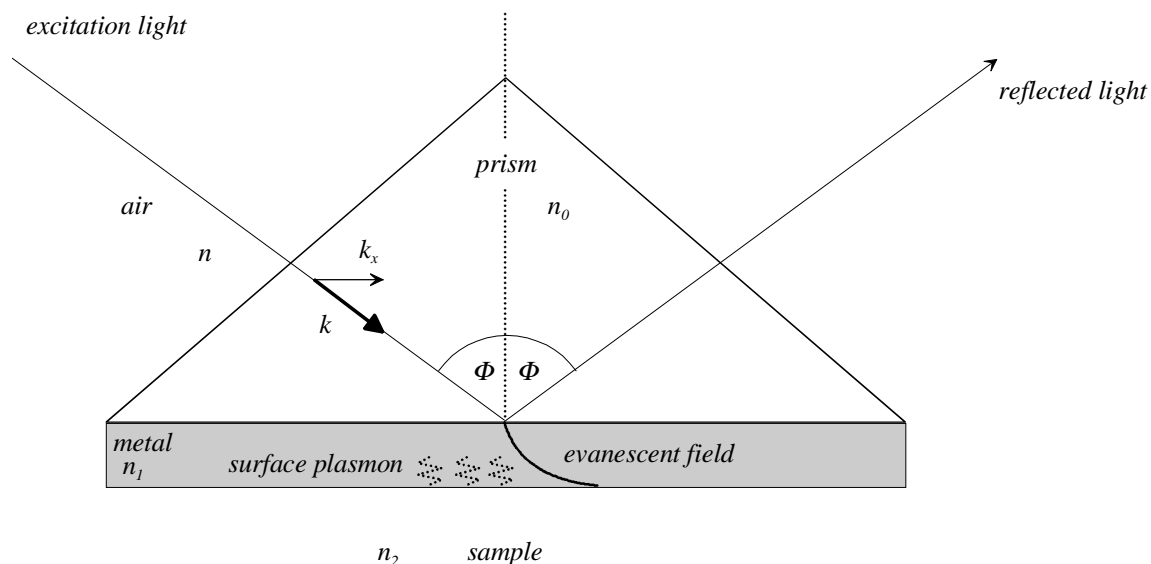
Fig. 4: Kretschmann structure.

The metal layer has a thickness of approximately 50 nm. A thinner layer is not recommended because it may produce a back-reflection of light into the prism. A thicker layer would decrease the efficiency of the resonance. With a layer of 50 nm the energy of the evanescent field produced by the light is almost totally transferred to the surface plasmons (Kieser, 1998).

The excitation of the surface plasmons is recognised as a decrease of intensity in the reflected light. This minimum corresponds to the conditions of resonance. A change in the index of refraction at the surface of the metal shifts the angle of resonance. The minimum of reflected intensity corresponds to a band because the absorption of the light is slightly widened. This is due to the attenuation of the electron oscillation along the interface metal/prism as a function of the absorption coefficient of the metal.

2.2.3. Different conditions of measurements

2.2.3.1.   Mass transport-controlled

The rate of mass transport is directly proportional to the ligand concentration, so that if mass transport is limiting, the rate of ligand binding to the surface provides a direct measure of the ligand concentration and the signal is independent of the analyte-ligand affinity at the surface. For this, the density on the surface has to be quite high and the

flow very low. The concentration of free ligand is chosen in order to give a linear slope. This method allows to determine the active concentration of the ligand according to Onsager's theory and also to measure inhibition curves and to calculate inhibition constants.

- Active concentration

Since the slope (dR/dt) is proportional to the binding onto the surface, it is also proportional to the active concentration of antibody ($[A_{bulk}]$). This concentration can be calculated from equation (24) according to Christensen (1997)

$$\frac{dR}{dt} = \frac{\left(L_m \cdot L_r \cdot [A_{bulk}] \cdot G \cdot MW\right)}{\left(L_m + L_r\right)} \tag{24}$$

where dR/dt is the slope of the signal, L_m and L_r are Onsager's coefficients, G is the concentration of available sites on the matrix (RU·mm^2/ng), and MW is the molecular weight (g/mol). The Onsager's coefficients are defined by equations (25) and (26)

$$L_m = \left(\frac{D^2 \cdot \text{flow}}{h \cdot b \cdot l}\right) \tag{25}$$

$$L_r = k_a' \cdot G \tag{26}$$

where D is the diffusion coefficient (m^2/s), h, b, l are the dimensions of the cell (m) and k_a' is the apparent association rate constant (l·mol^{-1}·s^{-1}).

In equation (24), $[A_{bulk}]$ and L_r are unknown. More than two equations can be written by varying the flow. The system of equations can be solved and the two unknowns can be calculated.

- Inhibition curves

The initial slope (k) was calculated with a linear fit in the program BIAevaluation. These values are used to draw the inhibition of the binding of the antibody to the derivative immobilised at the surface by the analyte in solution versus the concentration of analyte in solution.

$$[\text{free analyte}] = \left(1 - \frac{k}{k_0}\right) \cdot 100 \tag{27}$$

where k_0 is the slope in absence of analyte, i.e. the maximal slope and [free analyte] is the concentration of analyte (M).

The test mid-point corresponds to the concentration of antigen required to inhibit the binding of the antibody to the analyte derivative immobilised at the surface of 50 %, and can be read from this curve. The inhibition curves are fitted with the logistic function in agreement with Dudley et al. (1985).

The affinity constant defined in equation (2) can then be calculated from the test mid-point (TMP) according to Piehler et al. (1997)

$$K_A = \frac{2 + \sqrt{2}}{\sqrt{2} \cdot [TMP] - [IgG]} \tag{28}$$

where [TMP] is the molar concentration of analyte at the test mid-point, and [IgG] is the active concentration of antibody.

2.2.3.2.   Kinetics-control

The association and dissociation rate constants can be quantify when the mass transport of analyte to the surface is not limiting. The surface density should be low and the flow must be fast enough to produce a narrow diffusion layer (Pellequer et Van Regenmortel, 1993).

The dissociation rate constant (k_{diss}) was calculated first. The dissociation rate constant was used to assess the association rate constant (k_{ass}).

$$Y = R_0 \cdot e^{-k_{diss} \cdot (t - t_0)} + offset \tag{29}$$

$$Y = \frac{k_{ass} \cdot Conc \cdot R_{max}}{k_{ass} \cdot Conc + k_{diss}} \cdot \left(1 - e^{(-(k_{ass} \cdot Conc + k_{diss}) \cdot (t - t_0))}\right) + RI \tag{30}$$

The parameters in the equations are Y: response at t, R_0: response at the start of the fit (RU), t: time (s), t_0: time at the start of the fitted data (s), *offset*: residual response at

infinite time (RU), *Conc*: molar analyte concentration (mol/l), R_{max}: maximum analyte binding capacity (RU), and *RI*: bulk refractive index effect (RU).

The association (K_A) and dissociation (K_D) constants of the reaction at the surface are calculated from the ratios of the rate constants:

$$K_A = \frac{k_{ass}}{k_{diss}} = \frac{1}{K_D} \qquad\qquad (31)$$

2.3.   REFLECTOMETRIC   INTERFERENCE   SPECTROSCOPY: RIFS

This method relies on the interferences produced by the reflection of white light at thin layers (Gauglitz et al. 1993).

Light is sent, reflected on an interface that defines a boundary between two different indices of refraction. According to the angle of incidence (Φ) and the indices of refraction of the two media, a part of the radiation is reflected with an angle (Φ_R) equal to the angle of incidence and the other part is transmitted with the angle Φ_T. Snell's Law of Reflection defines the relation between the angles and the refraction indices (n) (Hecht, 1989).

$$\boxed{n{\cdot}\sin\Phi = n_1{\cdot}\sin\Phi_T} \qquad (32)$$

For a superposition of several thin layers the reflection takes place at each interface.
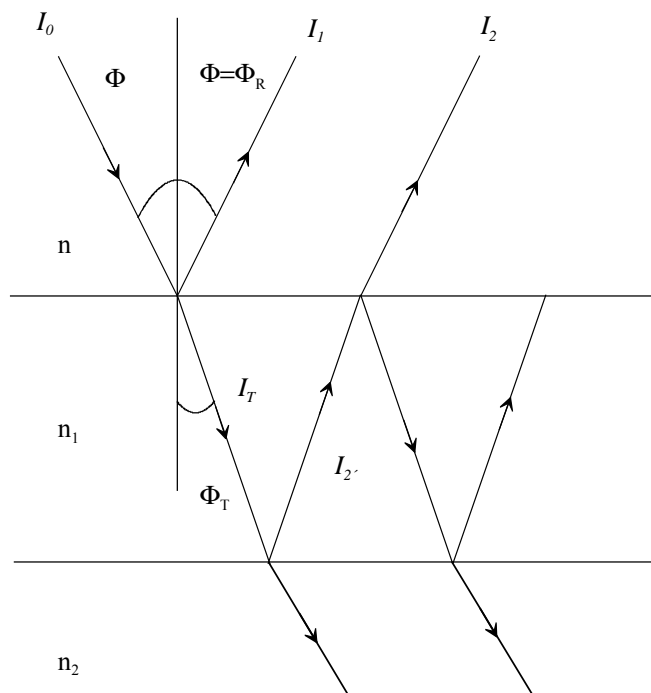
Fig. 5: Reflection and transmission of light in a system of parallel thin layers.

Moreover, if the layer thickness is smaller (0.5 to some 10 μm) than the length of coherence, constructive and destructive interferences are produced.
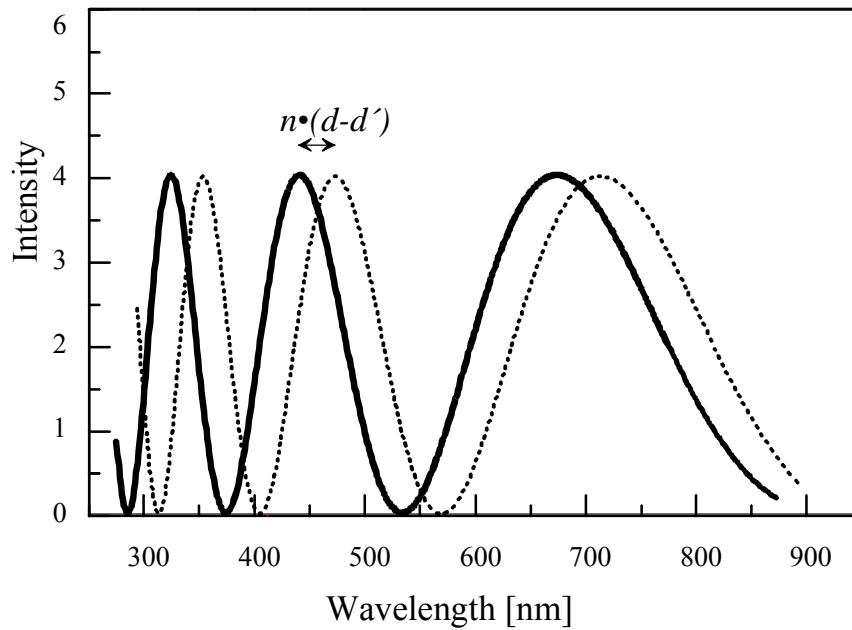
Fig. 6: Interference pattern caused by the reflection of light at several layers and shift of the pattern due to the augmentation of one of the layers.

For perpendicular incidence and weak reflectivity only the light reflected once (I_1) and twice (I_2) needs to be considered (Gauglitz et al., 1993, and Haake, 2000), see Fig. 5. The phase shift (δ) between (I_1) and (I_2) is defined by

$$\delta = \frac{2 \cdot \pi \cdot n_1 \cdot d_1 + \Theta}{\lambda} \qquad (33)$$

where d_1 represents the thickness of the middle layer with refractive index n_1, λ is the wavelength, and Θ is the transition of phase from n to n_1. The intensity of the reflected light is then equal to

$$I_R = I_1 + I_2 + 2\sqrt{I_1 \cdot I_2} \cdot \cos\left(\frac{4 \cdot \pi \cdot n_1 \cdot d_1 + \Theta}{\lambda} \right) \qquad (34)$$

As shown in Fig. 6, a change in the thickness layer due to specific binding to the modified transducer produces a shift in the interference pattern.

The RIfS method can also be employed to obtain kinetic constants and affinity constants.

The knowledge of the affinity constants is required to optimise homogeneous competitive assays, such as Fluorescence Resonance Energy Transfer, where two equilibria, defined by their affinity constant, are in competition.

2.4.   FLUORESCENCE RESONANCE ENERGY TRANSFER

2.4.1. Absorption and Fluorescence

2.4.1.1.   Absorption

The interactions between the electromagnetic properties of light and the molecular structure of the material produce the phenomena of absorption and emission.

The light is described by the following equation:

$$E = h \cdot \nu = \frac{h \cdot c}{\lambda}$$
(35)

E is the energy, ν is the frequency of the light, and λ represents the wavelength. H and c are respectively Planck's constant ($6.626 \cdot 10^{-34}$ J·s) and the speed of light in vacuum ($3 \cdot 10^{10}$ cm·s^{-1}) (Sharma and Schulman, 1999).

The electric field associated with the light allows charged particles, i.e. electrons, to absorb energy. This gain in energy transfers the molecule from the ground electronic state to an electronically excited state. However, a molecule cannot absorb light at any wavelength. Only light with a precise energy may be absorbed, defined by the exact difference of energy between the ground state (E_g) and the excited state (E_e) from the electronic transition.

$$E_e - E_g = h \cdot \nu$$
(36)

The position of the absorption band is associated with the energy of the electronic transition, whereas the intensity of the band represents the magnitude of the electronic transition (Sharma and Schulman, 1999).

The absorbed light depends of the nature and of the concentration of the molecule in solution. This relation is given by the Lambert-Beer law. In this law, A symbolises the absorbance, I and I_0 are respectively the intensity of the light transmitted through the absorbing sample and the initial intensity, C represents the concentration of the molecule (M), l is the path length of the light through the sample (cm), and ε is the

decadic molar absorption coefficient ($M^{-1} \cdot cm^{-1}$). The decadic molar absorption coefficient is specific for each molecule and for each wavelength.

$$A = -\log \frac{I}{I_0} = \varepsilon \cdot C \cdot l \qquad (37)$$

The molecular electronic absorption has a finite width due to the transition to several vibrational sub-levels inside the excited electronic state. These vibrational sub-levels are denoted by the vibrational quantum numbers $v = 0, 1, 2$ etc. All bands of absorption arise from the ground state vibrational level of the ground electronic state to several vibrational levels of the electronic excited state, therefore an absorption spectrum reflects the vibrational structure of the excited state (Sharma and Schulman, 1999). The several levels and possible transitions between the levels and sub-levels are presented in Fig. 7.

Not all theoretically possible transitions are allowed. The transition dipole moment defines the probability of the transition of the molecule from the initial state to the excited state. The transition dipole moments of the molecule in one state can be simplified by separating the spin function, the vibrational function, and the electronic wave function. Three rules limit transitions in complex molecules (Göpel and Ziegler, 1994, Atkins, 1999):

- The spin-interaction means the spin cannot change its multiplicity (singlet or triplet) during the transition.
- Laporte's rule for centrosymmetric compounds says that the initial and the excited wave functions cannot have the same symmetry (g and u).
- For reasons of symmetry the variation of the total orbital angular momentum (L) must be equal to 0 or ±1.

2.4.1.2.   Different possibilities of relaxation

Once the molecule has been excited to one of the excited electronic singlet states (S_1, S_2) it returns to its ground state (S_0). The absorption process takes about 10^{-15} s but the several possibilities to return to the ground state are slower, taking from 10^{-14} to several seconds. The various possibilities of relaxation are shown in Fig. 7.
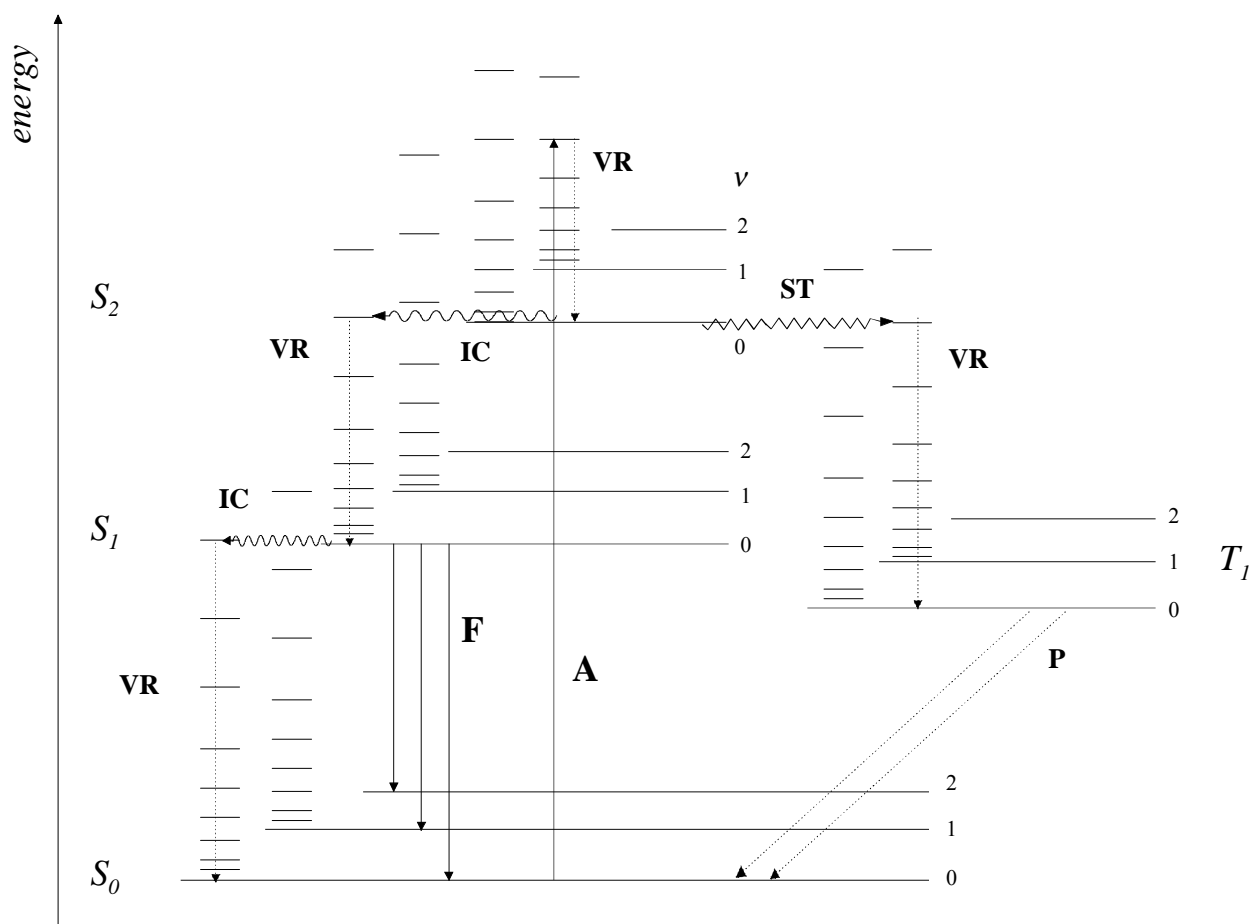
Fig. 7: Jablonski diagram, electronic absorption and numerous relaxation processes of molecules. Once the molecule is excited to one of the excited electronic singlet state (S_1, S_2) it returns to its ground state (S_0). The various possibilities of relaxation, staying in the singlet state, are the vibrational relaxation (VR), the internal conversion (IC) and the emission of fluorescence (F). Additionally, the excited triplet state (T_1) can be accessed for transitions under special conditions. The singlet-triplet intersystem crossing (ST) and the emission of phosphorescence (P) are then possible. (Göpel and Ziegler, 1994).

The vibrational relaxation refers to giving dispensing infrared quanta and kinetic energy to other molecules. This process takes place in the vibrational sub-levels within one electronic state in 10^{-14} to 10^{-12} s.

Contrary to vibrational relaxation, internal conversion takes place between two electronic states. If the lower vibrational level of the higher excited electronic state overlaps the upper vibrational level of the lower electronic state, the two electronic states are in a transient thermal equilibrium and the electrons can go to the lower

electronic state without loosing energy. After that vibrational relaxation takes place again. If there is little overlap between the two energy levels, the internal conversion may still take place by tunnelling. The internal conversion process is very rapid, taking 10^{-12} s.

From the electronic level S_1, if vibrational relaxation cannot take place, either a radiationless change of spin angular momentum conducts the molecule into a triplet state or a faster radiative deactivation named fluorescence can happen.

The transition from singlet spin to triplet spin is called singlet-triplet intersystem crossing. This process is normally forbidden, but there is a small probability that the change of spin may occur. The process that allows intersystem crossing is called spin-orbit coupling. It is the vectorial addition of the spin and the orbital angular momentum of the molecular electrons, which removes partially the distinction between the singlet and the triplet states. Because this transition is forbidden, lifetimes are quite long (10^{-8} s up to seconds).

Another mode of radiative deactivation is phosphorescence. The transition occurs between the lowest vibrational level of the triplet state to the ground singlet state. Therefore, it can only happen after an intersystem crossing process, which transfers the electron into the triplet state.

2.4.1.3.   Fluorescence

The last deactivation process described here is the emission of fluorescence. It takes place from the first excited electronic level to several vibrational sub-levels of the ground electronic state and therefore reflects the vibrational structure of the ground state. If the ground and the excited electronic states have identical vibrational spacings, the spectra of absorption and fluorescence will be mirror images of each other. The lifetime of fluorescent molecules is approx. 10^{-8} s, but the transition itself lasts 10^{-15} s. Because electrons arrive in several vibrational levels, one can think of vibrational relaxation as the next step to return the molecule to its ground state (Sharma and Schulman, 1999).

Intersystem crossing and internal conversion compete with fluorescence for deactivation of the electronic energy (Göpel and Ziegler, 1994). The ratio between the

rate constant of fluorescence (k_f) and the sum of the rate constants of all deactivation processes, including non-radiative deactivation modes (Σk_d), define the fluorescence efficiency which is also called quantum yield.

$$\Phi_f = \frac{k_f}{k_f + \Sigma k_d} \tag{38}$$

The reciprocal of the probability of fluorescence defines the lifetime of the lowest excited singlet state if fluorescence is the only mode of deactivation.

$$\tau_f^0 = \frac{1}{k_f} \tag{39}$$

The reciprocal of the sum of probability defines the mean lifetime the molecule spends in the excited state.

$$\tau_f = \frac{1}{k_f + \Sigma k_d} \tag{40}$$

It is also possible to define the quantum yield of fluorescence with these two lifetimes.

$$\phi_f = \frac{\tau_f}{\tau_f^0} \tag{41}$$

The intensity of the fluorescence emission is related to the molecular properties and can be derived from the Lambert-Beer law, equation (37) (Sharma et Schulman, 1999).

$$I_f = I_0 \cdot \phi_f \cdot (1 - 10^{-\varepsilon \cdot c \cdot l}) \cdot Z \tag{42}$$

with Z being a factor specific to the device. This expression can be simplified if the absorbance is extremely small.

$$I_f = I_0 \cdot \phi_f \cdot 2.3 \cdot \varepsilon \cdot c \cdot l \cdot Z \tag{43}$$

Fluorescent molecules can also deactivate by transferring their energy to another molecule. One of these transfers consists of Fluorescence (or Förster's) Resonance Energy Transfer (FRET).

2.4.2. FRET

FRET is described as a non-radiative transfer of energy between a fluorescent molecule called Donor and a second molecule defined as the Acceptor. But FRET does

not take place so easily, several conditions have to be met to observe FRET (Van der Meer et al., 1994).

- The quantum yield of the Donor has to be significant.
- The distance between the Donor and the Acceptor usually needs to be in the range of 1 to 10 nm.
- The Donor emission moment, the Acceptor absorption moment and their separation vector have to be in a favourable orientation to obtain a high orientation factor.
- The emission spectrum of the Donor must have a large overlap with the absorption spectrum of the Acceptor.
- The Donor and the Acceptor molecules must have strong electronic transitions.

2.4.2.1.   Quantum yield of fluorescence of the Donor

The efficiency of the transfer can be determined from the quantum yield of fluorescence in absence (ϕ_D) and in presence of the Acceptor molecule (ϕ_{DA}):

$$E_t = 1 - \frac{\phi_{DA}}{\phi_D} \qquad (44)$$

FRET is a supplementary way of deactivation, which competes with other normal deactivation modes described previously. The efficiency of the energy transfer can be defined in the same way as the efficiency of the fluorescence (Van Der Meer et al., 1994):

$$E_t = \frac{k_t}{k_t + k_f + \Sigma k_d} \qquad (45)$$

where k_t is the rate of energy transfer, and (as in equation (38)) k_f and Σk_d are respectively the rate of fluorescence of the Donor and the non-radiative modes of deactivation of the Donor.

2.4.2.2.   Distance between Donor and Acceptor

According to Förster's equation the rate of transfer is linked to the distance between the Donor and the Acceptor molecules R:

$$k_t = \left(k_f + \Sigma k_d \right) \cdot \left(\frac{R_0}{R} \right)^6 \qquad (46)$$

The efficiency of the transfer can also be defined with the distance between the Donor and the Acceptor by the following equation (Van Der Meer et al., 1994):

$$E_t = \frac{R_0^6}{R_0^6 + R^6} \qquad (47)$$

R_0 is defined as the distance at which the transfer efficiency is 50 %.

According to the Förster's theory R_0 is defined by:

$$R_0^6 = \frac{9000 \cdot \ln 10 \cdot \kappa^2 \cdot \phi_D \cdot J}{128 \cdot \Pi^5 \cdot n^4 \cdot N} \qquad (48)$$

κ^2 is the orientation factor of the Donor and Acceptor defined in the following chapter (2.4.2.3), J is the overlap integral between emission spectrum of the Donor and absorption spectrum of the Acceptor, n is the index of refraction, and N is the number of Avogadro ($6.02 \cdot 10^{23}$ per mole) (Dos Remedios and Moens, 1999).

2.4.2.3. Orientation factor

The orientation factor, κ^2, depends on three orientations: the emission transition moment of the Donor (TM_{ED}), the absorption transition moment of the Acceptor (TM_{AA}), and the distance between the Donor and the Acceptor molecules (R_{DA}).
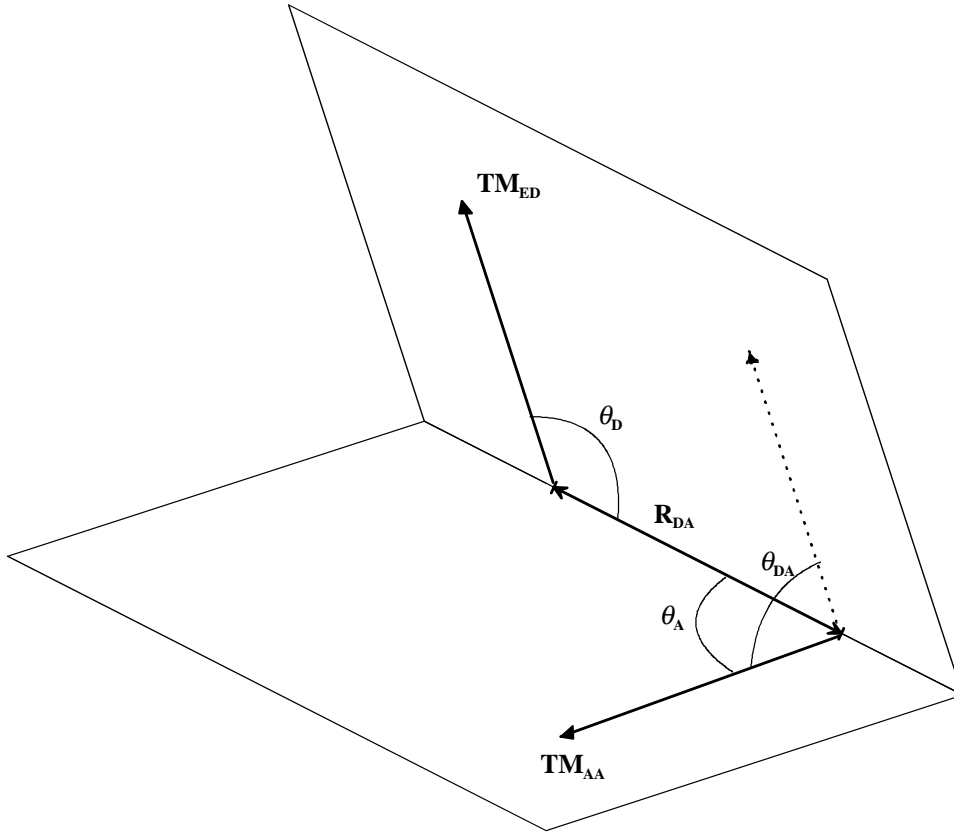
Fig. 8: Representation of the vectors and the angles defining the orientation factor.

The factor κ^2 is commonly expressed with the angles defined by these three unit vectors (Van der Meer, 1999).

$$\kappa^2 = \left(\cos\theta_{DA} - 3 \cdot \cos\theta_D \cdot \cos\theta_A\right)^2 \qquad (49)$$

The energy transfer is proportional to the orientation factor κ^2, therefore a high value is preferable. κ^2 varies between zero and four. The average value, if the three orientation vectors are randomly distributed, is equal to 2/3. κ^2 is equal to four when the emission transition moment of the Donor (TM_{ED}) and the absorption transition moment of the Acceptor (TM_{AA}) are parallel or antiparallel to the distance between the Donor and the Acceptor molecules (R_{DA}).

2.4.2.4. Spectral overlap

The overlap integral (*J*) defines the spectral overlap between the emission of the Donor and the absorption of the Acceptor. The wavelength of the light (λ), the molar extinction coefficient of the Acceptor at this wavelength, $\varepsilon_A(\lambda)$, and the fluorescence

spectrum of the Donor normalised on the wavelength scale, $F_D(\lambda)$, are combined to characterise the integral (Dos Remedios and Moens, 1999).

$$J = \int_0^\infty F_D(\lambda) \cdot \varepsilon_A(\lambda) \cdot \lambda^4 \cdot d\lambda \qquad (50)$$

3. Material and Methods

3.1.   <u>EQUIPMENT</u>

3.1.1. SPR device

Two commercial devices were employed: BIACORE 1000 and BIACORE 2000, from the firm Biacore, Uppsala, Sweden.

3.1.2. RIfS device

The RIfS system was set up using the following components:

A 5V/10W halogen light source, a Flow Injection Analysis (FIA) ASIA and auto-sampler from Ismatec, Wertheim-Mondfeld, Germany, an optical fiber in polymer PMMA with a diameter of 1 mm with fiber coupler (1x2) from MicroParts, Dortmund and a linear photodiode array MCS 410 from Carl Zeiss, Jena, Germany.

3.1.3. Fluorescence readers

The luminescence spectrometer LS50B and the fluorescence microtiterplate reader LSR200 were made by Perkin Elmer, Überlingen, Germany.

The experimental fluorescence nanotiterplate reader Bioscan 5 is made by Perkin Elmer Applied Biosystems, Überlingen, Germany. The device consists of a focused He-Ne laser (633 nm), which scans the area of the plate with a resolution of 10 μm. The device has an epi design: the excitation wavelength and the signal arrive and leave from the same side of the nanotiterplate (NTP). The signal is separated from the excitation before reaching the detector. The dichroic beam splitter transmits the signal and blocks the excitation wavelength. The signal passes a band-pass filter (665 nm – 680 nm) to the photo-multiplier tube (Schobel et al., accepted).

3.1.4. Secondary devices and material

- UV/Vis Spectrometer Specord M500 from Zeiss, Jena, Germany.

- UV/Vis Spectrophotometer Anthelie advanced, from Secomam, France.

- Biofuge 15 and Laborfuge 400R centrifuges, from Heraeus, Osterode, Germany.

- LKB optical unit UV-1, control unit UV-1 and rec 102 from Pharmacia Biotech, Uppsala, Sweden.

- Several piston-type pipettes from Eppendorf, Hamburg, Germany.

- Micro-dispenser device with micropipette from GeSIM, Grossermarkmannsdorf, Germany (Fischer-Fruholz, 1998).

- Micro-dispenser device with micropipette from Microdrop, Norderstedt, Germany (Schober et al., 1993).

- Vortex Genie 2 from Scientific Industries, New York, USA.

- Microtiterplate agitator MTS 2 from IKA-Labortechnik, Staufen i. Br., Germany.

- CM5 chips, with a carboxymethylated dextran matrix, from Biacore, Uppsala, Sweden.

- RIfS transducer with 10 nm Ta_2O_5 and 330nm SiO_2 on 1 mm D263 substrate, from Schott, Mainz, Germany.

- Special high-adsorption microtiterplates (MTP) made by Greiner, Germany

- Non binding white microtiterplates from Corning, USA

- Nanotiterplates (NTP) in Acrylnitril-Butadiene-Styrol-copolymer (ABS) made by BIAS, Bremen, Germany. The plates have a dimension of 2 x 2 cm^2, with 25 x 25 wells of 70 nl. The wells have the form of inverted truncated pyramids with a base of 600 µm and a depth of 400 µm.

- Transparent adhesive film with low fluorescence background, Arcare 7759, to cover the NTP, from Adhesives Research, Inc., Glen Rock, USA.

- Micro-concentrators "Microcon 30" with a pore size of 30 kDa from Millipore, Eschborn, Germany.

- The PD10 columns, Sephadex G-25 M from Pharmacia Biotech, Uppsala, Sweden.

3.2.   CHEMICALS

3.2.1. Antibodies and proteins

- The monoclonal IgG 15H11 as well as the immunogen BSA-(E2-7-CMO) were produced and given by the group of Prof. Cuilleron from the National Institute for Health and Medical Research (INSERM) at the hospital Debrousse in Lyon, France.

- The polyclonal antibodies against estrone, estradiol and estrogens and the haptens used in the immunogen substances (see Table 1) were produced by Dr. Ram Abuknesha from King's College, London.

	Anti-estrone-IgG	Anti-estradiol-IgG	Anti-estrogens-IgG
Abbreviation	α-E1-IgG	α-E2-IgG	α-ES-IgG
Immunogen	BSA-(E1-3-CME)	BSA-(E2-3-BA)	BSA-(E2-17-Hg) BSA-(E1-17-CMO)
Animal	Sheep	Rabbit	Sheep
Purification	With immunosorbent column with attached haptens	With immunosorbent column with attached haptens	With immunosorbent column with attached haptens

Table 1: polyclonal antibodies and respective immunogens.

- The monoclonal antibody against Rainbow Trout vitellogenin, called B8D8, was given by Prof. Hock, Chair of Botany, Technical University of Munich, Germany.

- Vitellogenin from Rainbow trout and estradiol induced plasma from rainbow trout were obtained from Dr. Halim Dizer, Department of Ecotoxicology, Technical University of Berlin, Germany.

- Synthetic wastewater was produced by the group of the Prof. Bilitewski, Institute for waste management and residual waste, Technical University of Dresden, Germany.

- Other proteins were ordered from Sigma, Deisenhofen, Germany.

3.2.2. Chemicals

The principal analytes and the numbering of the estrogens skeleton are shown in Fig. 9
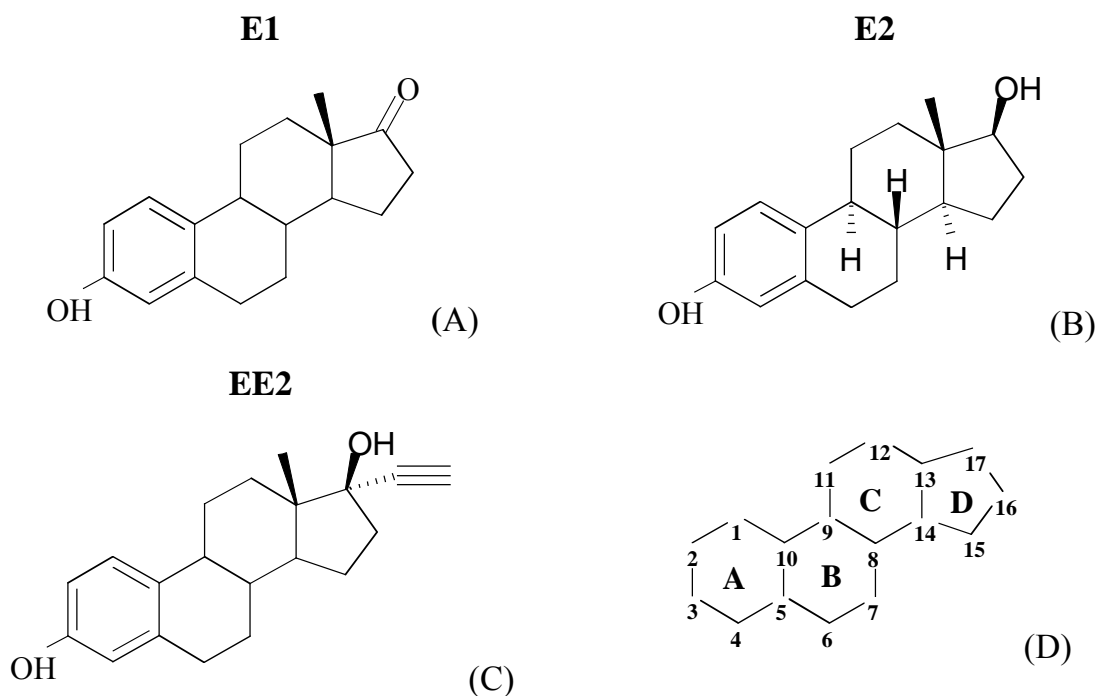
Fig. 9: Chemical structure of estrone (A) abbreviated E1, estradiol (B) abbreviated E2, ethinylestradiol (C) abbreviated EE2, and the numbering of the estrogens skeleton (D).

- The derivative 6-(O-carboxymethyl)oximinoestradiol was bought from Sigma, France.

- The estrogens and derivative sulfates and glucuronides were ordered from Sigma, Germany.

- The derivative 7-(O-carboxymethyl)oximinoestradiol coupled to BSA, which was the immunogen used to obtain the antibody 15H11, was offered by Prof. Cuilleron, from the National Institute for Health and Medical Research (INSERM), Lyon.

- Estrogen derivatives used for raising the polyclonal antibodies (see Table 1) were obtained from Ram Abuknesha, King's College, London.

- The NHS active esters of the dyes Cy5 and Cy5.5 were from Amersham Life Science, Braunschweig, Germany.

- The maleimide salt of the Alexa fluor 680 dye, Alexa680, was bought from Molecular Probes, Leiden, the Netherlands.

- Amine coupling kit with NHS/EDC from Biacore, Uppsala, Sweden.

- Other standard chemicals from Sigma and Riedel-de Haën, Germany.

3.2.3. Solutions

- Phosphate buffered saline (PBS)

  150 mM NaCl

  50 mM KH_2PO_4

  adjusted to pH 7.4 with KOH, 2M

- Carbonated buffer

  100 mM Na_2CO_3

  adjusted to pH 9.5 with $NaHCO_3$, 100mM

- Hepes Buffer Solution

  3.4 mM EDTA

  0.15 M NaCl

  0.005 % of P20

  10 mM Hepes

  pH is adjusted to 7.4

  Degazed in ultra sound bath for 15 min

- Regeneration solution for BIACORE for E2-6-CMO / 15H11

  30 mM NaOH

  7.5 % acetonitrile

- Regeneration solution for BIACORE for all other systems

  100 mM NaOH

  20% acetonitrile

- Regeneration solution for the RIfS

  HCl pH 1.6 followed by the mixture acetonitrile/bi-distilled water/propanoic acid in the proportions 50/50/1 or SDS 0.5 % in HCl pH 1.9.

3.3. **METHODS**

3.3.1. Surface modification

3.3.1.1.   SPR transducer

The derivative-BSA or BSA was immobilized on the surface of the chip as described in the Biacore system Manual (1991).

- NHS (0.05 M) and EDC (0.2 M) were mixed one to one, and 35 µl of the mixture were injected at a flow rate of 5 µl/min in one channel of a CM5 chip.

- The concentration of BSA-derivative or BSA used for kinetic and active concentration measurements was 10 µg/ml and 100 µg/ml respectively. 35 µl of BSA or BSA-derivative in acetate buffer pH 4 were injected at a flow rate of 5 µl/min.

- The surplus of active ester groups was blocked by a 7 min injection of a 1 M ethanolamine hydrochloride solution pH 8.5.

3.3.1.2.   RIfS transducer

The modification process is described in detail by Länge (2000) and Haake (2000).

- Immersing 20 min in a mixture of 40 % H_2O_2 and 60 % H_2SO_4 in an ultra sound bath

- rinse with bi-distilled water and dry with nitrogen

- 1 drop of glycidyloxypropyltrimethoxysilan (GOPTS) per transducer in a closed beaker for 1 hour

- rinse with dried acetone and dry with nitrogen

- one drop of a solution of aminodextran (AMD)/water (2/1) for 2 transducers in sandwich in a closed beaker saturated in water vapour overnight

- rinse with bi-distilled water and dry with nitrogen

- 1 mg of the derivative solved in 10 µl dimethylformamide (DMF) and 1 µl DIC per transducer for 6 hours in a closed beaker saturated in DMF vapour

- rinse with bi-distilled water and dry with nitrogen

3.3.1.3.   NTP

The NTP was modified as follows to reduce the non-specific adsorption:

- bath of 5 % Polyethylenimine in water overnight
- rinse thoroughly 15 min in a bath of bi-distilled water
- bath of 3 mg/ml of BSA in PBS overnight
- rinse thoroughly with bi-distilled water.

3.3.2. Labelling

The processes of labelling described previously by Schobel et al. (1999) have been slightly modified.

3.3.2.1.   IgG-Cy5

The dye is conditioned in a capsule adapted to label 1 mg of protein (155000 Da) with a degree of labelling between 4 and 12. The protocol was modified to obtain different degrees of labelling.

500 µg or 1 mg IgG was dissolved in carbonated buffer pH 9.4 (1 mg/ml) and 1/3 to 1 of the dye capsule diluted in 10 µl DMF was added to the protein solution. The fluorophore/protein ratio of each labelling is detailed in 3.3.3.3. Protein and fluorophore were mixed and incubated for 30 min. The labelled proteins were separated from the free dye either on a microcon concentrator 30, rinsed with PBS pH 7.4 (12000 g, 5 min/250 µl) till the filtrated solution is colourless, or on a column Sephadex G-25 with PBS.

3.3.2.2.   BSA-Cy5.5

The dye is conditioned in a capsule adapted to label 1 mg of protein (155000 Da) with a degree of labelling between 2 and 4. The protocol was modified according to the molar mass of BSA (69000 Da).

3 mg BSA was dissolved in 1 ml carbonated buffer pH 9.4, and one dye capsule diluted in 20 µl DMF was added to the protein solution. This was mixed and incubated for 30 min. The labelled proteins were separated from the free dye either on a Microcon concentrator 30 (12000 g, 5 min/250 µl) and rinsed with PBS, pH 7.4

(12000 g, 5 min/250 µl) till the filtrated solution is colourless, or on a column Sephadex G-25. PBS was the elution solution in both separation methods.

3.3.2.3.   Derivative-(BSA-Cy5.5) or derivative-BSA

The analyte derivative has to be transformed in NHS-ester. The analyte derivative was dissolved in dimethylformamide (DMF, 10 mg/ml). A 1.1-fold molar excess of N-hydroxysuccinimide (NHS) was added, and the mixture was stirred with a magnetic stirrer and cooled in an ice bath. Then a 1.1-fold molar excess of N, N´-dicyclohexylcarbodiimide (DCC) was added. The mixture was cooled and stirred for 20 min. The reaction continued stirring overnight. The reagents were centrifuged (12000 g) and the supernatant containing the NHS ester of the derivative was taken. The derivative was considered as totally transformed in NHS ester.

The derivative was then coupled to BSA. BSA was dissolved in a carbonated buffer pH 9,4 (5 mg/ml, 72.5 µM). The molar quantity of derivative in DMF added to the BSA-Cy5.5 was 6 to 10 times higher than that of BSA. The reaction took place for 30 min. The excess of derivative was separated either by filtration on Microcon concentrator 30 (12000 g, 5 min/250 µl) and rinsed three times with PBS, pH 7.4 (12000 g, 5 min/250 µl), or on a column Sephadex G-25 for the derivative coupled to Cy5.5.

3.3.3. Measurements

3.3.3.1.   BIACORE

• For measuring the active concentrations the theoretical concentrations were chosen in order to give a linear response: 7.5 nM for αE1, 100 nM for αE2, 50 nM for αES. The theoretical concentration in ascitic fluids for the monoclonal IgG 15H11 was unknown. Several dilutions of the ascites were tested between 1/390 and 1/3000. The sample was injected at different flow rates from 2 µl/min up to 100 µl/min (Richalet-Sécordel et al, 1997).
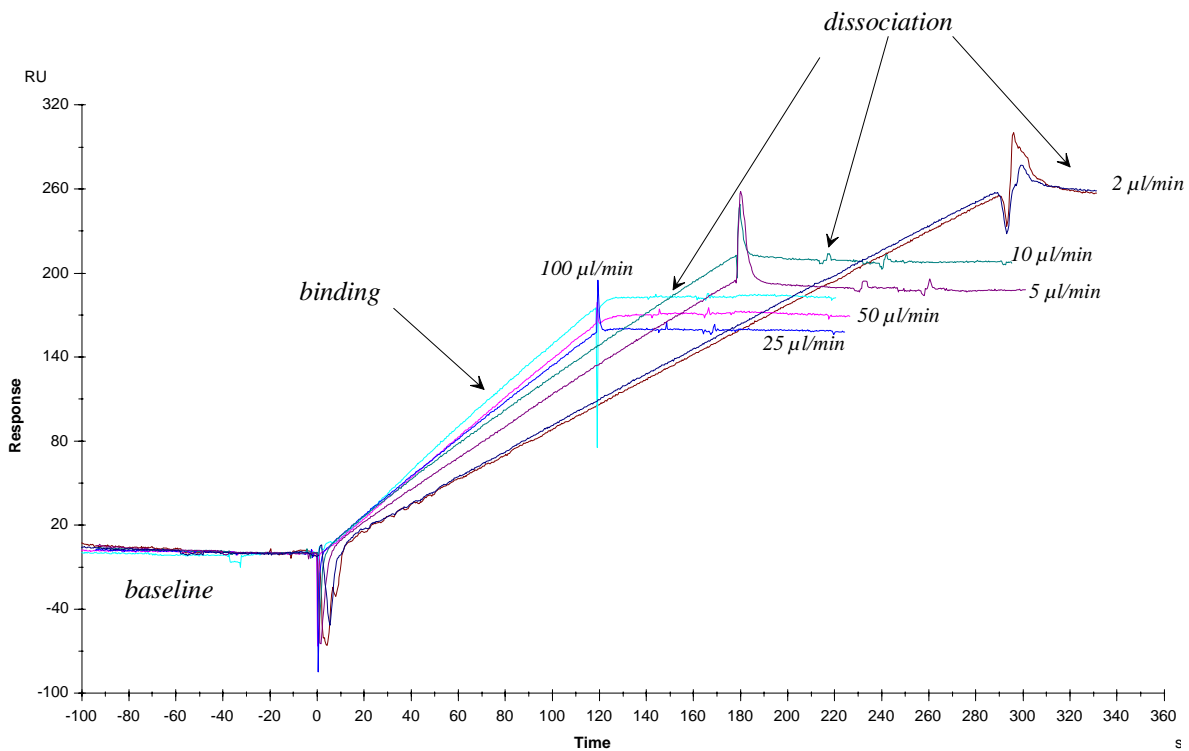
Fig. 10: Example of sensorgram obtained for the determination of the active concentration. The flow rate increases from 2 µl/min to 100 µl/min.

- The binding kinetics were measured with several concentrations of the antibody (Zeder-Lutz et al., 1997). The theoretical concentrations used were for αE1 between 15 nM and 0.9 nM, for αE2 and αES between 30 nM and 1.8 nM. The active concentrations used for 15H11 varied between 6.2 and 35.6 nM. A solution of inhibitor at a concentration of 1 µM was injected for the dissociation of the antibody in order to avoid re-binding. 140 µl of the antibody solution was injected at the flow rate of 20 µl/min for the association phase and the dissociation was observed for 600 s. Finally, the flow-cells were regenerated.
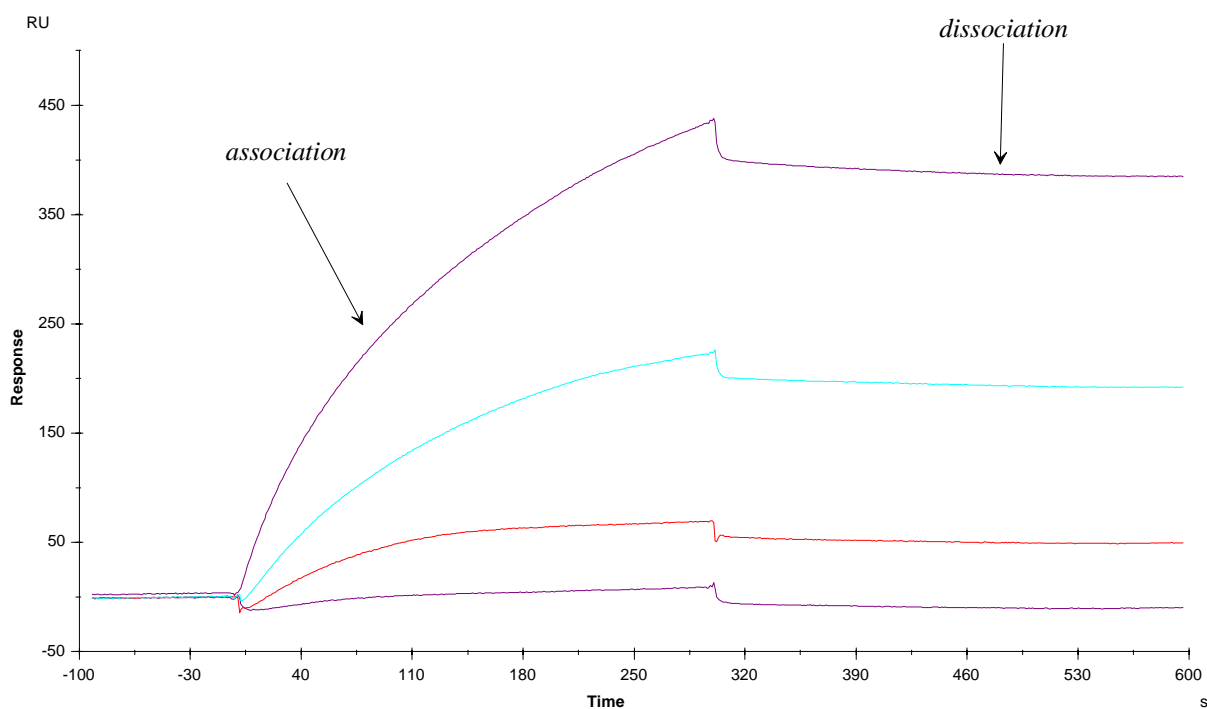
Fig. 11: Example of sensorgram obtained for the determination of the kinetic rates.

- The inhibition curves were measured under conditions of high surface density and low flow. The active concentration of antibodies used for 15H11 was 2.5 nM, and the concentrations used for the polyclonal IgGs are given in Table 9. The tested analytes are estrone, estradiol and ethinylestradiol, estradiol-3-sulfate and estradiol-17-glucuronide. Analytes were used at concentrations between 0.01 µg/l and 3000 µg/l. IgG and analytes were pre-incubated 10 min, and injected together for 2.5 min at 20 µl/min. Dissociation was measured for 100 s. Afterwards followed the regeneration.

3.3.3.2. RIfS

The protocol from Piehler et al. (1997) was slightly modified. The flow rate was fixed to 40 µl/min, and 1ml was injected on the transducer. The antibody concentration was chosen in order to give a slope of approximately 1 pm/s, which corresponds to 250 ng/ml for αE1 and 500 ng/ml for αE2 and αES. Each measurement was repeated three times to obtain an average value with a standard deviation. The inhibition curves, representing the slope as a function of the concentration on a semi-logarithmic scale, were fitted with the logistic function.
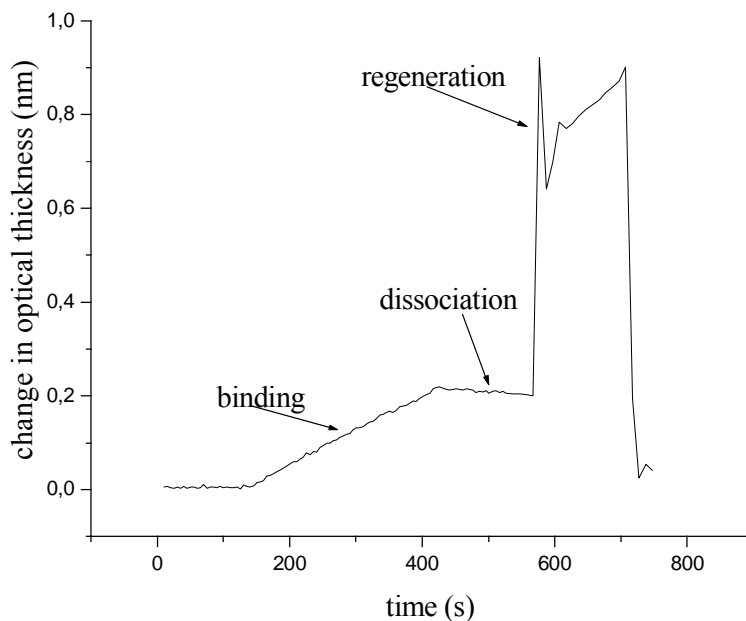
Fig. 12: Example of RIfS measurement.

3.3.3.3.   UV-Vis

The absorption spectra were measured with a split of 1 nm and a speed of 120 nm/min. The pure solvent was used as reference. The solution was diluted to give an absorbance smaller than two. The recorded wavelengths varied between 220 nm and 800 nm.

- The unknown molar absorbance of some substances was determined by preparing several solutions with variable concentration. The slope of the linear regression of the absorbance as a function of the concentration was equal to the decadic molar absorption coefficient.

- The degree of labelling was calculated with the following equation (Schobel et al. 1999):

$$\frac{[F]}{[P]} = \frac{\varepsilon_{P,278nm} \cdot A_{F,\lambda\max}}{\varepsilon_{F,\lambda\max} \cdot \left(A_{278nm} - K \cdot A_{F,\lambda\max}\right)} \tag{51}$$

with the indices $_P$ and $_F$ representing the protein and the fluorophore, A being the absorption, ε the decadic molar absorption coefficient, $[P]$ and $[F]$ the concentration of the protein and of the fluorophore respectively. K corrects the absorbance of the dye at 278 nm. The required characteristics are given in Table 2.

	IgG	BSA	VTG	Cy5	Cy5.5	Alexa680
MW (g/mol)	150000	69000	145000	792	1312	1000
λ_{max} (nm)	278	278	278	653	681	679
$\varepsilon_{\lambda max}$ (l/mol·cm)	201700	45540	87000	250000	190000	143000
K				0.05	0.13	0.03
Reference	Wells et al., 1966	Cohn et al., 1947	Byrne et al., 1989	Mujumdar et al., 1993	Mujumdar et al., 1996	See 4.2.1

Table 2: Required characteristics of the proteins and fluorophores for the determination of the labelling degree. K defines the percentage of absorbance of the fluorophore at the absorption wavelength of the protein.

The decadic molar absorption coefficient of the vitellogenin (*A*= 0,6 for 1mg/ml of VTG) was given in a private communication by the Dr. Halim Dizer, TU Berlin, Germany, and calculated in l·mol^{-1}·cm^{-1} according to the molar weight of 145000 g/mol.

3.3.3.4. FRET

The assay can be decomposed in two steps. All measurements were done in PBS containing 0.1 mg/ml OVA to reduce the non-specific adsorption at the surface of the plate.

The first step was the so-called titration which determines the analyte derivative-Cy5.5 / antibody-Cy5 ratio with the highest quenching of the Donor (Cy5). The solution of the labelled antibody (50 % of the total volume) was mixed and incubated for 10 min with a solution (50 % of the total volume) at variable concentrations of the labelled derivative, and then measured. The ratio which presents the highest quenching of the Donor was chosen for the next step.

The second phase was the competitive immunoassay where the free analyte in various concentrations added to the previously defined ratio of labelled derivative/labelled antibody. The free analyte (80 % of the total volume, 0.01-3000 µg/l) and the antibody (10 %) were incubated for 10 min before the derivative (10 %) was added. Before the measurement 10 min of incubation were necessary.

Concerning the NTP, the dispensing was done in a closed plexiglas box with high humidity and the NTP was cooled on a Peltier element to avoid evaporation. Once the pipetting was finished the plate was covered with a thin plastic film for the measurement (Schobel, 1999, and Stemmler, 1999).

- For the titrations in cuvettes with the LR50B the device measured a wavelength range in scan-mode, between 662 nm and 800 nm, and calculated the average of 3 spectra. The split was set to 5 nm and the scan speed to 120 nm/min. The excitation wavelength was 647 nm. For the calibration curves the device operated in time-mode, with 647 nm as excitation wavelength and a split of 5 nm, for 120 s.

- In the MTP with the LSR200 each well was excited at 640 nm and the fluorescence was integrated at 667 nm for 30 s.

In the NTP with the Bioscan the parameters were adjusted as follows: 40 mW for the light intensity, 150 mm/s for the scan speed, a frequency of 12500 kHz, and 1000 V for the photomultiplier voltage. The read-out of the whole plate required 2.8 min and gave an image of 1000·1000 pixels, see Fig. 13 (A). Then a mask was placed on the picture, see Fig. 13 (B), and the integration of the signal gave the intensity in each well.
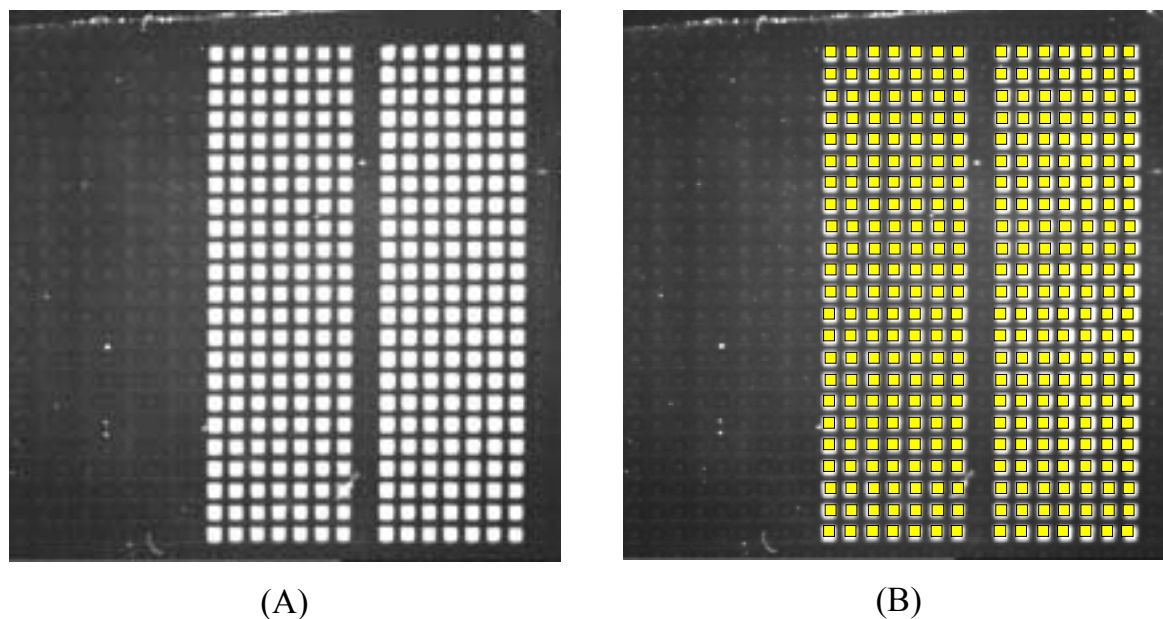
Fig. 13. (A) Example of an image of the measured NTP, (B) Position of the mask on the image of the NTP for the integration of the signal.

3.3.3.5.   PSFIA

Special high adsorption MTPs were coated with Vitellogenin (VTG, 50 nM) in PBS, 200 µl / well, overnight at 4°C. The plate was rinsed twice with PBS and blocked with 0,5 % BSA in PBS, 300 µl / well, 2 h at room temperature. The plate was emptied and filled with 250 µl of B8D8 and VTG: 125 µl of B8D8 2 nM in 0,5 % OVA in PBS were mixed with 125 µl of VTG (variable concentrations) in 0,5 % OVA in PBS. The plate was incubated overnight at 4 °C. 200 µl were taken from this plate and measured in a non-binding white MTP under the same conditions as for the FRET assay. The conditions of coating and incubation from Stemmler (1999) were modified.

3.3.4. Evaluation

After deleting the regeneration phase the sensorgrams obtained with SPR were normalised to a common origin, corresponding to the beginning of the specific interactions. The reference measurement (BSA immobilised) was subtracted from the response to correct for non-specific adsorption.

3.3.4.1.   Active concentration with SPR

The active concentration of the antibody was calculated with the software BIAconc developed by Christensen (1997). The theory was explained in 2.2.3.1. Care must be taken to reduce the error of the active concentrations according to Richalet-Sécordel et al. (1997). Each slope was divided in several intervals. The number of intervals and the size of the intervals were chosen in order to fulfil the following criteria. The standard deviation on the average active concentration [A_{bulk}] including all intervals (± standard deviation) as well as the standard deviation on the active concentration defined by one interval (χ^2) have to be the smallest possible. A good agreement has to be found between the slope measured at the different flow rates by linear regression, dR/dt_{reg}, and the ideal slope fitted by introduction of the calculated [A_{bulk}] and L_r, dR/dt_{fir}. The experimental slopes, fitted by linear regression, have to be determined with good χ^2 values for each interval. Finally, the values of L_r should decrease from the first to the last interval.

3.3.4.2.   Fitting of the kinetic measurements

The dissociation and association rate constants were calculated with the program BIAevaluation 3.1 using the equations given in 2.2.3.2. Two parameters indicated the quality of the fitting: the standard deviations and the residual plot. The standard deviations of k_{diss} and k_{ass} has to be small. The difference between the experimental and the calculated data for each point, represented by the residual plot, has to be randomly scattered around the x axis.

3.3.4.3.   Fitting of the inhibition and calibration curves

The inhibition (SPR and RIfS) and calibration (FRET) curves were fitted on a half logarithmic scale with the logistic function (Dudley et al, 1985). Each concentration was measured three times to determine the standard deviation.

$$I = \frac{I_{max} - I_{min}}{1 + \left(\dfrac{[A]}{[TMP]}\right)^s} + I_{min} \qquad (52)$$

$I_{\max}$ and $I_{\min}$ were the maximal and minimal intensities, $[A]$ the concentration of analyte, $[TMP]$ the test mid-point, and s was the slope at the inflection point.

The limit of detection is calculated with the concentration corresponding to the blank (no analyte) value added to three times the standard deviation of the blank value. The signalling range (SR) is represented by

$$SR = \frac{I_{\max} - I_{\min}}{I_{\max}} \cdot 100 \qquad (53)$$

The curve can be normalised between 0 and 100 % (B/B_0) according to the following equation (Hock, 1995):

$$\frac{B}{B_0} = \frac{I - I_{min}}{I_{\max} - I_{\min}} \cdot 100 \qquad (54)$$

The working range can be calculated from this representation. It is defined as the range of concentrations corresponding to 10 % - 90 % of the signal.

Concerning the measurement of unknown concentrations, the error of the unknown concentration is defined by the error of the signal divided by the slope of the fitting function at this point (Dudley, 1985).

The propagation of the errors in the calculations are calculated according to Hofmann (1982).
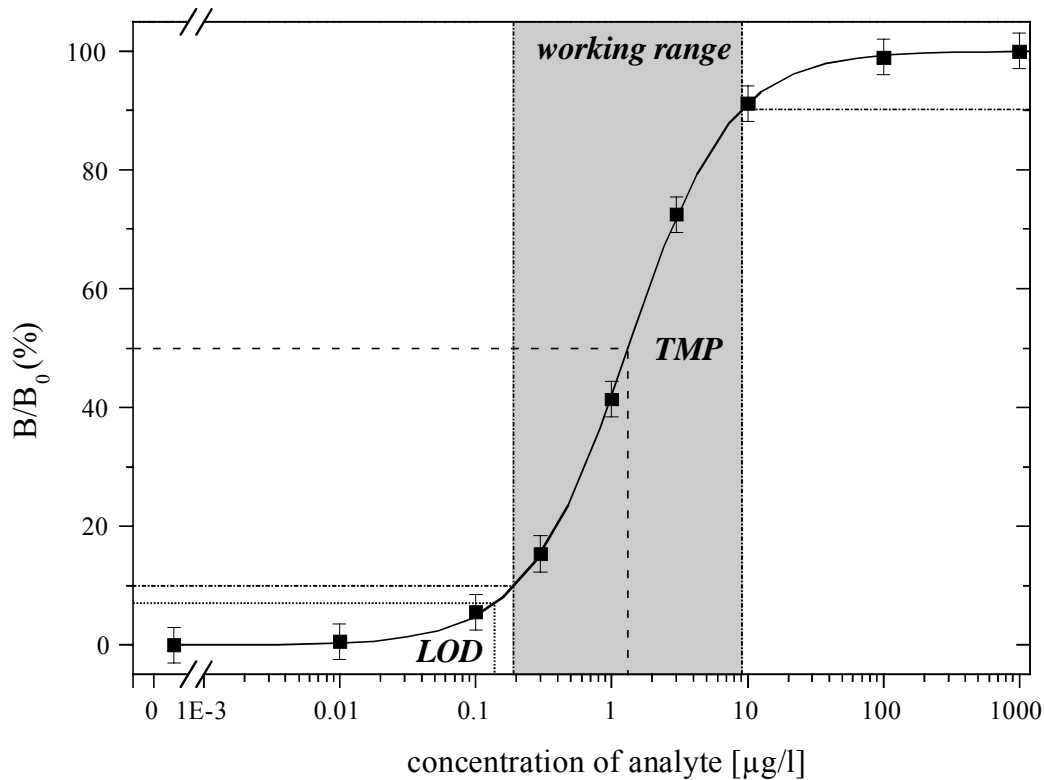
Fig. 14: Example of a calibration curve (FRET) with the analytical definitions. The limit of detection (LOD) is represented by a dotted line, the test mid point (TMP) is indicated by a dashed lined and the working range is defined by the grey area.

3.3.4.4.   Comparison of two series of measurements

To determine whether some measurements realised under different conditions (devices, surface of the transducer, method of determination) are comparable or significantly different, two non-parametric tests have to be applied. The Wilcoxon matched-pairs signed ranks test to compare two groups constituted by the same pairs, and the Mann Whitney's test to compare the median of independent samples (Barlow, 1989, and Massart et al., 1988).

In the Wilcoxon's matched pairs signed rank test the difference for each pair is calculated. Any pair with zero difference get thrown away. The number of remaining pairs is called N. The values of the differences are ranked first without regard to sign starting with the smallest value. Then the same sign is given as to the corresponding difference. The sum of the ranks for positive differences and the sum of the ranks for

the negative difference are calculated. The null hypothesis is that the two groups are equivalent. If this hypothesis is true, it is expected that the sum of all ranks for positive differences is close to the sum of ranks for negative differences. The smaller sum (T) is compared with the critical value T(N, α), α being the significance level. If the calculated T value is equal or smaller than the critical value of T, the null hypothesis is rejected.

For the Mann-Whitney's test the two groups called A and B, with N_A and N_B the number of data in each group respectively, are grouped and ranked. The lowest value has the rank one. The sums of the ranks of each group is calculated and called R_A and R_B. The U_A and U_B values can be calculated according to the following equations:

$$U_A = N_A \cdot N_B \cdot \frac{N_A \cdot (N_A + 1)}{2} - R_A$$

(55)

$$U_B = N_A \cdot N_B \cdot \frac{N_B \cdot (N_B + 1)}{2} - R_B$$

(56)

The smaller U value is compared to the critical $U(N_A, N_B, \alpha)$. The null hypothesis being that the groups are equivalent, the U_A and U_B values should be equal. If the smaller calculated U value is inferior or equal to the critical U value, the null hypothesis is rejected.

4. Results and Discussion

4.1. CHARACTERISATION OF 15H11 IgG BY SPR

The analyte derivatives-BSA were difficult to immobilise and the conditions of immobilisation were slightly changed. The concentration was increased to 100 µg/ml (for the kinetics) and 500 µg/ml (for active concentration measurements and inhibition curves), the pH was reduced to 3 instead of 4, and each immobilisation step was repeated twice.

4.1.1. Active concentration

Since the response varied considerably as a function of the dilution, the measurements of the active concentration of the monoclonal antibody 15H11 were repeated at various dilutions of the ascitic fluids.

Dilution of the ascites	Measured active concentration (nM)	Calculated concentration at undiluted level (µM)
1/3000	2.6 ± 0.3	8 ± 1
1/1560	8.3 ± 0.7	13 ± 1
1/780	15 ± 1	12 ± 1
1/390	36 ± 2	13.9 ± 0.7

Table 3: Measurements of the active concentration at different dilution levels. The concentration at undiluted levels is the active concentration in ascites.

The concentration at undiluted levels is the measured active concentration multiplied by the factor of dilution. The calculated concentration in ascitic fluids seems to reduce when the ascites are strongly diluted. This could be explained by a loss of activity in strong diluted solution. The active concentrations were used for all further calculations (kinetic rate constants and inhibition curves).

4.1.2. Kinetics and thermodynamics

The kinetic rate constants of 15H11 were compared at several temperatures between 10 and 30 °C for the two derivatives E2-6-CMO and E2-7-CMO immobilised at the surface (Fig. 15 and Fig. 16).
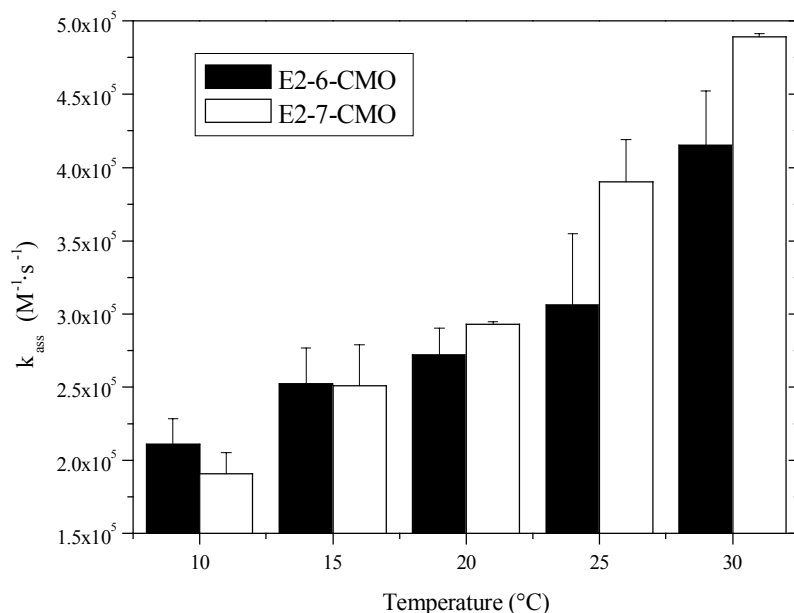
Fig. 15: Association rate constants for 15H11 with (E2-6-CMO)-BSA and for 15H11 with (E2-7-CMO)-BSA at several temperatures.
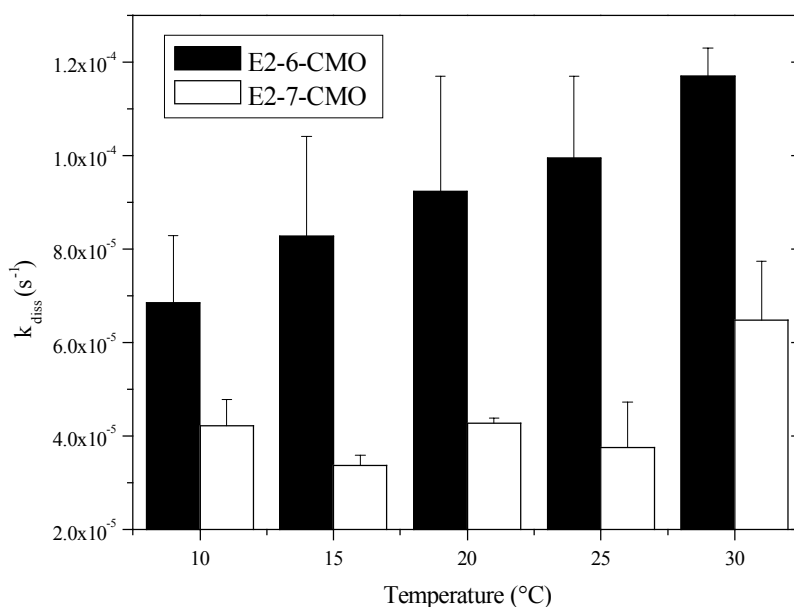
Fig. 16: Dissociation rate constants for 15H11 with (E2-6-CMO)-BSA and for 15H11 with (E2-7-CMO)-BSA at several temperatures.

The k_{ass} for (E2-6-CMO)-BSA and (E2-7-CMO)-BSA increased with the enhancement of the temperature. Only the k_{diss} for (E2-6-CMO)-BSA increased with the temperature whereas the k_{diss} for (E2-7-CMO)-BSA was insensitive to the temperature.

The k_{diss} is always smaller for E2-7-CMO than for (E2-6-CMO)-BSA. The complex with (E2-6-CMO)-BSA dissociated more quickly than the one with (E2-7-CMO)-BSA.

The kinetic rate constants allow to calculate the affinity constants between 15H11 and the two analyte derivatives immobilised at the surface. The affinity constants are shown in Fig. 17. The dissociation constants, not shown, are the inverse of the affinity constants.
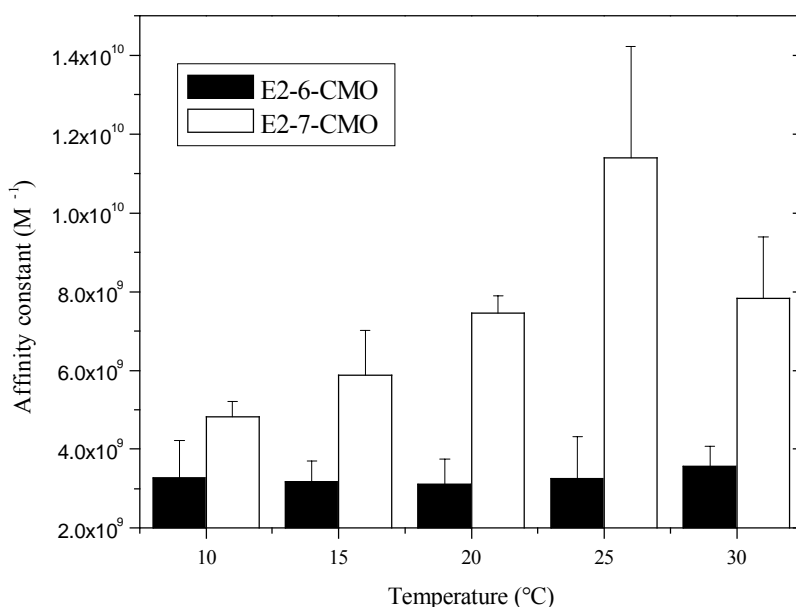
Fig. 17: Affinity constants determined by kinetic measurements for 15H11 with (E2-6-CMO)-BSA and for 15H11 with (E2-7-CMO)-BSA at several temperatures.

For the complex with the derivative (E2-6-CMO)-BSA the association and dissociation constants were unaffected by changes of temperature since both rate constants increased to the same degree with the temperature.

Because k_{ass} increases and k_{diss} stayed stable with temperature the affinity and dissociation constants of (E2-7-CMO)-BSA respectively increased and decreased with temperature up to 25 °C. It is difficult to say if this tendency was reversed above 25 °C since only one higher temperature (30 °C) was tested. At higher temperature the presence of bubbles could not be avoid and the measurements were unreliable.

In keeping with the values of k_{ass} and k_{diss}, K_A of (E2-7-CMO)-BSA was always higher than K_A of (E2-6-CMO)-BSA, while K_D was lower for (E2-7-CMO)-BSA. The 15H11/(E2-7-CMO)-BSA complex was more stable than the 15H11/(E2-6-CMO)-BSA. This confirms the results of the binding specificity of Rousselot et al. (1997), which indicates that the 15H11 has less affinity for the E2-6-CMO than for the E2-7-CMO.

The increase of the affinity constants with the increase of the temperature could indicate that the enthalpic contribution to the interaction is small (Wild et al., 2001).

The measurements of the kinetic rate constants made at several temperatures between 10 °C and 30 °C in steps of 5 °C allowed to determine some thermodynamic characteristics such as the enthalpy and the entropy changes of the reaction.

The graphical representations done to obtain the thermodynamical values for the system 15H11 and E2-6-CMO are summarised in Fig. 18, Fig. 19 and Fig. 20. The same process was used to obtain the values for 15H11 and E2-7-CMO. Finally, the results obtained from the graphical representations for 15H11 with E2-6-CMO and for 15H11 with E2-7-CMO are summarised in Table 4.
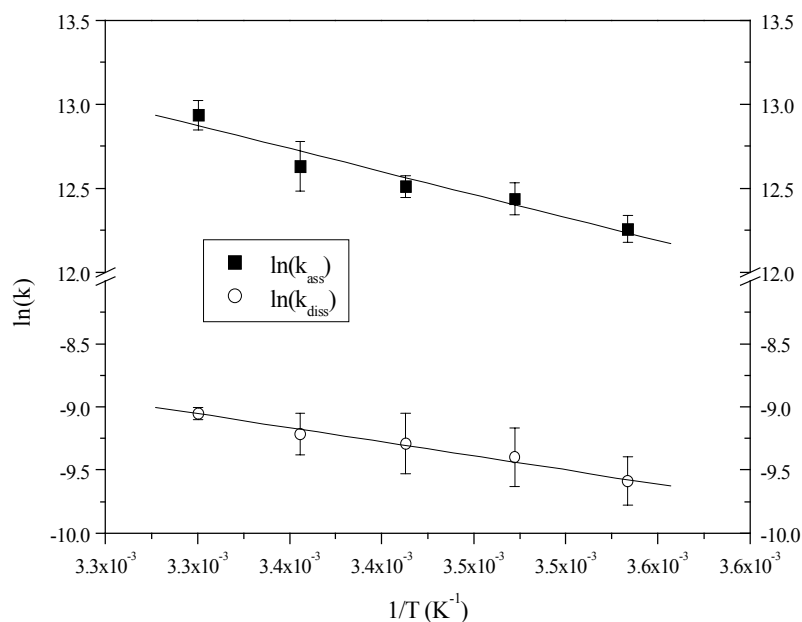
Fig. 18: ln(k_{ass}) and ln(k_{diss}) as a function of the inverse of the temperature, also called Arrhenius plot, see equations (9) and (10).

The linear regression for the logarithm of k_{ass} gave a slope of –2700 ± 400 and a correlation coefficient R = -0.97, whereas the linear regression for the logarithm of k_{diss}

presented a slope equal to –2200 ± 100 and R= -0.99. The slopes allowed to calculate the energy of activation (ΔE).
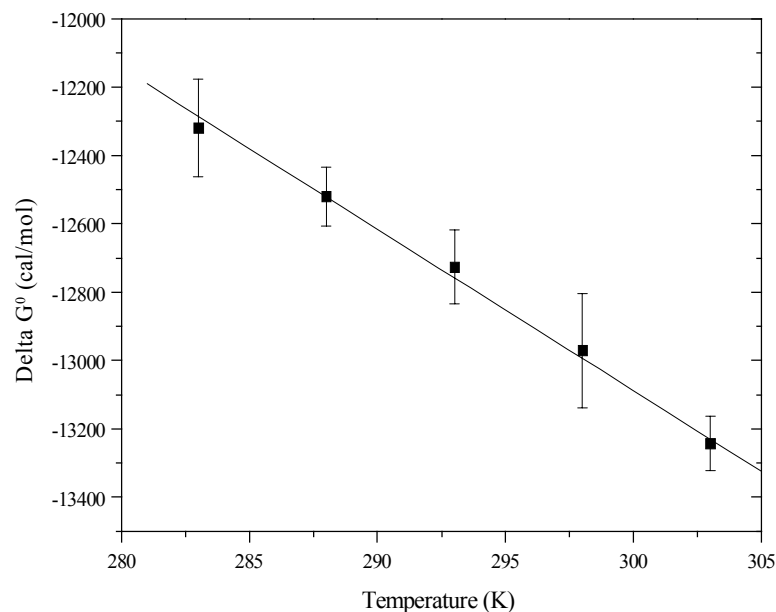
Fig. 19: ΔG^0 as a function of temperature, see equation (8).

The linear regression of the Gibbs free energy change (ΔG^0) as a function of the temperature gave a slope of –47 ± 2 and an intercept value of 1000 ± 500. The correlation coefficient R was –0.998. The slope contained the variation of the entropy of the reaction, and the intercept value gave the variation of the enthalpy.

Fig. 20: ln(k_{ass}/T) and ln(k_{diss}/T) as a function of the inverse of the temperature, see equations (12) and (13).
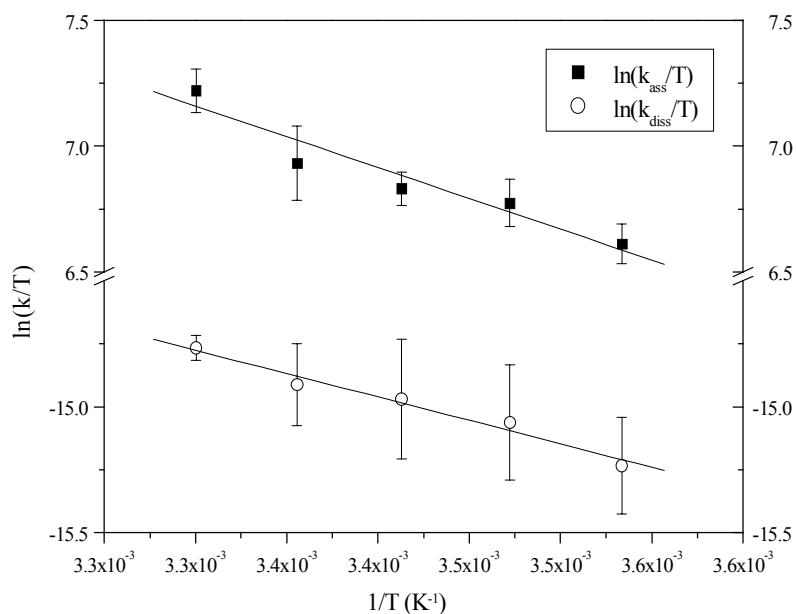
The linear regressions of $\ln(k_{ass}/T)$ and $\ln(k_{diss}/T)$ as a function of the inverse of the temperature give for k_{ass} a slope of -2400 ± 400 and an intercept value of 15 ± 1, with a correlation coefficient of -0.96, and for k_{diss} a slope equal to -1900 ± 200, an intercept value of -8.6 ± 0.6 and a R of -0.99. The variation of the entropy of the activated complex (ΔS^*) was given by the slope whereas the enthalpy of the activated complex (ΔH^*) is proportional to the intercept values. The differences between the association and dissociation values gave the variations of the entropy and the enthalpy of the reactions.

	(E2-6-CMO)-BSA	(E2-7-CMO)-BSA
ΔH^0 (cal/mol)	1020 ± 40	5500 ± 600
ΔS^0 (cal/mol.K)	47.0 ± 0.2	65.4 ± 0.9
ΔE_a (cal/mol)	5400 ± 200	7890 ± 90
ΔE_d (cal/mol)	4430 ± 60	3200 ± 600
ΔH^*_a (cal/mol)	4700 ± 200	8380 ± 40
ΔH^*_d (cal/mol)	3700 ± 90	2700 ± 600
ΔS^*_a (cal/mol·K)	-17.6 ± 0.8	-4.9 ± 0.1
ΔS^*_d (cal/mol·K)	-64.4 ± 0.3	-69.4 ± 2.1

Table 4: Thermodynamical characteristics for the systems 15H11 with E2-6-CMO and 15H11 with E2-7-CMO: ΔH^0 is the variation of enthalpy of the reaction, ΔS^0 is the variation of the entropy of the reaction, ΔE is the energies of activation, and the * symbolises the activated complex.

The ΔH^0 and ΔS^0 values are the average of the several possibilities of calculation with the graphical representations. The binding of the *IgG* to the analyte derivative is entropy-driven for both analyte derivatives since $-T\cdot\Delta S^0$ is considerably higher than ΔH^0: 13800 cal/mol > 1020 cal/mol at 293K for E2-6-CMO, and 19200 cal/mol >5500 cal/mol at 293 K for E2-7-CMO. This confirms that the complex formation is mainly entropy-driven.

The activation energy of association (ΔE_a) and dissociation (ΔE_d) represents the thermal energy required to overcome a hypothetical energy barrier that impedes association and dissociation of a molecular complex. Since this activation energy of association includes the effect of temperature on water viscosity (3.8-4.7 kcal/mol) the energy barrier corresponding to the association of the antibody to the analyte derivatives is low: a maximum of 1.6 kcal/mol for E2-6-CMO and 4.1 kcal/mol for E2-7-CMO (Wild et al., 2001). The association is not limited by the diffusion, a slight rearrangement of the paratope of the antibody may take place.

4.1.3. Inhibition curves

The different inhibition curves recorded for the IgG 15H11 are shown in Fig. 21. The concentration of IgG, [L], is 2.5 nM. The fitting of the curve with the logistic function gave the TMP.
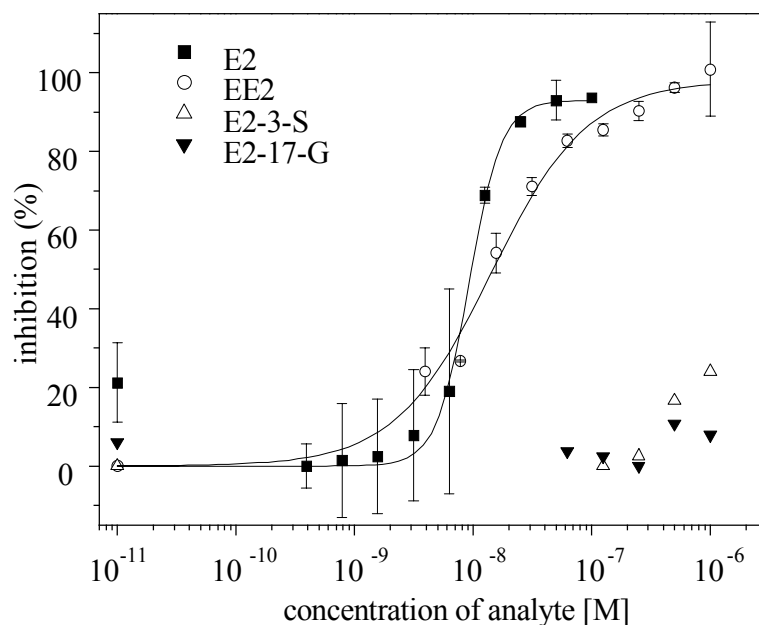
Fig. 21: Inhibitions curves of 15H11 with estradiol (E2), ethinylestradiol (EE2), estradiol-3-sulfate (E2-3-S) and estradiol-17-glucuronide (E2-17-G). The active concentration of 15h11 was 2.6 nM.

The TMP, $1.4 \cdot 10^{-8} \pm 0.1 \cdot 10^{-8}$ M for EE2 and $9.2 \cdot 10^{-9} \pm 0.9 \cdot 10^{-9}$ M for E2, gave affinity constants of $2.0 \cdot 10^{8} \pm 0.2 \cdot 10^{8}$ M^{-1} for EE2 and $3.3 \cdot 10^{8} \pm 0.3 \cdot 10^{8}$ M-1 for E2. These results indicate that ethinylestradiol is recognised by 15H11 with lower affinity than estradiol. The sulfate derivative in position 3 and glucuronide derivative in position 17 are not recognised by the antibody.

Rousselot et al. (1997) found an affinity constant of $2.4 \cdot 10^{10}$ M^{-1} for the complex 15H11/E2 from a Scatchard plot. Differences could be due to the indirect method used by these authors. But the fact that the 15H11 shows a higher specificity for the phenolic A ring than for the D ring is confirmed since 15H11 binds to EE2, which is the estradiol slightly modified in position 17. But it did not bind to other modified estradiol.

4.1.4. Conclusion

➢ The determination of the active concentration showed that the active concentration varied according to the dilution.

➢ The monoclonal IgG 15H11 was found to be reactive to the analyte derivatives E2-6-CMO and E2-7-CMO. The affinity to E2-6-CMO is independent of the temperature and always lower than the affinity to E2-7-CMO. The affinity constant of 15H11 for E2-7-CMO increased with increasing temperature between 10 and 30 °C.

➢ Both interactions where entropy-driven.

➢ The antibody showed high affinity for the analytes estradiol and ethinylestradiol and seemed to be more sensitive to modifications in the ring A than in the ring D. This should imply that the ring A plays an important role in the binding with the antibody 15H11.

4.2.   DETERMINATION OF LABELLING DEGREE

4.2.1. Determination of decadic molar absorption coefficient

The decadic molar absorption coefficient required to determine the labelling degree was successfully measured for several analyte derivatives: E1-3-CME, E1-17-CMO, E2-17-Hg and E2-3-MA as well as for the fluorophore Alexa680. One example of the linear regression is shown for the analyte derivative E1-3-CME in Fig. 22. The values of the wavelength of absorbance and the decadic molar absorption coefficient are given in Table 5.

This process did not work for two analyte derivatives which are not enough soluble: E2-3-BA and E2-3-IBA. The labelling degree for these two analyte derivatives has been determined only with RIfS.
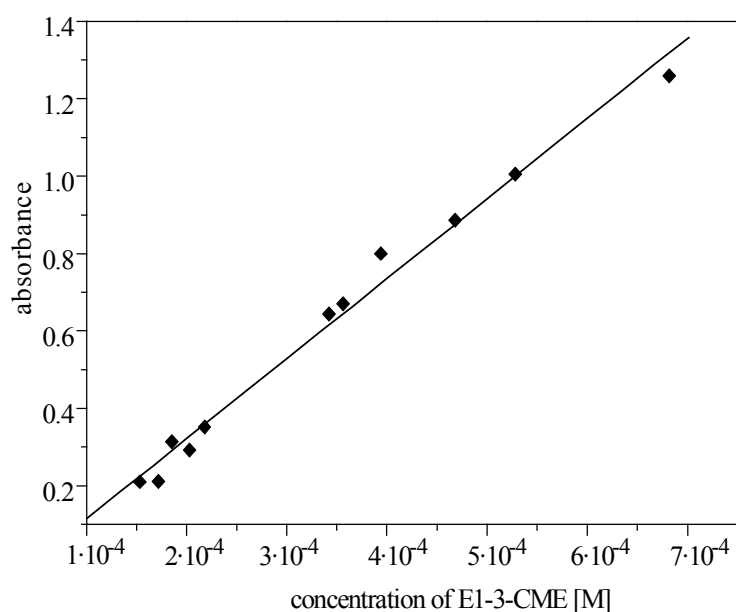
Fig. 22: Linear regression for the determination of the decadic molar absorption coefficient of E1-3-CME at 278nm in PBS.

The linear regression gave a slope of 2070 ± 80 $M^{-1} \cdot cm$ which defined the decadic molar absorption coefficient of E1-3-CME. The correlation coefficient R was equal to 0.99.

	λ_{max} (nm)	$\varepsilon_{\lambda max}$ (mol/l·cm)	R
E1-3-CME	278	2070 ± 80	0.99
E1-17-CMO	278	1630 ± 40	0.99
E2-17-Hg	281	1940 ± 40	0.99
E2-3-MA	278	1100 ± 20	0.99
Alexa680	679	143000 ± 3000	0.99
Alexa680	278	4000 ± 300	0.99

Table 5: The wavelength of absorbance and the decadic molar absorption coefficient of some analyte derivatives and of the fluorophore Alexa680 determined by the linear regression of the absorbance of the substance as a function of its molar concentration. R is the correlation coefficient of the linear regression.

The linear regressions were good since the correlation coefficients were almost equal to 1. The errors on the decadic molar absorption coefficient were therefore quite small, between 1.9 and 6.5 %.

4.2.2. Determination of labelling degree

The labelling degrees of antibodies and analyte derivatives are summarised in Table 6. Degree of labelling of proteins (IgG, vitellogenin and BSA) were characterised only with UV-Vis spectroscopy, whereas the degree of labelling of the analyte derivatives were measured with UV-Vis and/or RIfS.

Protein-fluorophore	Labelling degree with UV-Vis	Labelling degree with RIfS
αE1-Cy5	1:1,7	n.d.
αE1-Cy5	1:7,7	n.d.
αE2-Cy5	1:2	n.d.
αES-Cy5	1:1	n.d.
αES-Cy5	1:2	n.d.
(E1-3-CME)-BSA-Cy5.5	15.8:1:2.9	3.8:1:2.9
(E1-3-CME)-BSA-Cy5.5	18:1:2.9	1.9:1:2.9
(E1-3-CME)-BSA-Cy5.5	11:1:2.9	0.8:1:2.9
(E1-3-CME)-BSA-Cy5.5	1.7:1:1	0.7:1:1
(E1-3-CME)-BSA-Cy5.5	0.7:1:1.3	1:1:1.3
(E2-3-BA)-BSA-Cy5.5	n.d.	5:1:1.3
(E1-17-CMO)-BSA-Cy5.5	6:1:1	1.8:1:1
(E1-17-CMO)-BSA-Cy5.5	9.5:1:1.7	6.9:1:1.7
(E2-17-Hg)-BSA-Cy5.5	1:1:1.3	n.d.
(E2-3-IBA)-BSA-Cy5.5	n.d.	n.d.
(E2-3-MA)-BSA-Cy5.5	0.6:1:1.3	n.d.

Table 6: Labelling degrees of the antibodies, proteins and analyte derivatives, determined with UV-Vis spectroscopy and/or RIfS.

The labelling degree of analyte derivatives is always higher with UV-Vis than with RIfS , particularly for the high labelling degree (>ten) determined with UV. The decadic molar absorption coefficients of the analyte derivatives are too small to quantify properly the number of analyte derivatives per molecule of BSA. The labelling degree of E2-3-IBA was determined neither by UV-Vis spectroscopy nor by RIfS, because it was insoluble and it did not bind to the IgG. Since it did not bind to the IgG it was not employed for the FRET assay.

4.2.3. Conclusion

➢ Decadic molar absorption coefficient was determined for several analyte derivatives and for the fluorophore Alexa680. The values of the analyte derivatives are small, particularly in comparison to the decadic molar absorption coefficient of the fluorophores.

➢ The degree of labelling was determined either with UV-Vis spectroscopy or with RIfS for all required labelled analyte derivatives.

4.3.   CHARACTERISATION OF POLYCLONAL ANTIBODIES

The labelling degree for antibodies used in all SPR measurements was 1.7 dye per molecule of αE1, and 2 dyes per αE2 and αES.

4.3.1. Active concentration of the antibodies by SPR

Using the method explained in 2.2.3.1 the active concentration of the antibodies was determined with SPR. The measurements were realised before and after labelling the antibodies with the Donor fluorophore. The results are given in Fig. 23. The IgG αES should bind to the two haptens used in the immunogen: E1-17-CMO and E2-17-Hg. But once E2-17-Hg immobilised on the transducer the signal was much too weak to quantify the active concentration.
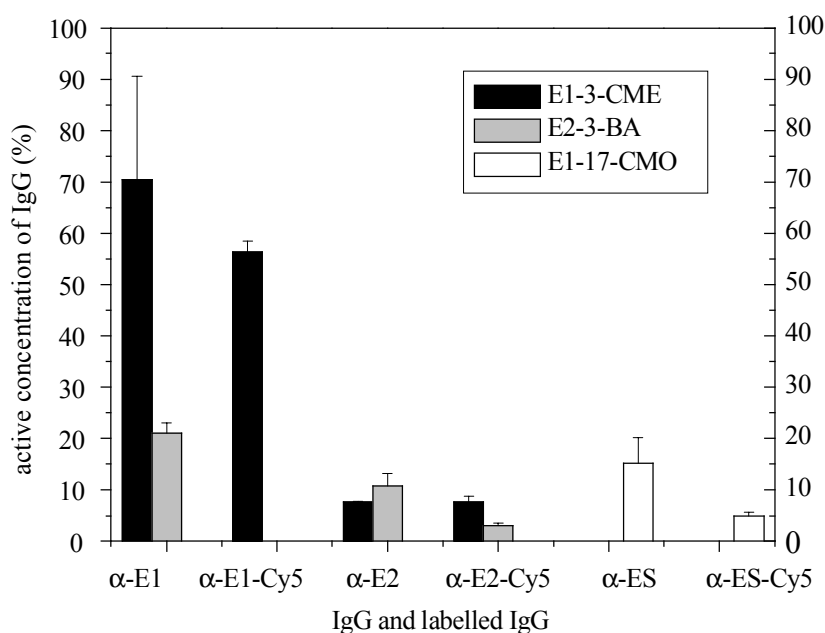
Fig. 23: Active concentration of the polyclonal antibodies to the reactive analyte derivative immobilised at the surface before and after labelling of the antibodies with the Donor fluorophore. 100 % correspond to the concentration of purified IgG in solution of PBS measured by absorbance at 278 nm.

Firstly, the antibodies are not 100 % active. α-E1 is highly active, 70 %, whereas α-E2 and α-ES have a much reduced active concentration, between 10 % and 20 %.

This may be explained by the difference of preparation and/or purification. α-E1 is delivered lyophilised, and stored at – 20 °C. α-E2 and α-ES are delivered in form of a precipitate in a solution of ammonium sulfate stored at 4 °C. The precipitate has to be separated from the ammonium sulfate solution, solved in PBS and rinsed with PBS on Microcon. The purification steps may be a cause of this difference in the initial percentage of active concentration.

Secondly, a reduction of the active concentration was observed after labelling, This decrease can be explained by the binding of dye in or near the binding site. The probability to disturb the binding site by labelling increases with a high degree of labelling but this diminution of the active concentration can not be foreseen (Vigorito et al., 1995). The measurement of the active concentration of the antibody has to be done after the labelling. The active concentrations are used in all subsequent calculations.

4.3.2. Kinetic rate constants with SPR

The kinetic rate constants and affinity constants at the surface were determined for each reactive IgG/analyte derivative pair. The results are summarised in Fig. 24 and Fig. 25.

Polyclonal antibodies do not have one affinity constant since they consist in a population of several antibodies with several affinities. The apparent measured affinity constant represents the average affinity constant of the population of antibodies. The population of polyclonal antibodies is heterogeneously shared around this average affinity constant. According to the conditions of the assay and particularly to the concentration of the antibody used different apparent affinity constants could be measured.
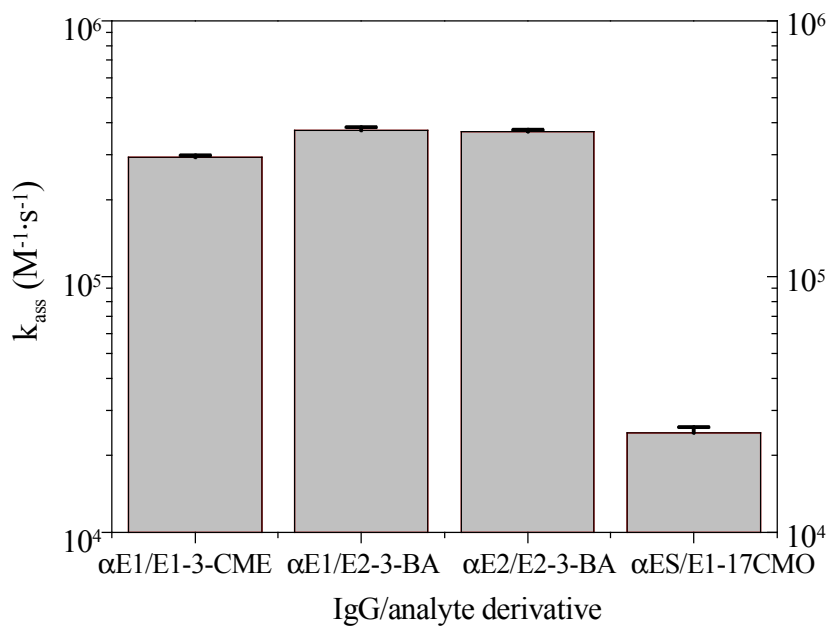
Fig. 24: Association rate constants of the IgG/analyte derivative.
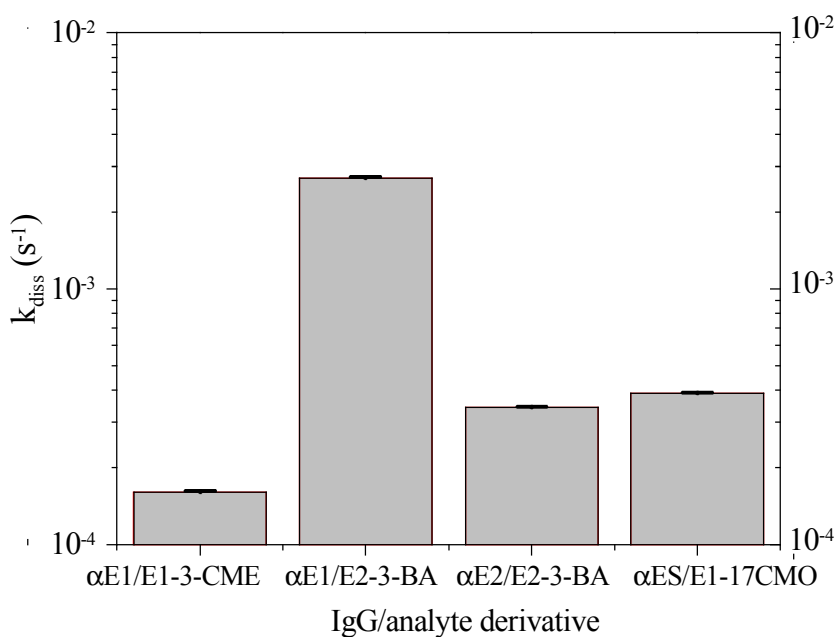
Fig. 25: Dissociation rate constants of the IgG/analyte derivatives.

The association and dissociation rate constants are used to calculate the affinity constant between the antibody and the analyte derivative immobilised at the surface.
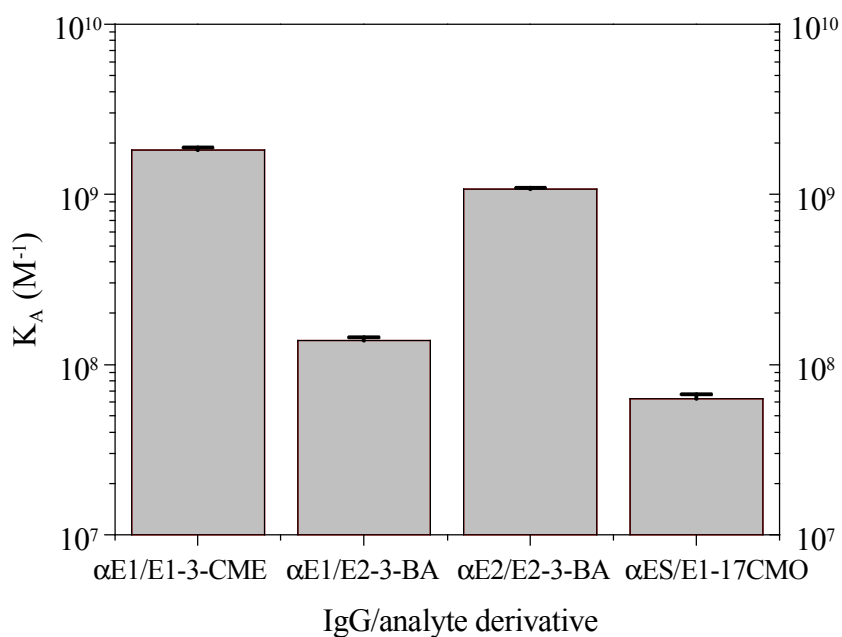
Fig. 26: Affinity constants of the IgG/analyte derivative at the surface.

The two pairs anti E1 with E1-3-CME and anti E2 with E2-3-BA associate rapidly and dissociate slowly, giving affinity constants around 10^9 M^{-1}. Anti E1 binds rapidly to E2-3-BA but dissociates also rapidly, the association constant is then lower than for the pairs anti E1/E1-3-CME and anti E2/E2-3-BA, around 10^8 M^{-1}. The affinity constant of anti ES with E1-17-CMO is also low ($7 \cdot 10^8$ M^{-1}) because antibody and analyte derivative associate and dissociate slowly. In the next paragraph (4.3.3), the affinity constants of the antibody analyte derivative pairs determined by kinetic measurements are compared to the same affinity constants determined by inhibition tests.

4.3.3. Affinity in solution with SPR

The affinity constants in solution for the three antibodies were calculated for all cross reactive analytes and analyte derivatives with the inhibition curves. The affinity of the labelled IgGs was also calculated. Examples of inhibition curves for labelled and unlabelled IgG are shown in Fig. 27. All results are summarised in *Table 7*.
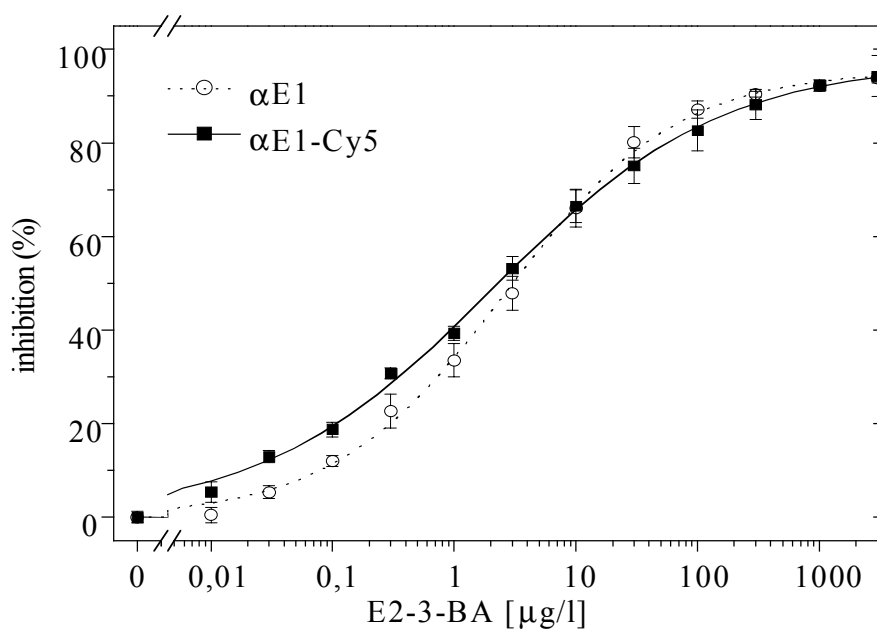
Fig. 27: Inhibition curves of anti-estrone by E2-3-BA and of anti-estrone-Cy5 by E2-3-BA. [IgG] = 7.5 nM.

IgG	analyte	IgG active[M]		TMP [M]		KA [M-1]	
αE1	E1	7.E-10 ±	2.E-10	3.E-09 ±	2.E-09	1.1E+09 ±	8.E+08
αE1	E2	7.E-10 ±	2.E-10	6.E-08 ±	2.E-08	4.E+07 ±	1.E+07
αE1	EE2	7.E-10 ±	2.E-10	*		*	
αE1	E1-3-CME	5.E-09 ±	2.E-09	7.E-09 ±	2.E-09	8.2E+08 ±	1.E+09
αE1	E2-3-BA	5.E-09 ±	2.E-09	1.1E-08 ±	1.E-09	3.E+08 ±	1.E+08
αE1-Cy5	E1	4.2E-09 ±	2.E-10	4.E-09 ±	2.E-09	2.E+09 ±	5.E+09
αE1-Cy5	E2	4.2E-09 ±	2.E-10	1.4E-07 ±	2.E-08	1.8E+07 ±	3.E+06
αE1-Cy5	E1-3-CME	4.2E-09 ±	2.E-10	4.E-09 ±	1.E-09	3.E+09 ±	5.E+09
αE1-Cy5	E2-3-BA	4.2E-09 ±	2.E-10	6.2E-09 ±	6.E-10	8.E+08 ±	2.E+08
αE2	E1	1.6E-09 ±	4.E-10	*		*	
αE2	E2	1.6E-09 ±	4.E-10	1.E-07 ±	2.E-08	2.5E+07 ±	6.E+06
αE2	EE2	1.6E-09 ±	4.E-10	*		*	
αE2	E2-3-BA	1.6E-09 ±	4.E-10	8.E-09 ±	2.E-09	3.5E+08 ±	9.E+07
αE2-Cy5	E2	9.E-10 ±	2.E-10	6.E-08 ±	2.E-08	4.E+07 ±	1.E+07
αE2-Cy5	E2-3-BA	4.5E-10 ±	9.E-11	9.E-09 ±	3.E-09	2.9E+08 ±	9.E+07
αES	E1	2.3E-09 ±	8.E-10	8.E-09 ±	2.E-09	4.E+08 ±	1.E+08
αES	E2	5.E-09 ±	2.E-09	1.1E-08 ±	1.E-09	3.2E+08 ±	9.E+07
αES	EE2	5.E-09 ±	2.E-09	1.8E-08 ±	3.E-09	1.6E+08 ±	5.E+07
αES	E1-17-CMO	2.3E-09 ±	8.E-10	8.E-09 ±	5.E-09	4.E+08 ±	3.E+08
αES	E2-17-Hg	5.E-09 ±	2.E-09	1.34E-08 ±	7.E-10	2.4E+08 ±	4.E+07
αES-Cy5	E1	7.5E-10 ±	9.E-11	5.E-09 ±	2.E-09	6.E+08 ±	2.E+08
αES-Cy5	E2	1.5E-09 ±	2.E-10	5.3E-09 ±	8.E-10	6.E+08 ±	1.E+08
αES-Cy5	EE2	7.5E-10 ±	9.E-11	7.E-09 ±	2.E-09	4.E+08 ±	1.E+08
αES-Cy5	E1-17-CMO	1.5E-09 ±	2.E-10	9.E-10 ±	5.E-10	>6E+08	
αE1	E1	1.3E-09 ±	1.E-10	6.8E-09 ±	9.E-10	4.1E+08 ±	7.E+07
αE1	E2	1.3E-09 ±	1.E-10	1.1E-07 ±	5.E-08	2.2E+07 ±	9.E+06
αE1	E1-3-CME	1.3E-09 ±	1.E-10	3.E-09 ±	1.E-09	1.0E+09 ±	7.E+08
αE1-Cy5	E2-3-BA	1.3E-09 ±	1.E-10	2.6E-09 ±	2.E-10	1.4E+09 ±	3.E+08
αE1-Cy5	E1-3-CME	1.3E-09 ±	1.E-10	2.2E-09 ±	9.E-10	2.E+09 ±	1.E+09
αE1	E2-3-BA	1.3E-09 ±	1.E-10	6.E-09 ±	1.E-09	4.6E+08 ±	9.E+07

*Table 7: Affinity constants between IgG and analyte or analyte derivative in solution, calculated with the TMP of the inhibition curves (equation 28). The white background indicates the measurements where the analyte derivative immobilised was homologous to the IgG: E1-3-CME for αE1, E2-3-BA for αE2 and E1-17-CMO for αES. The grey background indicates the measurements with the αE1 and E2-3-BA immobilised at the surface. The asterisk * indicates that 50 % of inhibition was not reached and the affinity could not be calculated.*

The affinity between αES-Cy5 and E1-17-CMO could not be calculated, but the affinity must be higher than the affinity between αES-Cy5 and E2 ($6 \ 10^8 \, M^{-1}$).

In both cases the active concentration of IgG was the same, therefore the TMP can be directly compared. The TMP with E1-17-CMO was smaller than the TMP for E2, indicating a higher affinity.

First it was tested if the affinity constants, measured by inhibition curves with different analyte derivatives at the surface are comparable. The affinity constants for anti E1 to its several analytes or analyte derivatives seemed almost identical when the surface is modified with E1-3-CME or E2-3-BA. The ratio of the affinity determined with E2-3-BA and E1-3-CME at the surface varied between 0.38 and 1.91. Since the measured pairs were exactly similar, only the analyte derivative immobilised at the surface changed, the Wilcoxon paired signed rank test was applied to the six pairs. The calculated T values were 10 and 11. The smaller value, 10, being larger than the critical value U(6, 10%) equal to 2, the null hypothesis, that the two groups are similar was accepted. This result confirmed, that there is no systematic difference between the groups.

Then, a critical point was to ensure that the labelling did not influence the K_A. No systematic difference was observed. The affinity constant for anti ES-Cy5 to E1-17-CMO could not be determined, and these pairs (ES/E1-17-CMO and ES-Cy5/E1-17-CMO) were therefore not used in the test. To confirm that the labelling of the IgG had no influence on the affinity of the antibody for the analyte, the Mann-Whitney test was applied. The sums of the ranks obtained were 108 for the affinity constants concerning the native IgG, and 145 for the affinity constants of the labelled IgG. The corresponding U values were 79 and 42. The smaller value was larger than the critical U(11, 11, 10%) equal to 34. This confirmed that the two groups were similar and therefore the labelling did not influence the affinity constant.

An important consequence is that the affinity constants of one antibody for its analyte derivatives and for the analyte can be compared before the labelling to predict the performances of the FRET calibration curves.

The αES bound to the analyte derivative E2-17-Hg in solution with high affinity but, as explained in chapter 4.1.1, the IgG did not bind to the derivative immobilised on the transducer.

The affinity of the antibodies for the derivatives was determined by kinetics as well as by inhibitions curves. The results are summarised in Table 8 and were compared by the Mann-Whitney test.

IgG / derivative	K_A by kinetics	K_A in solution
αE1 / E1-3-CME	$1,82 \cdot 10^9 \pm 5 \cdot 10^7$	$8 \cdot 10^8 \pm 9 \cdot 10^8$
αE1 / E2-3-BA	$1,38 \cdot 10^8 \pm 6 \cdot 10^6$	$3 \cdot 10^8 \pm 1 \cdot 10^8$
αE2 / E2-3-BA	$1,07 \cdot 10^9 \pm 2 \cdot 10^7$	$3.5 \cdot 10^8 \pm 9 \cdot 10^7$
αES / E1-17-CMO	$6,3 \cdot 10^7 \pm 4 \cdot 10^6$	$3 \cdot 10^8 \pm 3 \cdot 10^8$

Table 8: Comparison of the affinity constants determined by kinetic measurements and by inhibition curves.

The calculated U values were both equal to 8 what was much higher than the critical value of U(4, 4, 10%) equal to 1. This indicated that the affinity constants determined by kinetics, were comparable with the constants determined by inhibition tests.

4.3.4. Affinity constants in solution with RIfS

The affinity constants could be determined in the same way with the RIfS device. Inhibition curves were measured and the affinity constants were calculated with the test mid-point of the curves. For the required active concentration the values obtained previously with the SPR device were used (see 4.3.1). The results are summarised in Table 9.

IgG	analyte	IgG active [M]		TMP [M]		KA [M^{-1}]	
αE1	E1	1.2E-09 ±	3.E-10	2.7E-09 ±	2.E-10	1.284E+09 ±	3.E+06
αE1	E2	1.2E-09 ±	3.E-10	3.7E-09 ±	4.E-10	8.4E+08 ±	5.E+07
αE1	EE2			*		*	
αE1	E1-3-CME	1.2E-09 ±	3.E-10	2.E-09 ±	1.E-09	2.E+09 ±	2.E+09
αE1	E2-3-BA	1.2E-09 ±	3.E-10	2.5E-09 ±	3.E-10	1.46E+09 ±	8.E+07
αE2	E1	3.6E-10 ±	8.E-11	9.E-09 ±	3.E-09	2.7E+08 ±	8.E+07
αE2	E2	3.6E-10 ±	8.E-11	1.7E-08 ±	2.E-09	1.4E+08 ±	2.E+07
αE2	EE2	3.6E-10 ±	8.E-11	9.E-07 ±	3.E-07	2.6E+06 ±	7.E+05
αE2	E2-3-BA	3.6E-10 ±	8.E-11	6.4E-08 ±	5.E-09	3.8E+07 ±	3.E+06
αES	E1	5.E-10 ±	2.E-10	1.90E-09 ±	6.E-11	1.57E+09 ±	5.E+07
αES	E2	5.E-10 ±	2.E-10	4.2E-09 ±	5.E-10	6.3E+08 ±	6.E+07
αES	EE2	5.E-10 ±	2.E-10	4.2E-09 ±	3.E-10	6.3E+08 ±	3.E+07
αES	E1-17-CMO	5.E-10 ±	2.E-10	2.3E-09 ±	3.E-10	1.2E+09 ±	1.E+08
αE1	E1	2.5E-10 ±	8.E-11	1.8E-09 ±	1.E-10	1.45E+09 ±	4.E+07
αE1	E2	2.5E-10 ±	8.E-11	6.2E-09 ±	5.E-10	4.0E+08 ±	3.E+07
αE1	EE2	2.5E-10 ±	8.E-11	4.3E-08 ±	4.E-09	5.7E+07 ±	5.E+06
αE1	E2-3-BA	2.5E-10 ±	8.E-11	2.9E-09 ±	2.E-10	8.9E+08 ±	3.E+07
αE1	E1-3-CME	2.5E-10 ±	8.E-11	1.0E-09 ±	2.E-10	2.9E+09 ±	6.E+08

Table 9: Affinity constants determined with the test mid-point of the inhibition curves measured with RIfS . The asterisk * indicates that the TMP was not reached, and the K_A could not be calculated.

It was not possible, as for the results with SPR, to compare the affinity constants determined with two different derivatives (E1-3-CME and E2-3-BA) immobilised at the surface. A minimum of five pairs are required to apply a Wilcoxon paired signed rank test.

In order to compare the values of the affinity constants determined with RIfS and with the BIACORE the Wilcoxon paired signed rank test was applied to the two series. The calculated T values are 3 and 52 for the sum of the ranks of negative differences and the sum of the ranks of the positive differences respectively. The smaller value was equal to the critical value U(10, 1%)=3. The difference between the groups was significant.

A comparison with SPR results showed also that the extremely low affinity ($2,6 \cdot 10^6$ M^{-1}) of αE2 for EE2 could be detected with RIfS, but not with SPR.

4.3.5. Conclusion

➢ The labelling of the antibody and the separation of the antibody from the ammonium sulfate solution can strongly influence the active concentration.

➢ For the SPR method as well as for the RIfS method the affinity constants measured for αE1 to its homologous and its several heterologous reactants by inhibition curves were the same with the two possible analyte derivatives immobilised at the surface: E1-3-CME and E2-3-BA.

➢ The affinity constants determined for the labelled and unlabelled antibodies were comparable. The labelling did not influence the affinity constants. K_A value of one antibody for one analyte can be compared to K_A value of the same antibody for one analyte derivative before the labelling.

➢ The affinity constants determined by kinetics were not significantly different from the affinity constants determined by inhibition curves.

➢ The results obtained with RIfS were significantly different from the results obtained with SPR. This difference could be explained by the different conditions of measurement with both devices.

4.4.   FRET Simulations and optimisation of the assay

In order to determine the influence of the critical parameters on the FRET assay, simulations were realised. The definition of the two affinity constants with the concentrations at the equilibrium and the law of action mass equations (57) – (59) allow to simulate under special conditions the calibration curves for diverse affinity constants.

With K defining the affinity constant and [IgG] representing the concentration for labelled antibody, [Ag] the antigen, [Der] the labelled analyte derivative, [IgG-Ag] and [IgG-Der] the analyte-labelled antibody-complex and labelled analyte derivative-labelled antibody-complex respectively, the law of action mass equations are:

$$[IgG]_0 = [IgG] + [IgG-Der] + [IgG-Ag] \qquad (57)$$

$$[Der]_0 = [Der] + [IgG-Der] \qquad (58)$$

$$[Ag]_0 = [Ag] + [IgG-Ag] \qquad (59)$$

where brackets with the indication "$_0$" indicate the total concentration, and brackets are used for the concentrations at equilibrium.

The assumptions used to simplify the simulations (Schobel, 1999) are the following:

1) The antibody is considered as monoclonal and any bivalence is taken into account.

2) The binding of the labelled analyte derivative with the labelled antibody results in total quenching of the Donor, there is no residual fluorescence of the Donor.

3) The Acceptor does not emit fluorescence.

4) The binding of the free analyte to the labelled antibody does not change the spectroscopic characteristics of the Donor.

Under these assumptions the fluorescence is caused by the free antibody and the antigen-antibody complex. The signal is proportional to the sum of these concentrations. For the graphical representations, the signal was normalised to 100 %.

In this chapter, the limit of detection is defined as the lowest concentration of the working range, corresponding to a signal of 10 %.

4.4.1. Variation of the affinity constants

Fig. 28 shows simulated calibrations where both affinity constants are equal and range between 10^7 and 10^{10} M^{-1}. It demonstrates the influence of the affinity constants on the normalised fluorescence. The test mid-point and the working range are given in Table 10. The concentration of IgG was $3.3 \cdot 10^{-9}$M, and the concentration of analyte derivative ($2.8 \cdot 10^{-6}$ M – $2.8 \cdot 10^{-9}$ M) was chosen in order to give the quenching maximum.
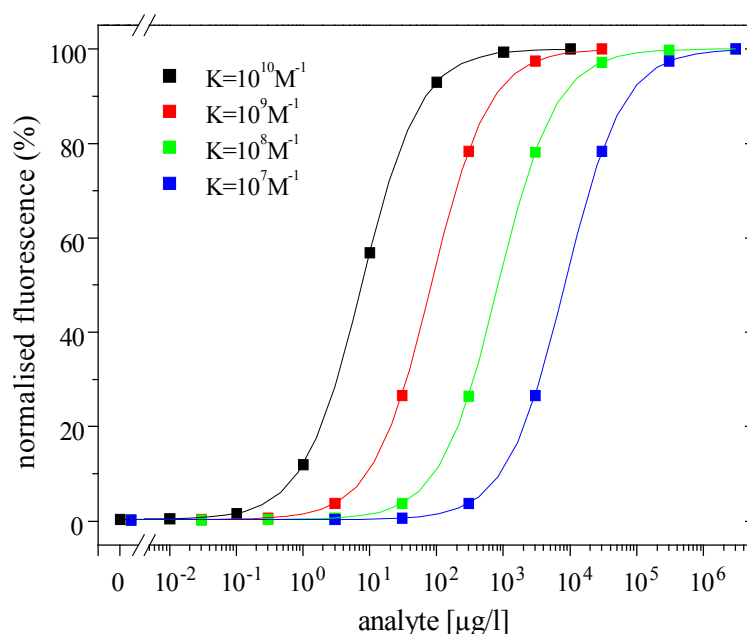
Fig. 28: Simulated calibrations curves with FRET, with affinity constants of the antibody to the analyte and to the analyte derivative equal and varying between 10^7 and 10^{10} M^{-1}.

K(IgG-Ag)=K(IgG-Der), [M^{-1}]	Working Range, [$\mu g/l$]	TMP, [$\mu g/l$]
10^7	907-73901	8360 ± 50
10^8	90-7540	842.3 ± 0.6
10^9	9-739	83.6 ± 0.5
10^{10}	0.8-67.7	7.60 ± 0.02

Table 10: Characteristics of the calibration curves simulated in Fig. 28.

Fig. 29 shows simulated calibrations where the ratio of the affinity constants varies between 0.01 and 100. The affinity constant between the antibody and the analyte derivative, K(IgG-Der), was fixed to 10^9 M^{-1} and the affinity constant between the antibody and the analyte, K(IgG-Ag), varied between 10^7 and 10^{11} M^{-1}. The concentration of IgG was $3.3 \cdot 10^{-9}$ M, and the concentration of analyte derivative ($3 \cdot 10^{-8}$ M) was chosen in order to give the quenching maximum. The simulation demonstrates the influence of the ratio of the constants on the normalised fluorescence. The test mid-point and the working range are given in Table 11.
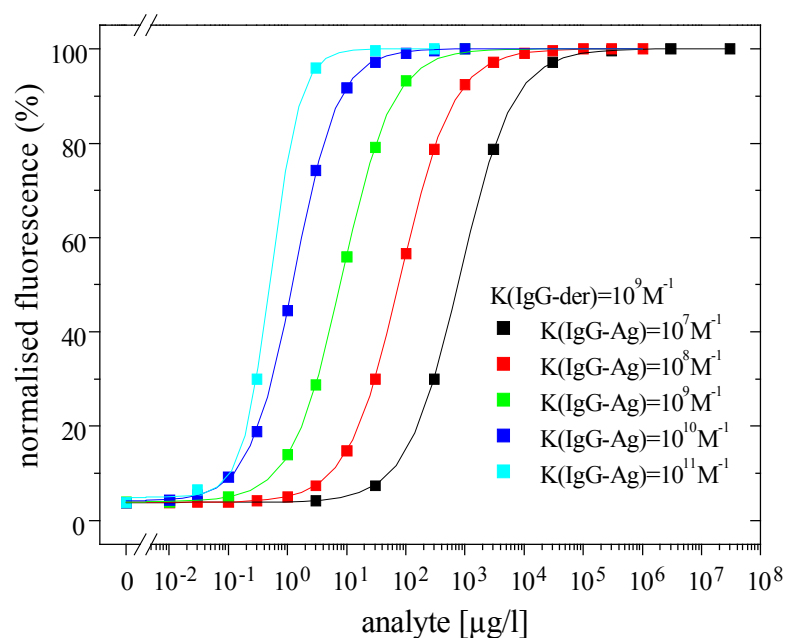

Fig. 29: Simulated calibrations curves with FRET, with different affinity constants of the antibody to the analyte and varying between 10^7 and 10^{11} M^{-1}. The affinity constant of the antibody to the analyte derivative was fixed to 10^9 M^{-1}.

K(IgG-Ag)/K(IgG-Der)	Working Range, [µg/l]	TMP, [µg/l]
0.01	87-7842	824 ± 2
0.01	9-774	82.0 ± 0.1
1	0.98-72.64	8.4 ± 0.1
10	0.20-8.55	1.29 ± 0.01
100	0.16-1.82	0.53 ± 0.02

Table 11: Characteristics of the calibrations curves simulated in Fig. 29.

The simulations show the influence of the ratio between the affinity constants as well as the influence of the values of the affinity constants. When both affinities were equal, the highest affinity (10^{10} M^{-1}) gave the lowest test mid-point (7.6 µg/l). The range of concentrations that can be measured, was smaller (0.8-68 µg/l), but the low LOD (0.85 µg/l) allowed to quantify small concentrations of analyte. High affinity systems are therefore preferable.

In the case of different affinity constants, the LOD was lower (0.16 µg/l and 0.20 µg/l) when the affinity of the antibody was higher for the analyte than for the analyte derivative. Affinity of the antibody higher for the analyte derivative than for the analyte produced high LOD (9 µg/l and 87 µg/l) and the range of concentrations was shifted to high concentrations. In order to obtain a low LOD the affinity of the IgG for the analyte has to be higher than the affinity for the analyte derivative.

4.4.2. Variation of the concentration of analyte derivative

Fig. 30 shows simulated calibrations where the concentration of analyte derivative varied for a fixed concentration of IgG. The test mid-point, signalling range (SR) and the working range are given in Table 12. The concentration of IgG was $3.3 \cdot 10^{-9}$ M and the affinity constants were equal to 10^9 M^{-1}.
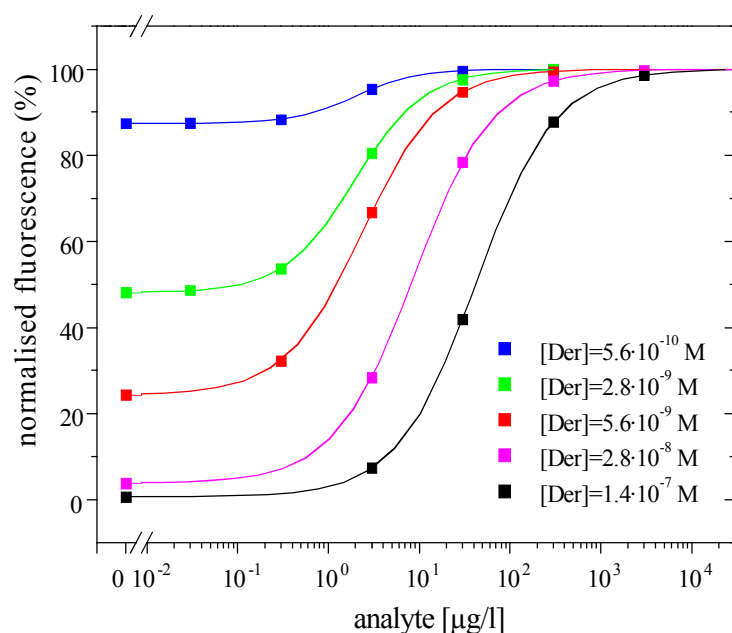
Fig. 30: Simulated calibrations curves with FRET, with variable concentrations of analyte derivative and fixed concentration of IgG equal to $3.3 \cdot 10^{-9}$ M. The two affinity constants are equal to 10^9 M^{-1}.

Concentration of derivative, [M]	TMP, [µg/l]	Working Range, [µg/l]	Signalling Range, (%)
$1.4 \cdot 10^{-7}$	42.3	4.7 – 381.9	99
$2.8 \cdot 10^{-8}$	8.75	0.6 – 75.3	96
$5.6 \cdot 10^{-9}$	2.37	0.3 – 19.9	76
$2.8 \cdot 10^{-9}$	1.94	0.3 – 13.4	52
$5.6 \cdot 10^{-10}$	1.99	0.4 – 10.5	13

Table 12: Characteristics of the simulations with variable concentrations of analyte derivative, shown in Fig. 30.

The results show clearly that the higher the concentration of analyte derivative, the higher the signalling range (99 %) but also the higher the LOD (4.7 µg/l). A reduction of the concentration of analyte derivative by a factor of 5 or 25 consequently decreased the LOD to 0.6 or 0.3 µg/l without reducing the SR too much (96 or 76 %). Further reduction of the concentration did not improve the LOD, but decreased the SR.

4.4.3. Conclusion

➢ The affinity constants considerably influence the performance of the assay, and the higher the affinities the smaller the TMP and the LOD.

➢ Best results are obtained if the affinity of the antibody is lower for the analyte derivative than for the analyte since this reduces the TMP.

➢ The chosen concentration of analyte derivative is also consequent since a lower concentration can considerably reduce the LOD but at the same time decreases the signalling range of the calibration curve.

➢ A compromise has to be found where the LOD is in a region of low concentration and the signalling range is not too small: it means a system with high affinities, where the affinity of the IgG is higher for the analyte than for the analyte derivative and with a concentration of analyte derivative as small as possible.

4.5. FLUORESCENCE IMMUNOASSAY WITH THE POLYCLONAL IGG

4.5.1. Wastewater measurements

The calibrations were recorded in a PBS buffer. A background of 1 mg/ml of OVA was required to reduce the non-specific adsorption of the protein. The calibrations curves of estrone, estradiol and ethinylestradiol are shown in Fig. 31.
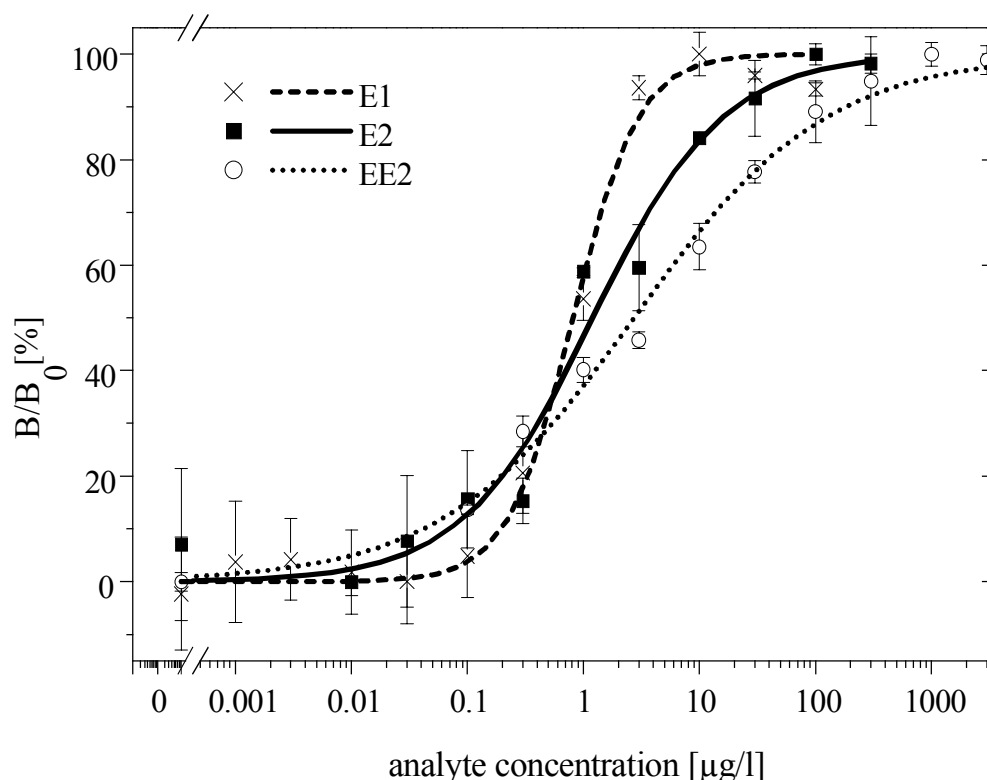
Fig. 31: Calibrations of E1 with αE1 and E1-3-CME, of E2 with αE1 and E1-3-CME and of EE2 with αES and E1-17-CMO. [IgG]=0.25 µg/ml and [Der]= 10 µg/l in each calibration curve.

The only preparation step for the samples was the degassing. The same background protein concentration is used as for the calibration curves. A correction for waste matrix water was required. We corrected the matrix effect by measuring the fluorescence of the Donor in the matrix (PBS or wastewater) with free analyte but in absence of the Acceptor. The fluorescence of the Donor is constant in each matrix but differs from one matrix to the other. The signal in wastewater is referenced to the

fluorescence of the Donor in absence of an Acceptor in wastewater: the intensity of fluorescence of the spiked samples was divided by the fluorescence of the Donor in the wastewater and multiplied by the fluorescence of the Donor in the buffer solution before to be reported on the calibration curve to give the concentration of analyte. This type of reference is allowed because it can be done with any sample, it does not require a sample of the matrix not contaminated by the analyte.

The measured intensity values are reported in the equation of the logistic function to determine the measured concentrations. The results are summarised in

Table 13.

analyte	true concentration [μg/l]	signal [%]	measured concentration [μg/l]	recovery rate [%]
estrone	0.5	31 ± 3	0.48 ± 0.04	96
	1	61 ± 3	1.09 ± 0.07	109
	2	80 ± 2	2.0 ± 0.1	100
estradiol	0.5	23 ± 3	0.26 ± 0.09	52
	1	40 ± 4	0.7 ± 0.2	70
	3	61 ± 3	2.2 ± 0.6	73
ethinylestradiol	0.5	27 ± 1	0.38 ± 0.06	76
	2	43 ± 4	1.5 ± 0.6	75
	5	57 ± 9	5 ± 3	100

Table 13: Summarised results of the measurements of spiked wastewaters.

The measurements were done directly in wastewater and without pre-concentration. The recovery rates of the three concentrations measured for E1 and EE2 were found to be between 74 – 110 %. Only the lowest concentration of E2 showed a small recovery rate of about 50 %, which could not be explained. For accuracy the recovery rates have to be in the range of 70 – 120 % according to the Association of Official Analytical Chemistry (AOAC) (Parker, 1991). The method is suitable to measure the concentration of one estrogen in synthetic wastewater.

4.5.2. Optimisation of the assay according to the simulations and affinity constants

The antibody αE1 was labelled with approximately 7 dyes and αE2 and αES were labelled with 2 dyes. All titrations were performed in a cuvette. Two examples for αES are given in Fig. 32.

(A)

(B)
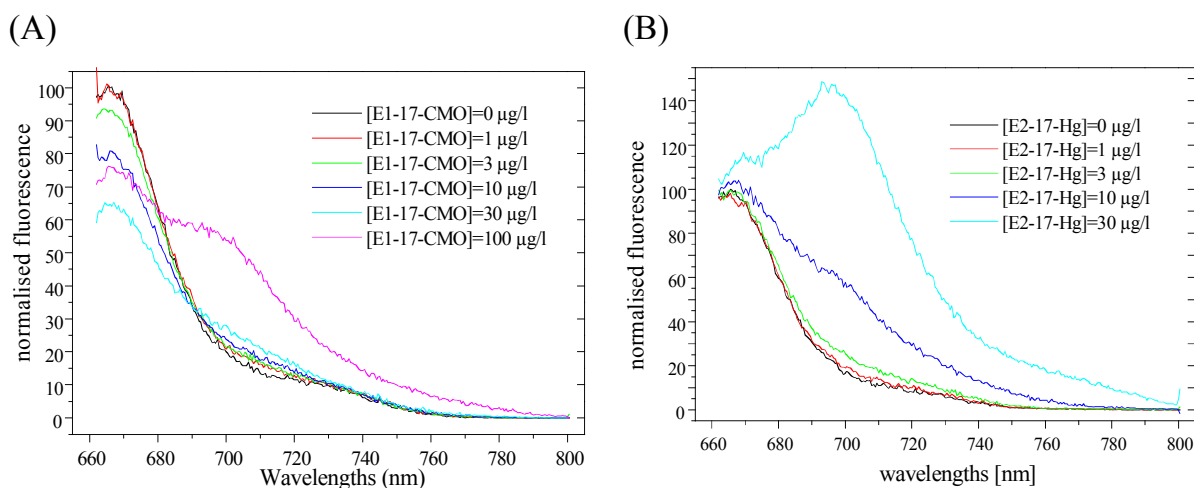
Fig. 32: Titrations of αES [1 µg/ml], (A) with E1-17-CMO, (B) with E2-17-Hg.

An assay of titration of αES with E1-17-CMO was unsuccessfully attempted. No quenching was observed, this confirmed the results obtained with SPR: once the derivative was immobilised or generally speaking modified in position 17, by binding to the BSA, the derivative did not bind anymore to the IgG.

Titrations of αE2 with E2-3-IBA and E2-3-MA were also measured, but no quenching was observed.

There were three combinations possible to quantify E1. E1 binds to αE1 and αES. αE1 has affinity with E1-3-CME but it cross-reacts also with E2-3-BA, and αES binds only with the analyte derivative E1-17-CMO. This allows to quantify E1 by three different approaches: αE1 / E1-3-CME / E1, αE1 / E2-3-BA / E1 and αES / E1-17-CMO / E1. For E2 there is an additional possibility αE2 / E2-3-BA / E2, which makes 4 possibilities for E2. EE2 reacts only with αE. There is just one possibility to quantify EE2: αES / E1-17-CMO / EE2. The results are shown for estrone in Fig. 33 and Table 14, and for estradiol, in Fig. 34 and Table 9.

The FRET results are compared with the ratio of the affinity constants to see if the influence of the affinity constants observed in the simulations can be found.

To calculate the ratio of the affinity constants determined with SPR, the average of the affinity constants with unlabelled and with labelled IgG was used.
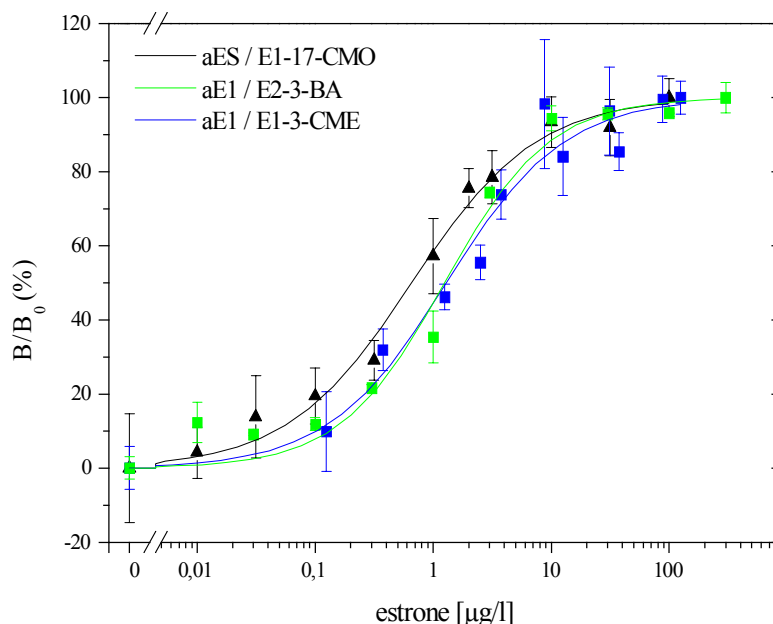
Fig. 33: Calibration curves of estrone by αES with E1-17-CMO, by αE1 with E1-3-CME and by αE1 with E2-3-BA.

	$K_{(IgG-Ag)}/K_{(IgG-Der)}$ RIfS	$K_{(IgG-Ag)}/K_{(IgG-Der)}$ SPR	TMP [µg/l]	WR [µg/l]
αE1/E1-3-CME	0.6	0.9	1.3 ± 0.2	0.11-16.04
αE1/E2-3-BA	0.9	3	1.2 ± 0.2	0.28-8.66
αES/E1-17-CMO	1.3	1.2	0.7 ± 0.1	0.06-8.70

Table 14: Ratio of the affinity constant of the antibody and the analyte, and the affinity constant of the antibody and the analyte derivative, and characteristics of the measured FRET calibration curves of estrone.

The lowest concentration of estrone was obtained with the αES IgG and E1-17-CMO; the two other systems showed a performance slightly inferior. This corresponded to the results expected according to the ratio of the K_A values measured with RIfS. This

was the only system where the affinity of the IgG was smaller for the analyte derivative than for the analyte. The two other systems with αE1 and E1-3-CME or E2-3-BA showed an affinity larger for the analyte derivative than for the analyte, therefore the LOD and the TMP were higher.

With SPR, the results are not so evident. The ratio of the affinities with the pair αE1 and E2-3-BA obtained with SPR and with RIfS are completely different, that is why these results are supposed to be defective; they are not discussed here. With the exception of this pair, the lowest LOD should be obtained, as with RIfS, with αES IgG and E1-17-CMO, where the ratio is larger than one. The ratio with αE1 and E1-3-CME being slightly smaller than one, the results with FRET are presumed worse. The expected FRET results, according to the affinity constants determined by SPR, correspond quite well to the measured FRET calibration curves.
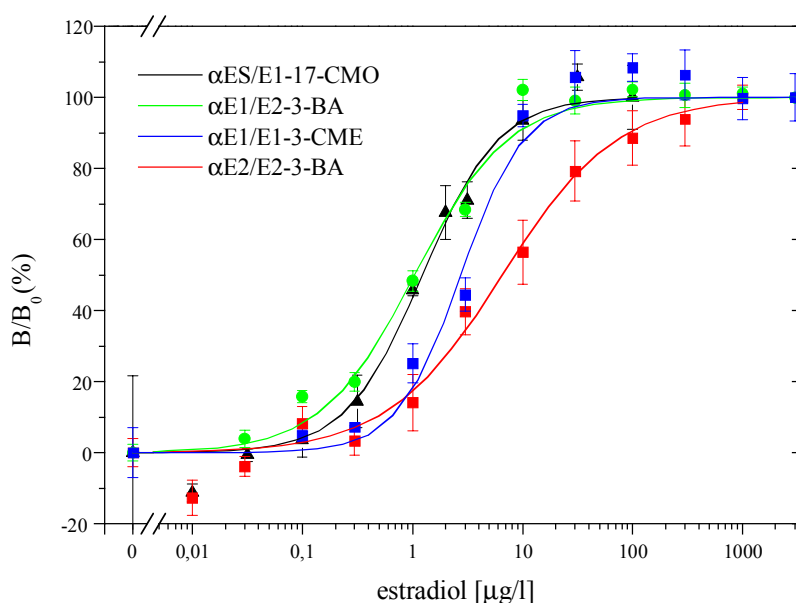

Fig. 34: Calibration curves of estradiol by αES with E1-17-CMO, by αE1 with E1-3-CME, by αE1 with E2-3-BA and by αE2 with E2-3-BA.

	$K_{(IgG-Ag)}/K_{(IgG-Der)}$ RIfS	$K_{(IgG-Ag)}/K_{(IgG-Der)}$ SPR	TMP [µg/l]	WR [µg/l]
αE1/E1-3-CME	0.4	0.01	2.8 ± 0.5	0.69-11.46
αE1/E2-3-BA	0.6	0.05	1.0 ± 0.1	0.17-8.31
αES/E1-17-CMO	0.5	1.1	1.2 ± 0.1	0.17-7.30
αE2/E2-3-BA	4	0.1	6.6 ± 1.0	0.31-99.5

Table 15: Ratio of the affinity constant of the antibody and the analyte, and the affinity constant of the antibody and the analyte derivative, and characteristics of the measured FRET calibration curves of estradiol.

The results obtained with αE1 and E2-3-BA and αES and E1-17-CMO were comparable concerning the TMP (around 1 µg/l) as well as the LOD (0.17 µg/l). The LOD (0.3 and 0.7 µg/l) and TMP (2.8 and 6.6 µg/l) were much higher with the αE1/E1-3-CME and αE2/E2-3-BA pairs. This corresponds quite well to the results expected from RIfS. The ratio for αE1/E2-3-BA and αES/E1-17-CMO are similar and smaller than one. The ratio for αE1/E1-3-CME was much smaller. Although the ratio for αE2/E2-3-BA is much larger than one with RIfS, the LOD is high, which can be explained by the low values of the affinities, one order of magnitude smaller than the affinities of the other systems for estradiol.

The ratio for αES/E1-17-CMO was however smaller than one, which explained that the LOD and TMP are larger than these obtained previously for estrone. The calibration of E1 with αES and E1-17-CMO had a TMP of 0.7 µg/l and a LOD of 0.06 µg/l, and the ratio of the affinities was larger than one.

With both SPR and RIfS, the best ratio was obtained with αES/E1-17-CMO, yielding the lowest LOD with the FRET assay. The ratio with αE1 and E2-3-BA is smaller, and the two systems αE1 with E1-3-CME and αE2 with E2-3-BA show low ratios (0.05 and 0.07), leading to high LOD (0.31 and 0.69 µg/l) and high TMP.

When the ratios of RIfS and SPR were extremely different it may be possible that the minimal antibody concentration required to detect the high affinity constant was not detectable. An important point to determine the affinity constant in the bulk flow is the

used concentration of antibody. According to Piehler et al (1997) the concentration of antibody used has to be lower than the reciprocal of the affinity constant in order the form and the position of the curve depend on the affinity constant. If the antibody concentration is too high the curve is defined only by the concentration of antibody. However it was impossible to reduce the concentration of antibody because the slope of the signal was already extremely small.

The Wilcoxon matched pairs signed ranks test applied to the affinity constants measured with RIfS and with SPR, showed that the results were not comparable. But the same test applied to the ratio of the affinity constants, between analyte and analyte derivative showed that the ratio obtained with RIfS are comparable with the ratio obtained with SPR. The test applied to all ratios, given in Table 14 and Table 15, gave calculated U values of 14, larger than the critical value U(7, 10 %) equal to 4. This confirmed that both methods were suitable to predict the order of the FRET calibration curves.

The test was not applicable to each analyte individually (pairs in one table), because of the too small number of pairs: 3 pairs for estrone and 4 pairs for estradiol.

4.5.3. Conclusion

➢ FRET allowed to make measurement in synthetic wastewater with good recovery rates between 72 and 109 %. The required preparation of the sample consisted only of degassing. The difference of intensity in different matrices was corrected by a simple reference method.

➢ The affinity constants obtained with the RIfS method allowed to predict which system antibody and analyte derivative could detect the smallest concentration of each analyte.

➢ The ratios of affinity constants obtained with the SPR method are considered comparable with the ratios of affinity constants obtained with the RIfS method according to the applied Wilcoxon test.

4.6.   MINIATURISATION OF THE FRET ASSAY

The repartition of the excitation light on the nanotiterplate was not homogeneous and required a correction. Measurements of several concentrations of Cy5 in solution were carried out to determine the limit of detection, which was $5 \cdot 10^{-9}$ M of Cy5. These parameters were previously described by Schobel (1999) and Stemmler (1999).

4.6.1. Establishment of the assay in nanotiterplates

The assay has to be adapted to the NTP. The first step was the transfer of pre-incubated samples. Titration and calibration curves are shown in Fig. 35 and Fig. 36.

Fig. 35: Titration of 3 μg/ml of anti E1-Cy5 (1:7.7) with (E1-3-CME)-BSA-Cy5.5 (1:1:2.9). The black squares represent the intensity in the MTP and the empty circles represent the intensity in the NTP. The solutions were pre-incubated and then transferred in one step to the NTP.

The results in the MTP and in the NTP are comparable: the highest quenching is achieved with the same concentration of analyte derivative, 10 μg/l, and the signalling range can be considered as equivalent.

Fig. 36: Calibration of estrone with 3 µg/ml of anti E1-Cy5 (1:7) and 10 µg/l of (E1-3-CME)-BSA-Cy5.5 (1:1:2.9). The black squares represent the intensity in the MTP and the empty circles represent the intensity in the NTP. The solutions were pre-incubated and then transferred in one step to the NTP

The comparison of the measurement in MTP and the measurements of the sample transferred to the NTP showed the results were similar. The signalling range remained constant and equal approximately to 60 % and the test mid-points of the two calibrations curves are also very similar (8.8 ± 0.6 µg/l in MTP and 9 ± 2 µg/l in NTP).

In a second step, each solution was pipetted sequentially into the NTP, exactly like for the MTP, and the equilibria between IgG, analyte and analyte derivative took place in the NTP.

Fig. 37: Titration of 3 μg/ml of anti E1-Cy5 (1:7.7) with (E1-3-CME)-BSA-Cy5.5 (1:1:2.9). The black squares represent the intensity in the MTP and the empty circles represent the intensity in the NTP.
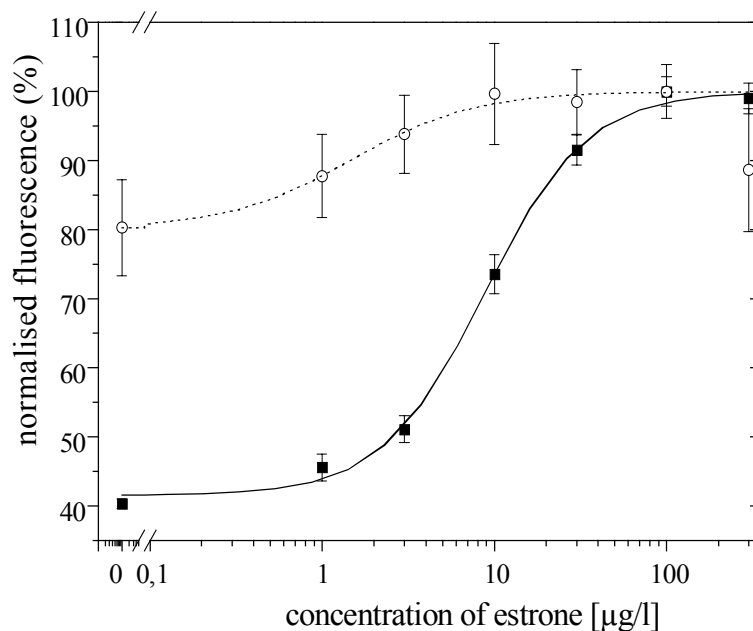
Fig. 38: Calibration of estrone with 3 μg/ml of anti E1-Cy5 (1:7) and 10 μg/l of (E1-3-CME)-BSA-Cy5.5 (1:1:2.9). The black squares represent the intensity in the MTP and the empty circles represent the intensity in the NTP.

The signalling range for the titration curve was reduced from 60 % in the MTP to 45 % in the NTP but the concentration of analyte derivative giving the highest quenching was the same: 10 µg/l.

Concerning the calibration the curves were no more comparable. The signalling range was considerably reduced from 60 % to 20 %. And the TMP, 8.8 ± 0.6 µg/l in the MTP shifted to 1 ± 1 µg/l in the NTP.

The problem is thought to be due to the adsorption of protein (IgG and/or BSA-derivative) on the surface of the NTP. The increase of the ratio surface/volume from 8.8 cm^{-1} in the MTP to 76 cm^{-1} in the NTP is probably responsible of this high non-specific adsorption. In order to prevent this adsorption the surface of the plate had to be treated. One of the most well-known methods to reduce the non-specific adsorption is the coating of the surface with a protein, like BSA (Peterfi et al., 2000). The NTP was coated with a solution of 3 mg/ml of BSA in PBS overnight at 4°C. The results obtained are shown in Fig. 39 and Fig. 40.
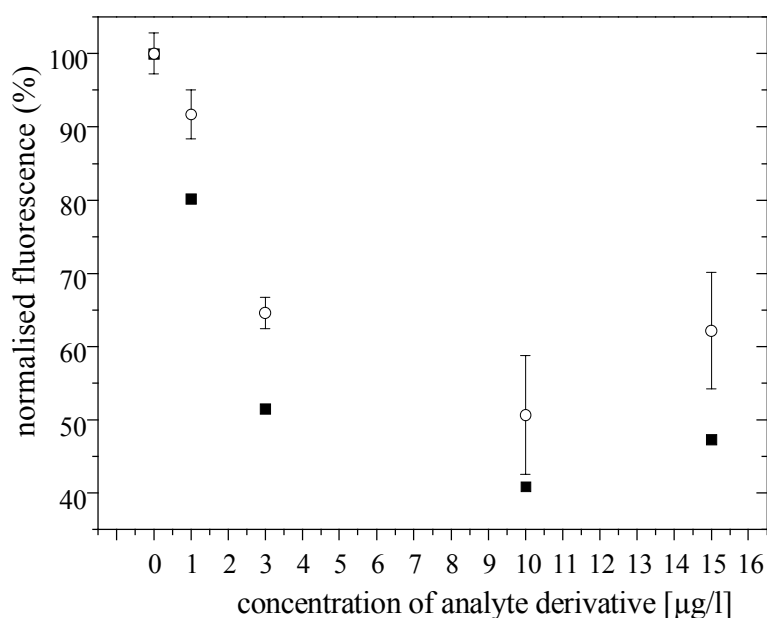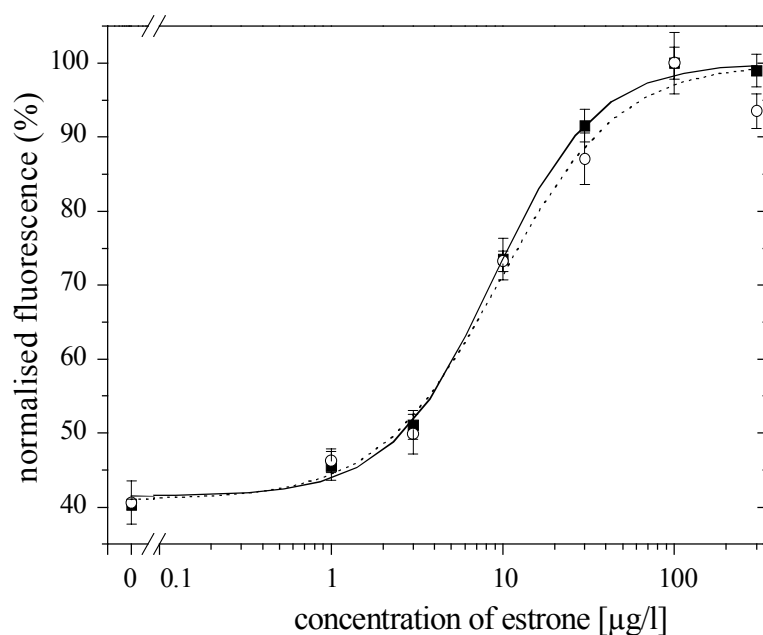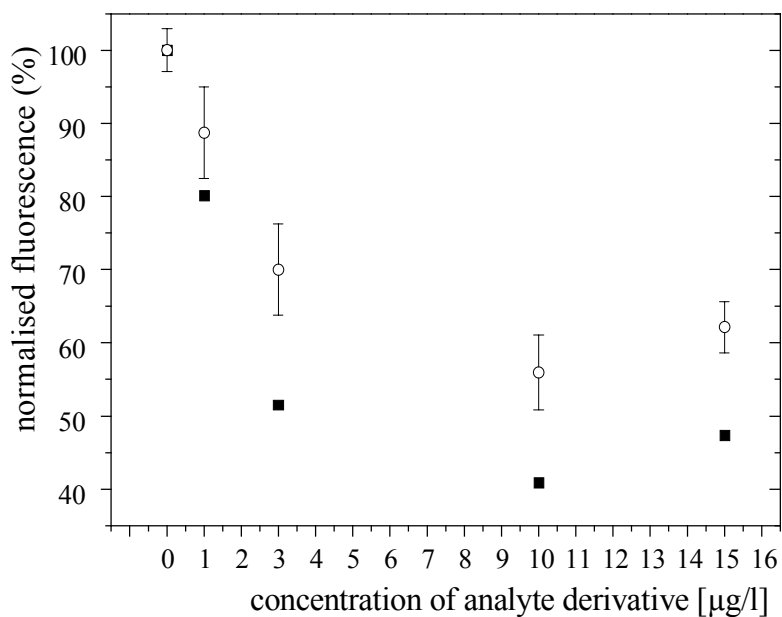

Fig. 39: Titration of 3 µg/ml of anti E1-Cy5 (1:7.7) with (E1-3-CME)-BSA-Cy5.5 (0.7:1:1.3). The black squares represent the intensity in the MTP and the empty circles represent the intensity in the BSA coated NTP.
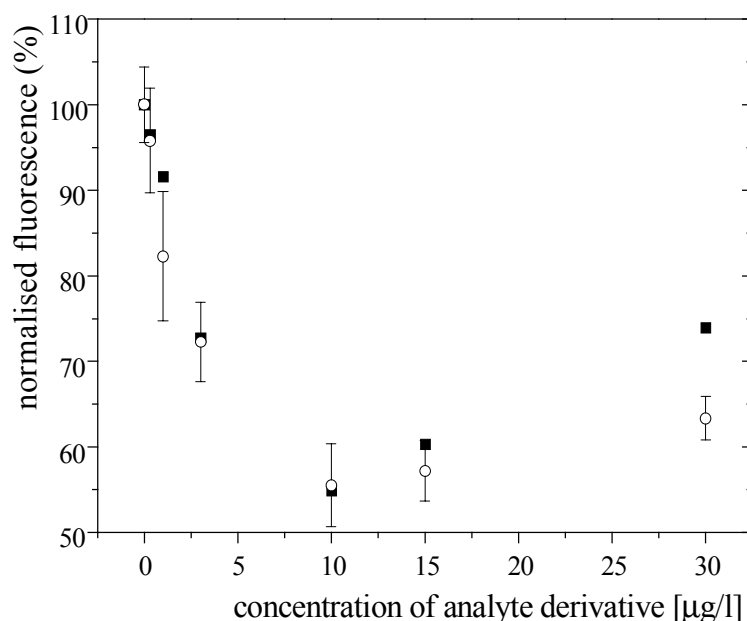
The standard deviation of the measurements in the NTP were still important but the signalling range was comparable (45 %), as well as the optimal concentration of analyte derivative (10 µg/l).
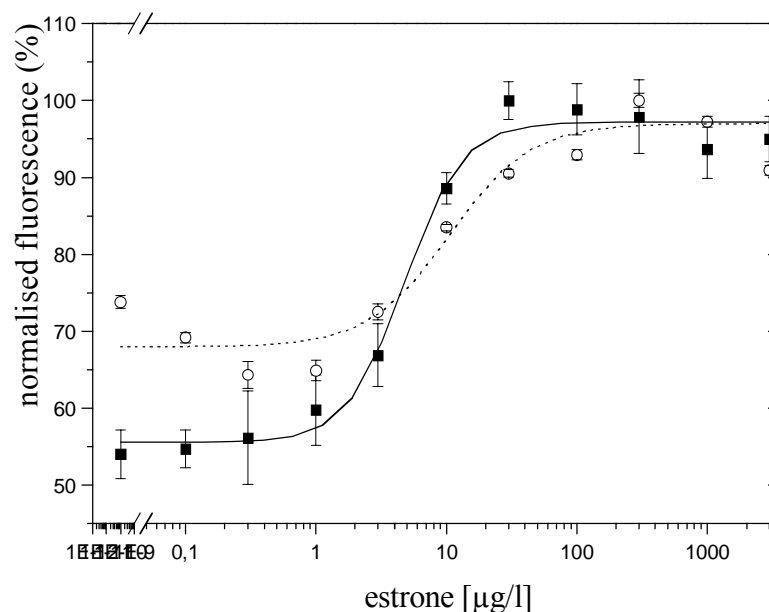
Fig. 40: Calibration of estrone with 3 µg/ml of anti E1-Cy5 (1:7.7) and 10 µg/l of (E1-3-CME)-BSA-Cy5.5 (0.7:1:1.3). The black squares represent the intensity in the MTP and the empty circles represent the intensity in the BSA coated NTP.

The calibration in the NTP was better but the signalling range was still reduced (30 %) in comparison to the results in the MTP (45 %).

Different other coating solutions, known to reduce the non-specific adsorption, were tested in regard to the improvement of the signalling range and the TMP for the calibration in the NTP. The three most important variables for the adsorption of protein on a solid phase are the temperature, the time and the concentration. The conditions most frequently chosen for the incubation are overnight at 4°C, but the time can be shortened by increasing the temperature and the concentration (Tijssen, 1992). The coating solutions were made in PBS, one or several concentrations were tested. The NTP were coated overnight at 4°C and gently rinsed with bi-distilled water. All tested coating solutions are listed below.

- Aminodextran (AMD) 260 kDa, dilution 1/10 (m/v) in water (Castilho et al., 2000)

- Polyethylenimine at 1-5 % (Grondahl et al., 2000) + AMD, dilution 1/10 + glutaraldehyde 2,5 % (Velev, 1997) + BSA 10 mg/ml 2 h RT. Glutaraldehyde was used to fix the protein shell of AMD.
- Casein, dilution of 2 ml of a solution at 5 % in 10 ml (Peterfi and Kocsis, 2000)
- PEI (1-5 %) + Casein 5 %, dilution of 2 ml in 10 ml
- skimmed milk powder, 3 mg/ml
- calf serum, 3 mg/ml
- PEI (1-5 %) + calf serum, 3 mg/ml
- PEI 0,5 % + alginic acid 0,5 % (Morra and Cassineli, 1999)

It was also attempted to modify covalently the NTP according to the protocols below.

- Carboxylation by oxidation with $KmnO_4$, activation of the acid groups by a water soluble carbodiimide or NHS/EDC and grafting of AMD according to Zammatteo et al. (1996)
- Carboxylation by oxidation with NaOH 8 % for 24 h, activation of the acid groups by NHS/EDC and binding of AMD according to Kürner et al. (2000)

A few compounds were added to the solution in an attempt to reduce the non-specific adsorption and increase the signalling range:

- Tween 0.01, 0.05, and 0.1 % (Kuwabara et al., 1999)
- octyl-b-glucopyranoside 0.02, 0.1, 0.5 and 1 %
- non-specific IgG 0.1 g/l and 0.05 g/l

All these methods did not bring better results than PEI + BSA, and some of them were time-consuming.

The results are shown only for the best method with polyethylenimine (PEI) and BSA (Fig. 41). PEI is known to enhance the surface charge and to promote the electrostatic interaction (Grondahl et al., 2000). As expected the pre-treatment with the PEI improved the coating of BSA. Two solution of PEI were tested: 1 % and 5 %.
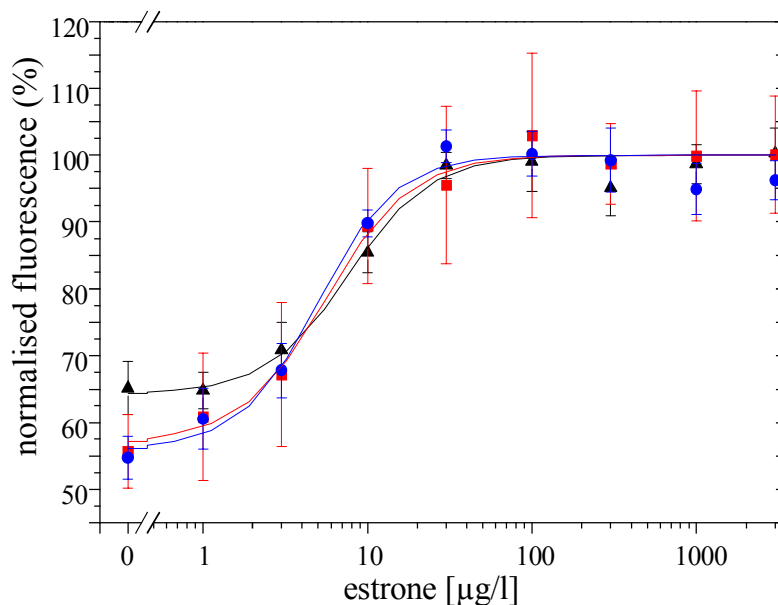
Fig. 41: Calibration curve of estrone with anti-E1-Cy5 (1:7.7) and 10 µg/l of (E1-3-CME)-BSA-Cy5.5 in the MTP (red square), in the NTP coated with 5 % PEI and BSA (blue circle) and in the NTP coated with 1 % PEI and BSA (black triangle).

The results in the MTP are comparable with the results in the NTP (with 5 % of PEI), as well for the TMP (5.0 ± 0.7 µg/l in the MTP and 5.6 ± 0.5 in the NTP) as for the signalling range (44 ± 1 % in the MTP and 43 ± 1 % in the NTP). The coating of the NTP with 5 % of PEI and 3 mg/ml of BSA prevents the adsorption of the protein on the surface of the NTP. 1 % of PEI was not enough since the signalling range was slightly smaller (36 ± 1 %) and the TMP larger (7.7 ± 0.9 µg/l).

The next step is the reduction of the concentration of IgG to reduce the TMP.

4.6.2. Reduction of the IgG concentration

The concentration of IgG was reduced from 3 µg/ml to 2 and to 1 µg/ml IgG. The corresponding titrations were performed in the NTP. For 3 µg/ml of IgG the required concentration of (E1-3-CME)-BSA-Cy5.5 was 20 µg/l, it was reduced to 10 µg/l for 2 µg/ml of IgG and finally to 7 µg/l for 1 µg/l of IgG. The calibration curves for 1 µg/ml of IgG are shown in Fig. 42, and the results of all calibration curves are summarised in Table 16.
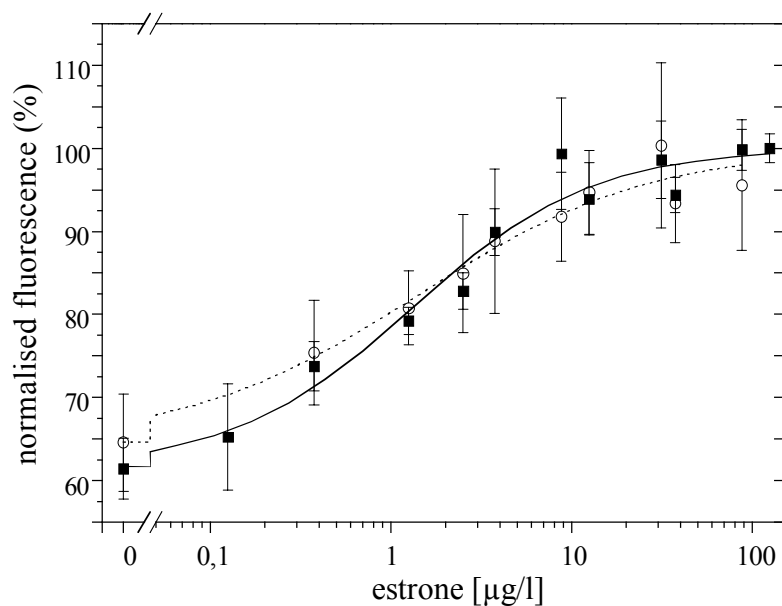
Fig. 42: Calibration of estrone with anti-E1-Cy5 (1:7.7, 1 µg/ml) and (E1-3-CME)-BSA-Cy5.5 (1:1:2.9, 7 µg/l). The full line represents the measurements in the MTP and the dotted line the measurements in the NTP.

	IgG [µg/ml]	TMP [µg/l]	Signalling Range (%)	Working Range [µg/l]
MTP	3	6 ± 1	48	1.66-20.15
	1	1.3 ± 0.3	38	0.11-15.93
NTP	3	7 ± 1	45	1.0-42.0
	2	3.7 ± 0.3	40	0.7-19.6
	1	1.4 ± 0.4	35	0.06-35.14

Table 16: Characteristics of the calibration curves, concentration of IgG, test midpoint, signalling range and working range.

The concentration of IgG could be reduced successfully down to 1 µg/ml for the calibration curve in NTP coated with PEI and BSA. The results were comparable in the MTP and in the NTP. However, the standard deviation of the measurements in the NTP was much larger than the one in the MTP. This was presumed to be due to the dispenser device (microdrop device used only for this part 4.6.2), which must be improved.

4.6.3. Conclusion

➤ Although the plastic NTP showed a high non-specific adsorption which considerably reduced the signalling range in comparison to the signalling range in the MTP, it was possible to avoid it by coating the NTP with PEI and BSA. This preparation of the NTP allowed to obtain the same results in the NTP as in the MTP. The concentration of IgG was reduced down to 1 µg/ml to improve the performance of the assay.

4.7.   VITELLOGENIN ASSAYS

4.7.1. FRET measurements with the usual fluorophores

The monoclonal antibody B8D8 was labelled with the Donor Cy5 to the labelling degree 1:4.6. The vitellogenin (VTG) was labelled with the Acceptor fluorophore Cy5.5 to the labelling degree 1:2.6. Since VTG (145 kDa) is much larger than the haptens (300 Da) used generally for the assay, BSA was not used with VTG. A titration of 1 µg/ml of B8D8-Cy5 was done with VTG-Cy5.5 (1 – 300 µg/l). No quenching of the Donor was observed. Two possibilities were considered to explain why the FRET did not work: either the distance between the two dyes was too large, because VTG is much larger than BSA, or the labelled compounds could not bind, because the labelling impedes the binding.

Several labelling degrees were tested to vary the distance between the dyes. The following degrees of labelling were unsuccessfully tested in titration assays: 1:6.6, 1:0.5, and 1:1 for VTG-Cy5.5, and 1:3.8 and 1:4.9 for B8D8-Cy5. It was also attempted to exchange the Donor and the Acceptor, since the Acceptor is supposed to have a higher labelling property than the Donor. B8D8 was labelled to 1:3.7 with Cy5.5, and VTG to 1:3.7 with Cy5. The titration assays did not show quenching of the Donor Cy5 with various concentrations of B8D8-Cy5.5.

Since the FRET assay was unsuccessful because the quenching of the Donor failed, the activity of the labelled compounds was tested in another assay, called Phase Separation Fluorescence Immuno-Assay (PSFIA) (Stemmler, 1999).

4.7.2. PSFIA measurements with the Cy5 labelled molecules

For this assay only one labelled compound is required. First, the binding of the labelled antibody was tested. To optimise the conditions of the assay several concentrations of VTG were used for the coating of microtiterplates, several concentrations of B8D8-Cy5 (labelling degree 1:5) were used for the fluorescence intensity measurement, several times of coating and times of incubation in the plate were tested. A high adsorptive microtiterplate was coated with vitellogenin in PBS,

[5·10^{-8} M], overnight at 4°C. The reference microtiterplate was treated in the same way but without protein. B8D8-Cy5 (250 µl, [5·10^{-9} M]) was incubated in the plate overnight at 4°C, then 200 µl was transferred into a non-adsorptive plate and the fluorescence of the B8D8-Cy5 in solution was measured. The results are shown in Fig. 43.
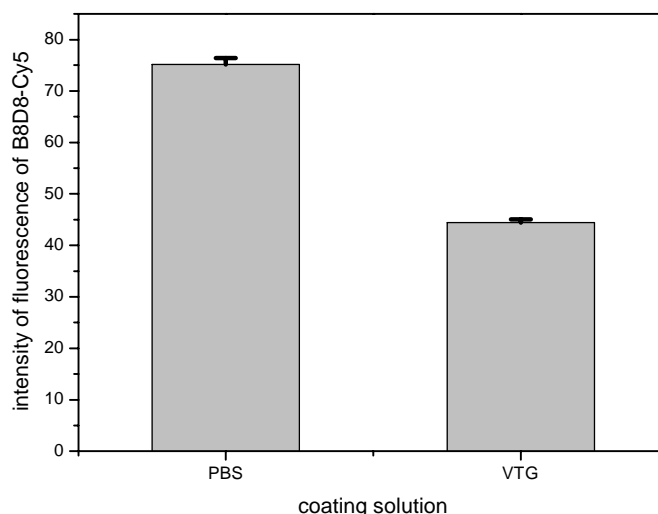
Fig. 43: Fluorescence of the B8D8-Cy5 after incubation overnight in a plate coated with PBS and vitellogenin. [B8D8]=5·10^{-9} M in PBS containing 0,5 % of BSA and [VTG] coating=5·10^{-8} M in PBS.

The "coating" without protein demonstrated that there is no non-specific adsorption of the B8D8-Cy5. The binding of the B8D8-Cy5 to the vitellogenin coated plate was specific. The labelling of the B8D8 did not disturb the binding with the vitellogenin.

To confirm that the binding between the B8D8-Cy5 and the VTG was specific, an inhibition test has to be done. The plate was coated with VTG [5·10^{-8} M]. Either B8D8-Cy5 [5·10^{-9} M], or B8D8-Cy5 together with 3000 ppb of VTG, were incubated in the plate. The measurements were compared to the non coated plate. The results are shown in Fig. 44.
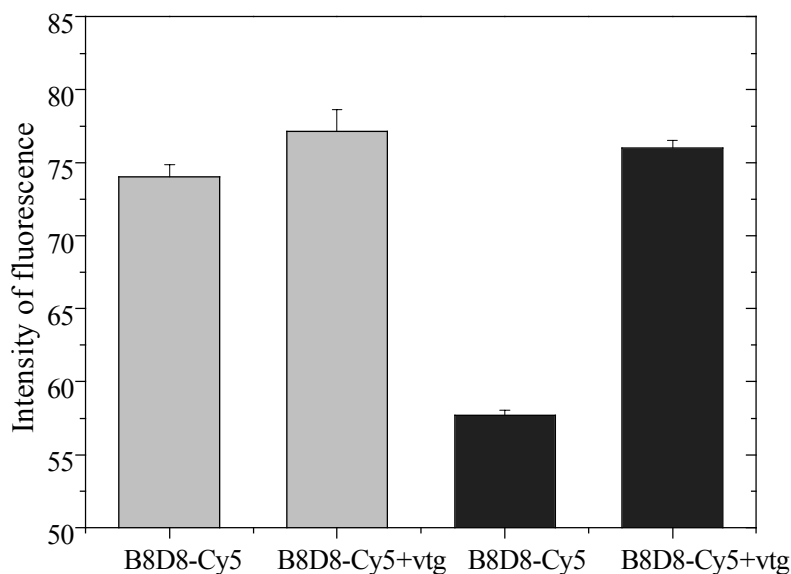
Fig. 44: Inhibition tests of the B8D8-Cy5 with vitellogenin in solution. The grey columns represent the measurements in the non-coated plates, and the black columns represent the measurement in the VTG coated plates.

The intensities of B8D8-Cy5 in the non-coated plate and of VTG-inhibited B8D8-Cy5 in the non-coated plate were similar. These columns show the highest signal (77 fluorescence units) since the B8D8-Cy5 did not bind to the surface. The intensity of B8D8-Cy5 strongly decreased with the VTG coating, indicating binding of the B8D8 to the surface. The presence of a high concentration of VTG in solution with B8D8 in the incubation increased the fluorescence because B8D8 bound to the VTG in solution could not bind to the VTG on the plate. This confirmed that labelled B8D8 bound specifically to VTG.

We tested the activity of the labelled VTG-Cy5, but not of VTG-Cy5.5, since the plate reader is adapted to measure the fluorescence of Cy5. The labelling chemistry is the same for the dyes Cy5 and Cy5.5, both bind to the protein via amino groups. Hence different activities of VTG-Cy5.5 and VTG-Cy5 are not expected. The PSFIA described above was slightly modified: an adsorptive plate was coated with different concentrations of B8D8. A VTG-Cy5 solution (10^{-9} M, the optimal tested concentration) was incubated overnight. 200 µl of the solution were transferred into a non-binding plate, and the fluorescence of Cy5 was measured. Several concentrations

for the coating were tested to find the optimal conditions. The results are summarised in Fig. 45.
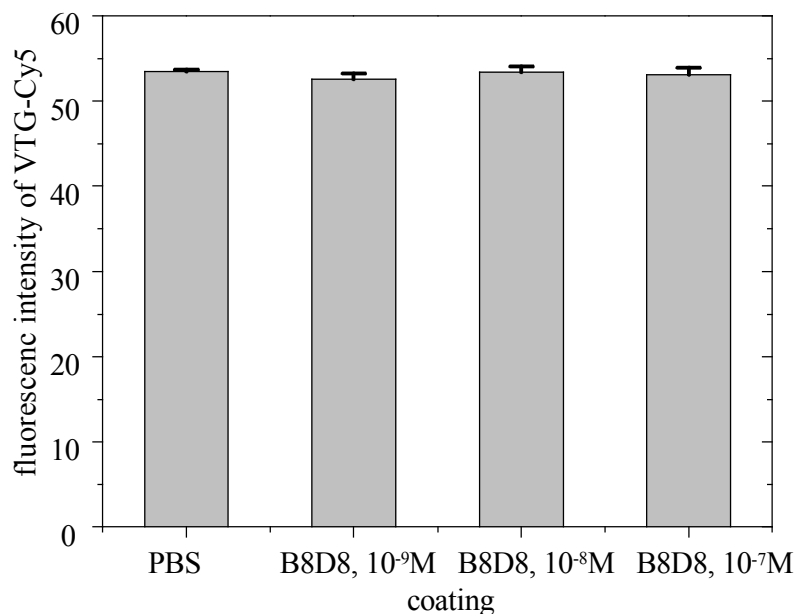
Fig. 45: Test of binding with B8D8 and VTG-Cy5 with several concentration of B8D8 for the coating.

Fig. 45 shows that the fluorescence signal was independent of the concentration of binding sites on the surface. The labelled vitellogenin has not bound to the B8D8-coated plate. VTG-Cy5 may be deactivated by the labelling procedure.

4.7.3. FRET with a new Acceptor fluorophore

Subsequently, we searched for a dye reacting to an active group in the protein different from the amino groups. The precondition for the new dye was a similar spectral characteristic as Cy5.5 (absorption at 675 nm and emission at 694 nm) to achieve a FRET with Cy5 as Donor. The dye Alexa680 (Molecular Probes, Leiden, the Netherlands) seems to fulfil the requirements. It absorbs at 679 nm and emits at 700 nm, and it binds covalently to proteins via thiol groups.

VTG was successfully labelled with Alexa680 with a ratio of 0.5 dye / VTG. But the titration of B8D8-Cy5, 1:3, 1 µg/ml by VTG-Alexa680 at different concentrations did not show any quenching of the Cy5 dye.

4.7.4. PSFIA with the alexa680 labelled vitellogenin

The activity of the VTG-Alexa680 was tested with the PSFIA. For the B8D8-Cy5 (1:3) the optimal concentration for the measurement was found to be 10^{-9} M. Several concentration of VTG for the coating were tested. The coating was done with PBS, VTG and VTG-Alexa680. The results are shown in Fig. 46.
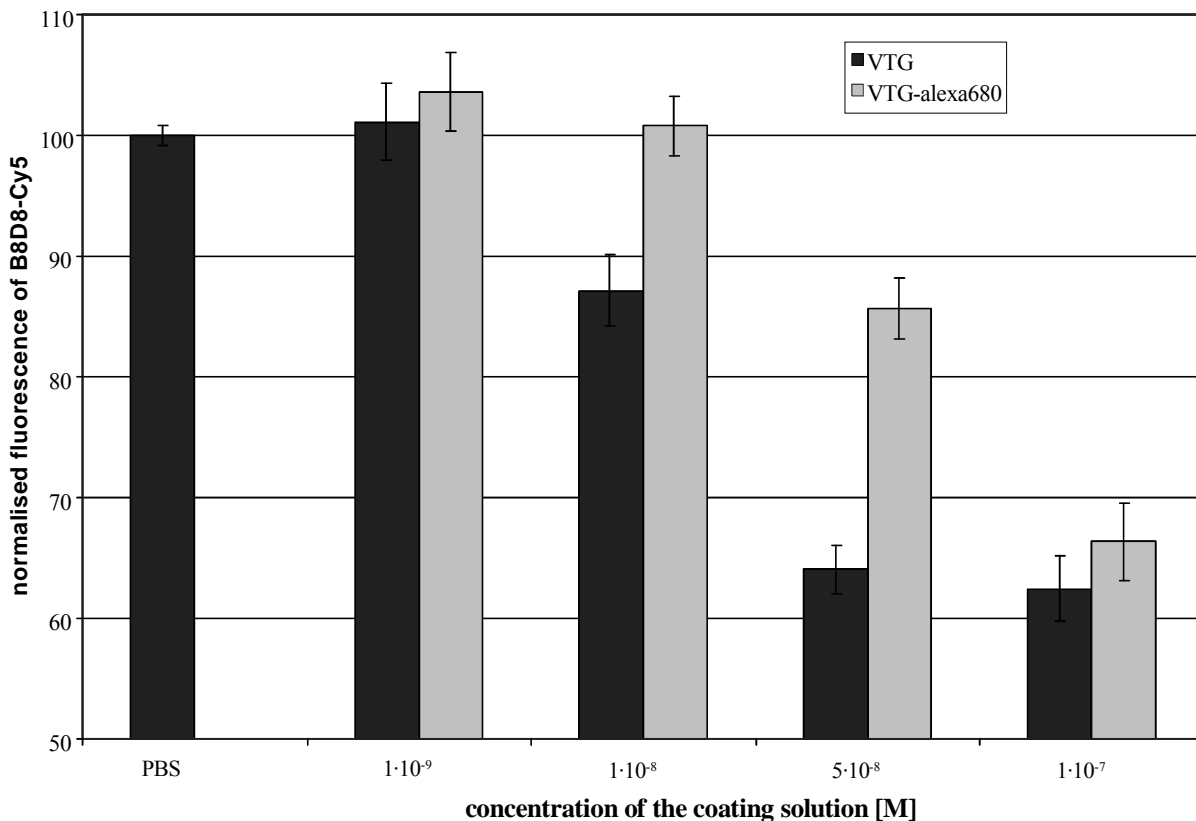
Fig. 46: Test of binding of B8D8-Cy5 to a VTG and VTG-Alexa680 coated plate. The signal corresponding to the coating with PBS being maximal, this binding signal is normalised to 100 %.

The natural VTG and the VTG-Alexa680 were able to bind to the B8D8. The binding capacity of the VTG did not seem to be damaged by the labelling.

The FRET assay may not have worked for several reasons: Cy5 and Alexa680 may not be an appropriate pair (this could be tested with another common hapten and antibody system) or the distance between the dyes may be too large.

4.7.5. Conclusion

➢ It was not possible to observe FRET between the labelled B8D8 and the labelled VTG.

➢ The binding of labelled IgG to immobilised VTG was demonstrated with a PSFIA.

➢ The VTG labelled on the amino groups could not bind to the immobilised IgG. Either the labelling of VTG avoids the binding or the immobilisation of the IgG impedes the binding.

➢ The binding of Cy5 labelled IgG to Alexa680 labelled VTG could be confirmed with a PSFIA.

5. Conclusions and Prospects

Several pairs of antibody and haptens were thermodynamically and kinetically characterised by Surface Plasmon Resonance (SPR) and/or by Reflectometric Interference Spectroscopy (RIfS). The monoclonal anti-estradiol antibody was fully characterised with SPR. The active concentration was determined as well as the kinetic rate constants and thermodynamic values such as enthalpy and entropy changes. The affinity constants of the antibody for several analytes and analyte derivatives were obtained by kinetic measurements as well as by inhibition curves. The polyclonal anti-estrone, anti-estradiol and anti-total estrogen antibodies were characterised with SPR and with RIfS . The RIfS method was used only to determine the affinity constants between antibody and analyte or analyte derivative in solution by inhibition curves. The SPR method was applied to determine the affinity constants by inhibition curves as well as by kinetic measurements using reagents immobilised on the surface. SPR was also used to measure the active concentration of the antibodies and the affinity constants of the labelled antibodies.

The monoclonal antibody 15H11 showed an apparent decrease of its active concentration when used a very low concentration, which had to be considered for all measurements. The analyte derivatives E2-6-CMO and E2-7-CMO bound both to the monoclonal antibody. The affinity to E2-6-CMO was independent of the temperature. The affinity between 15H11 and E2-7-CMO increased with the increase of the temperature between 10 and 25°C, which suggests that the interactions were entropy driven. The same observation was made for the reaction of E2-6-CMO with 15H11. These thermodynamic informations could help to adjust assay conditions in order to favour either the association or dissociation of the complex. The inhibition curves indicated that the antibody has a high affinity for the analytes estradiol and ethinylestradiol. The 15H11 seemed to be more sensitive to modifications in the ring A of estradiol than in the ring D, which could indicate that the ring A is more important for binding and could thus be more deeply buried in the binding site of the antibody,

than ring D. Molecular modelling may be able to suggest the position of the estradiol in the binding site and indicate which interactions are involved.

Measurements with the polyclonal antibodies showed a strong difference in active concentration between the native αE1 IgG (lyophilisated powder) and the αE2 and αES IgG (in ammonium sulfate solution). This could be due partially to the filtration step to separate the antibody from the ammonium sulfate solution and/or to the solution of elution of the purification step. The labelling of the antibody can influence strongly the active concentration: the active concentration of the antibodies was generally reduced after labelling in comparison to the native form. The affinity constants between antibody and derivatives were determined by kinetic as well as by inhibition curve, and the results were comparable according to the Mann Whitney test applied. The affinity constants determined by SPR with different derivatives immobilised at the surface were also considered similar. Finally, the affinity constants determined for the labelled and unlabelled antibodies were comparable. The labelling did not influence the affinity constants and the K_A values measured before the labelling could be used to predict the results of the FRET assay. The double measurements of affinity constants between antibody and analyte or analyte derivatives obtained from inhibition curves with SPR and RIfS allowed to compare the two methods. The results obtained with RIfS were significantly different from the results obtained with SPR. This difference could be explained by the different conditions of measurement with both devices and by the different concentrations of antibody used. The mass transport constant depends on flow cell dimensions and bulk flow rate. In SPR ($2·0.5·0.05$ mm^3) the dimensions of the flow cell are much smaller than in RIfS ($1·3·0.05$ mm^3) and the flow rate is larger in RIfS than in SPR. Since the mass transport constant is proportional to the cube root of the flow rate the effect of the flow rate on the mass transport is relatively small. But the larger size of the flow cell in the RIfS device may explained that the limiting conditions of mass transport are better fulfilled in RIfS. The measurements in SPR may not be made under mass transport control and the kinetic rate constant could influence the results. It should be possible to improve the mass transport limiting conditions by reducing the flow rate and increasing the surface binding capacity.

All binding reactions observed between the polyclonal antibodies and the analytes or analyte derivatives are summarised in Table 17.

	αE1	αE2	αES
E1-3-CME	x		
E2-3-BA	x	x	
E1-17-CMO			x
E2-17-Hg			*
E1	x	x	x
E2	x	x	x
EE2		x	x

Table 17: Heterologous and homologous reactions between polyclonal antibodies and analytes or analyte derivatives. x indicates a binding of the antibody with the hapten. * means that the binding of the antibody was observed only with the free hapten, no affinity was observed after the immobilisation of the hapten of a BSA molecule or on the surface of the transducer.

The Fluorescence Resonance Energy Transfer (FRET) assay requires labelling of two compounds, the antibody and the analyte derivative. The antibody was traditionally labelled with the Donor, Cy5, whereas the analyte derivative was labelled with the Acceptor, Cy5.5, through a Bovine Serum Albumin (BSA) molecule The labelling degrees were determined either by UV-Vis spectroscopy for the compounds with high decadic molar absorption coefficient, or with RIfS for the number of analyte derivatives per molecule of BSA.

Simulations of the FRET assay were done under special conditions which simplified the calculations. They showed the importance of each crucial parameter of the system: the concentration of analyte derivative, the affinity constants and the ratio between the affinity constants of the antibody to the analyte and to the analyte derivative.

The simulations showed clearly that the decrease of the concentration of the analyte derivative led not only to the reduction of the LOD but also to a decline of the signalling range. The affinity constants were extremely important since high affinity

led to low LOD and a lower affinity for the analyte derivative than for the analyte also reduced the LOD.

The affinity constants of the several antibodies for all cross-reactive analytes and analyte derivatives were calculated to compare the ratios between their respective affinities. These ratios were used in simulations to predict which IgG – analyte derivative pair should give the lowest LOD and test mid-point (TMP). The predicted results were compared with the measured FRET calibration curves. The affinity constants determined by the RIfS method allowed to predict correctly the results of the FRET calibration curves. The prediction was not as clear with the affinity constants determined by SPR as with the affinity constants determined by RIfS. For one IgG – analyte derivative pair (αE1 – E2-3-BA) predictions did not correspond with the FRET calibration curve. It was, however, possible for all other pairs to predict the order of the FRET results.

Since the simulations were simplified it was impossible to predict the signalling range. Since the Acceptor emits fluorescence and the Donor is not totally quenched, the signalling range can be reduced by the labelling degree. A study about the labelling degree and the signalling range would be of further interest.

The measurements of spiked wastewater samples were quite good; the calculated recovery rates indicated that the FRET method is suitable for the measurements of one estrogen in the sample.

Cross reactivity of antibodies can be an inconvenient as well as an advantage. The antibody can react with all its cross reactive substances in solution with several affinities and the presence of unknown cross-reactive substances in the solution could lead to determination of a wrong concentration of the quantified substance. On another hand the cross reactivity is helpful in the competitive immunoassay, where it allows to play with the sensitivity of the assay. An important point is to know to which substances can bind the antibody. The knowledge of limited heterologous reactions could be used to measure multi-analytes calibration curves with the help of a neural network.

The FRET assay was miniaturised and applied in a measurement volume of 70 nl. The problem caused by the reduction in volume was the non-specific adsorption of the proteins of the assay onto the nanotiterplate (NTP), which reduced drastically the signalling range. This adsorption had to be reduced by coating the plate. The only possibility to control if coating the plate prevented non-specific adsorption was to carry out the calibration in the NTP and to compare it with the calibration in the microtiterplate (MTP). The appropriate coating was 5 % of polyethylenimine followed by 3 mg/ml of BSA. The TMP was then reduced by reducing the concentration of IgG from 3 µg/ml to 1 µg/ml.

The next step to reduce the TMP would be to decrease the concentration of analyte derivative. This would decrease the signalling range. The reduction of the standard deviation of the measurements in the NTP could also be obtained by an improvement of the pipetting device or a better control of the evaporation/condensation in the NTP during the dispensing.

Finally, a FRET assay was used to quantify a big protein, vitellogenin. The protein and the monoclonal anti-vitellogenin antibody, B8D8 were successfully labelled respectively with Cy5 and Cy5.5, but no quenching was observed during the titration. In order to test individually each labelled compound a fluorescence immunoassay with phase separation (PSFIA) was developed. The labelled antibody was shown to bind to the coated vitellogenin microtiterplate but the labelled vitellogenin did not bind to the coated antibody microtiterplate. The labelling of the vitellogenin or the immobilisation of the IgG disturbed the binding. Another label was tested as Acceptor, Alexa680, instead of Cy5.5. The chosen label has the same spectral properties, wavelengths of absorption and emission, as Cy5.5 but it binds through another group of the protein. As with Cy5.5 no quenching was observed during the titration. The PSFIA was used once again to test the activity of the Alexa680 labelled vitellogenin. The Cy5-labelled antibody bound the native vitellogenin-coated microtiterplate as well as the Alexa680 labelled vitellogenin-coated microtiterplate. In this case the labelling did not impede the binding of the two compounds.

The reason why the FRET assay did not work has to be further studied. The first step would be to confirm that the Cy5.5-labelled vitellogenin is really not active. This

could be verified by testing the binding of the Cy5-IgG to the Cy5.5-vitellogenin coated microtiterplate.

6. Bibliography

Andersen H.R., Andersson A-M., Arnold S.T., Autrup H., Barfoed M., Beresford N.A., Bjerregaard P., Christiansen L.B., Gissel B., Hummel R., Bonefeld Jorgensen E., Korsgaard B., Le Guevel R., Leffers H., McLachlan J., Moller A., Nielsen .B., Olea N., Oles-Karasko A., Pakdel F., Pedersen K.L., Perez P., Skakkeboek N.E., Sonnenschein C., Soto A.M., Sumpter J.P., Thorpe S.M., Grandjean P. (1999) Comparison of short-term estrogenicity tests for identification of hormone-disrupting chemicals, *Environ. Health Pespect*. 107(Suppl.1), 89-108.

Arnaud P. (1991) *Cours de chimie physique*, Bordas, Paris.

Arts C.J., Kemperman P.T. and Van der Berg H. (1989) Oestrogen radioreceptor assay for multi-residue screening of bovin urine for oestrogenic anabolic compounds, *Food Addit. Contam.* 6(1), 103-115.

Atkins (1999) *Physical chemistry*, 6th edition, Oxford University Press, Oxford Melbourne Tokyo.

Barlow R.J. (1989*) Statistics*, John Wiley and sons, Chichester.

Belmont University, Course of biology 314: immunology, *http://www.belmont.edu/Science/Biology/Bio314/BIO314_Immunology.htm*.

BIACORE *system manual* (1991)

Bolt H.M., Schuhmacher U.S. and Degen G.H. (1998) Special aspects of endocrine modulators in human and environmental risk assessment of existing chemicals, archives of toxicology 72(11), A72-A75.

Borst D.W., Eskew M.R., Wagner S.J., Shores K., Hunter J., Luker L., Halte J.D., Hecht L.B. (2000) Quantification of juvenile hormone III, vitellogenin, and vitellogenin-mRNA during the oviposition cycle of the lubber grasshopper, *Insect*

Biochem. Mol. Biol. 30(8-9), 813-819.

Byrne B.M., Gruber M. and G. AB (1989) The evolution of egg yolk protein, *Prog. Biophys. Molec. Biol*. 53, 33-69.

Castilho L.R., Deckwer W.D. and Anspach F.B. (2000) Influence of matrix activation and polymer coating in the purification of human IgG with protein A affinity membranes, Journal of membrane science, 172(1-2), 269-277.

Christensen L.L.H. (1997) Theoretical analysis of protein concentration determination using biosensor technology under conditions of partial mass transport limitation, *Analytical Biochemistry* 249, 153-164.

Christiansen L.B., Pedersen K.L., Korsgaard B., Bjerregaard P. (1998) Estrogenicity of xenobioics in rainbow trout (Oncorhynchus mykiss) using in vitro synthesis of vitellogenin as biomarker, *Mar. Environ. Res*. 46(1-5), 137-140.

Cohn E.J., Hughes Jr. W.L. and Weare J.H. (1947) Preparation and properties of serum and plasma proteins XIII Crystallization of serum albumins from ethanol-water mixtures, *J. Am. Chem. Soc*. 69, 1747-1761.

Colborn T. (1991) Epidemiology of Great Lake bald eagles, *Environ. Health Perspect.* 33, 395-453.

Commission of European communities (1999), community strategy for endocrine disruptors, COM (1999) 706 final, Brussels

Cook J.W., Dodds E.C. and Hewett C.L. (1933) a synthetic oestrus-exciting compound, *Nature* 131, 205.

Day E.D. (1990) *Advanced Immunochemistry*, Wiley-Liss, New York.

Degen G.H., Bolt H.M. (2000) Endocrine disruptors: update on xenoestrogens, *Int. Arch. Occup. Environ. Health* 73(7), 433-441.

Degen G.H., Foth H., Kahl R., Kappus H., Neumann H.G., Oesch F., Schulte-

Hermann R. (1999) Hormonally active substances in the environment : xenoestrogens, *Umweltmed. Forsch. Prax.* 4(6), 367-374.

Dorn I.T., Neumaier K.R. and Tampe R. (1998) Molecular recognitioin of histidine-tagged molecules by metal-chelating lipids monitored by fluorescence energy transfer and correlation spectroscopy, *Journal of the American Chemical Society* 120, 2753-2763.

Dos Remedios C.G. and Moens P.D.J. (1999) Resonance energy transfer in proteins, *Resonance energy transfer*, John Wiley & Sons Ltd., Chichester.

Dudley R.A., Edwards P., Ekins R.P., Finney D.J., McKenzie I.G.M., Raab G.M., Rodbard D. and Rogers R.P.C. (1985), *Clin. Chem.* 31, 1264-1271

Feldman D. (1997) Editorial: Estrogens from plastic – Are we being exposed ?, Endocrinology 138(5), 1777-1779.

Fischer-Fruholz S. (1998) The handling of nanosamples on a chip, Am. Lab. 30(4), 46-51.

Fujii K., Hara A., Shiraishi M. (1998) Quantification of vitellogenin in red sea bream, *Suisan Zoshoku* 46(3), 355-366.

Garnier C., Barbier B., Gilli R., Lopez C., Peyrot V. and Briand C. (1998) Heat-shock protein 90 (hsp90) binds in vitro to tubulin dimer and inhibits microtubule formation, Biochemical and Biophysical Research Communications 250(2), 414-419.

Gauglitz G., Brecht A., Kraus G. and Nahm W. (1993) Chemical and biochemical sensors based on interferometry at thin (multi-) layers, Sensors and actuators B 11,21-27.

Gemsa D., Kalden J.R. and Resch K. (1991) Immunologie: Grundlagen – Klinik-Praxis, Georg Thieme Verlag, Stuttgart New York.

Glasstone S. (1960) *Texbook of physical chemistry*, McMillan and co, London.

Göpel W. and Ziegler C. (1994) *Stuktur der Materie: Grundlagen Mikroskopie und Spektroskopie*, B.G. Teubner Velagsgesellschaft, Stuttgart Leipzig.

Göpel W., Hesse J. and Zemel J.N. (1992) Chemical and biochemical sensors, sensors a comprehensive survey, VCH Verlagsgesellschaft mbH, Weinheim New York Basel Cambridge.

Grondahl L., Battersby B.J., Bryant D. and Trau M. (2000) Encoding combinatorial libraries: A novel application of fluorescent silica colloids, *Langmuir*, 16(25), 9709-9715.

Guillette L.J., Jr. Crain A., Rooney A.A. and Pickford D.B. (1995) Organisation versus activation: the role of endocrine-disrupting contaminants (EDCs) during embryonic development in wildlife, *Environ. Health Perspect.*, 103(7), 157-164.

Haake H.M. (2000), Doctoral Dissertation, University of Tübingen, Germany.

Hansen P.D., Dizer H., Hock B., Marx A., Sherry J., McMaster M. and Blaise C. (1998) Vitellogenin – a biomarker for endocrine disruptors, *Trends in Analytical Chemistry* 17(7), 448-451.

Hecht E. (1989) *Optik*, 2nd edition, Addison-Wesley, Bonn.

Hock B. (1995) Immunochemical assay of environmental pollutants using pesticides as an example, *Immunochemical detection of pesticides and their metabolites in the water cycle*, VCH, Heidelberg.

Hofmann D. (1982) Measurement errors, probability and information theory, *Handbook of measurement science vol. 1* Sydenham and Thorn (Eds.), John Wiley and sons, Ltd, Brisbane..

Huang C-H. and Sedlak D.L. (2001) Analysis of estrogenic hormones in municipal wastewater affluent and surface water using enzyme-linked immunosorbent assay and gas chromatography/tandem mass spectrometry, *Environ. Toxicol. Chem.* 20(1), 133-139.

Jackson T.M. and Ekins R.P. (1986) Theoretical limitations on immunoassay sensitivity. Current practice and potential advantages of fluorescent Eu^{3+} chelates as non-radioisotopes tracers, *J. Immunol. Meth*. 87, 13-20.

Karlsson R. and Roos H. (1997) Reaction kinetics, *Principle and practice of immunoassay*, Stockton press, New York.

Kieser B. (1998) Diplomarbeit, University of Tübingen, Germany.

Kittel C. (1986) *Introduction to solid state physics*, Joun Wiley & sons, Inc., New York..

Korach K.S. and McLachlan J.A. (1995) Techniques for detection of estrogenicy, *Environmental. Health Perspectives* 103(7), 5-8.

Körner W., Hanf V. Schuller W., Kempter C., Metzger J; Hagenmayer H. (1999) Input/output balance of estrogenic active compounds in a major municipal sewage plant in Germany, *Sci. Total Environ*. 225(1-2), 33-48.

Koya Y., Matsubara t., Ikeuchi T., Adachi S., Yamauchi K. (1997) Annual changes in serum vitellogenin concentrations in viviparous eelpout, Zoarces longates, *Comparative biochemistry and physiology part A, physiology* 118(4), 1217-1223.

Krishna A.G., Kumar D.V., Khan B.M., Rawal S.K. and Ganesh K.N. (1998) Taxol DNA interactions: fluorescence and CD studies of DNA groove binding properties of taxol, *Biochimica and Biophysica Acta – general subjects* 1381(1), 104-112.

Kürner J.M., Klimant I., Krause C., Preu H., Kunz W. and Wolfbeis O.S. (2000) Phosphorescent nanospheres as marker in optical chemo- and biosensing, *5th European conference on optical chemical sensors and biosensors: Europtode V*, Lyon-Villerbanne, France

Kuwabara T., Hasegawa M., Kawano M. and Takaichi S. (1999) Characterisation of violaxanthin de-epoxidase purified in the presence of tween 20: effects of dithiothreitol and pepstatin A, *Plant and cell physiology,* 40(11), 1119-1126.

Länge K (2000), Doctoral Dissertation, University of Tübingen, Germany.

Laune D. (1998) Thèse : *Dissection peptidique du paratope de l'anticorps : identification de résidus impliqués dans la reconnaissance antigénique, de peptides bioactifs et d'idiotopes peptidiques*, Université de Montpellier I.

Levi Y. (1999) Les micropolluants à effets modulateurs endocriniens, *Spectra. Anal.* 28(208), 19-22.

Liddell E. and Weeks I. (1996) *Antikörper-Techniken*, Spektrum Akademischer Verlag, Heidelberg – Berlin – Oxford.

Lopez de Alda M.J., Barcelo D. (2001) Determination of steroid sex hormones and related synthetic compounds considered as endocrine diseuptors in water by fully automated on-line solid-phase extraction-liquid chromatography-diode, *J. Chromatogr. A* 911(2), 20.3-210.

Lottspeich F. and Zorbas H. (Hrsg.) (1998) *Bioanalytik*, Spektrum Akademischer Verlag, Heidelberg – Berlin.

Massart D.L., Vandeginste B.G.M., Deming S.N., Michotte Y. and Kaufman L. (1988) *Chemometrics: a textbook*, Elsevier Science Publishers B.V., Amsterdam.

Matthiessen P. and Sumpter J.P. (1998) Effects of estrogenic substances in the aquatic environment *Fish Ecotoxicology* 86, 319-335.

Morra M. and Cassineli C. (1999) Non fouling properties of polysaccharide coated surfaces, *J. Biomater. Sci. Polymer*, 10, 1107-1124.

Mujumdar R.B., Ernst L.A., Mujumdar S.R., Lewis C.J. and Waggoner A.S. (1993) Cyanine dye labelling reagents: sulfoindocyanine succinimidyl esters, *Bioconjugate Chem.* 4, 105-111.

Mujumdar S.R., Mujumdar R.B., Grant C.M. and Waggoner A.S. (1996) Cyanine labelling reagents: sulfobenzindocyanine succinimidyl esters, *Bioconjugate Chem.*

7(3), 356-362.

Narita M., Ogawa N. and Hamada F. (2000) Fluorescent molecular recognition for endocrine-disrupting chemicals and their analogs by fluorescent hetero-modified cyclodextrin, *Analytical Sciences* 16, 701-705.

Nice E.C. and Catimel B. (1999) Instrumental biosensors: new perspectives for the analysis of biomolecular interactions, *BioEssays* 21, 339-352.

Oosterkamp A.J., Herraiz M.T.V., Irth H., Tjaden U.R., Van der Greef J. (1996) Reversed-phase liquid chromatography coupled online to receptor affinity detection based on the human estrogen receptor, *Anl. Chem.* 68(7), 1201-1206.

Parker G.A. (1991) Validation of methods used in the Florida department of agriculture and consumer services' chemical residue laboratory, *J. Assoc. Off. Anal. Chem.* 74(5), 868-871.

Pedersen S.N. Lindholst S. (1999) Quantification of the xenoestrogens 4-tert.-octylphenol and bisphenol A in water and in fish tissue based on microwave-assisted extraction, solid-phase extraction and liquid chromatography-mass spectrometry, *J. Chromatogr. A* 864(1), 17-24.

Pellequer J.L. and Van Regenmortel M.H.V. (1993) Measurement of kinetic binding constants of viral antibodies using a new biosensor technology, *J. Immunol. Methods*, 166(1), 133-143.

Peterfi Z. and Kocsis B. (2000) Comparison of blocking agent for an ELISA for LPS, *Journal of immunoassay*, 21(4), 341-354.

Phillips B. and Harrison P. (1999) Overview of the endocrine disruptors issue*, Issues in environmental science and technology XII Endocrine disrupting chemicals*, The royal society of chemistry, Cambridge.

Piehler J., Brecht A., Giersch T., Hock B. and Gauglitz G. (1997) Assessment of affinity constants by rapid solid phase detection of equilibrium binding in a flow

system, *Journal of Immunological Methods* 201, 189-206.

Rachkov A., McNiven S., El'skaya A., Yano K., Karube I. (2000) Fluorescence detection of β-estradiol using a molecularly imprinted polymer, *Anal. Chim. Acta.* 405, 23-29.

Raether H. (1988) *Surface Plasmons on Smooth and Rough Surfaces and on Gratings*, Springer Verlag, Berlin Heidelberg New York London Paris Tokyo.

Richalet-Sécordel P.M., Rauffer-Bruyère N., Christensen L.L.H., Ofenloch-Haehnle B., Seidel C. and Van Regenmortel M.H.V. (1997) Concentration measurement of unpurified proteins using biosensor technology under conditions of partial mass transport limitations, *Analytical Biochemistry* 249, 165-173.

Riedel-de Haën, ELISA –systems 17b-estradiol. Art. Nr 45164.

Rollerova E., Urbancikova M. (1999) Estrogenic potential of environmental compounds, *Biologia* 54(6), 625-634.

Rousselot P., Mappus E., Blachère T., Rolland de Ravel M., Grenot C., Tonnelle C. and Cuilleron C.Y. (1997) specific photoaffinity abelling of Tyr-49 on the light chain in the steroid-combining site of a mouse monoclonal anti-estradiol antibody using two epimeric 6α- and 6β-(5-azido-2-nitrobenzoyl)amidoestradiol photoreagents, *Biochemistry* 36, 7860-7868.

Routledge E.J. and Sumpter J.P. (1996) Estrogenic activity of surfactants and some of their degradation products assessed using a recombinant yeast screen, *Environ. Toxicol. Chem.* 15, 241-248.

Routledge E.J., Sheahan D., Desbrow C., Brighty G.C., Waldock M. and Sumpter J.P. (1998) Identification of estrogenic chemicals in STW effluent. 2. In vivo responses in trout and roach, *Environ. Sci. Technol.* 32, 1559-1565.

Santti R., Makela S., Strauss L., Korkman J., Kostian M-L. (1998) Phytoestrogens: potential endocrine disruptors in males, *Adv. Mod. Environ. Toxicol.* 24, 263-280.

Schmid E. and Fruhauf P. (1998) Instrumental methods for determination of steroids in water, *Wien. Mitt.: Wasser – Abwasser – Gewässer* 153, 17-32.

Schobel U, Egelhaaf H-J, Brecht A, Oelkrug D, Gauglitz G. (1999) *Bioconjugate Chem.* 10, 1107-1114.

Schobel U. (1999) Doctoral Dissertation, University of Tübingen, Germany.

Schobel U., Coille I., Brecht A., Steinwand M. and Gauglitz G. (accepted) Miniaturisation of a homogeneous fluorescence immunoassay based on energy transfer using nanotiterplates as high density sample carrier, *Anal. Chem.*

Schober A, Günther R., Schwienhorst A., Döring M. and Lindemann B.F. (1993) Accurate high speed liquid handling of very small biological samples, *Biotechniques* 15(2), 324-329.

Seifert M., Brenner-Weiss G., Haindl S., Nusser M., Obst U., Hock B. (1999) A new concept for the bio-effects-related analysis of xenoestrogens: hyphenation of receptor assays with LC-MS, *Fresenius J. Anal. Chem.*. 363, 767-770.

Seifert M., Haindl S., Hock B. (1999) Development of en enzyme linked receptor assay (ELRA) for estrogens and xenoestrogens, *Anal. Chim. Acta*. 386(3), 191-199.

Shahdeo K., Karnes H.T. (1998) Combining Immunoassays with chromatographic an electrophoretic separatrion techniques – a review, *Mikrochim. Acta* 129, 19-27.

Sharma A and Schulman S.G. (1999) *Introduction to fluorescence spectroscopy*, John Wiley and sons, inc., New York Chichester Weinheim Brisbane Singapore Toronto.

Sherry J., Gamble A., Hodson P., Solomon K., Hock B., Marx A., Hansen P. (1999) Vitellogenin induction in fish as an indicator of exposure to environmental estrogens: *Impact Assess. Hazard. Aquat. Contam*., 123-160, (Rao, Salem S. Eds) Lewis, Boca Raton.

Snyder S.A., Keith T.L., Verbrugge D.A., Snyder E.M., Gross T.S. Kannan K. Giesy

J.P. (1999) Analytical methods for detection of selected estrogenic compounds in aqueous mixtures, *Environ. Sci. Technol*. 33(16), 2814-2820.

Soto A.M., Sonnenschein C., Chung K.L., Fernandez M.F., Olea N., Serrano F. O. (1995) The E-SCREEN assay as tool to identify estrogens: an update on estrogenic environmental pollutants, *Environ. Health Perspect*. 103(Suppl.7) 113-122.

Stemmler I. (1999) Doctoral Dissertation, University of Tübingen, Germany.

Sumpter J.P. (1995) Feminized responses in fish to environmental estrogens, *Toxicology Letters* 82/83, 737-742.

Sumpter J.P. and Jobling S. (1995) Vitellogenesis as a biomarker for estrogenic contamination of the aquatic environment, *Environ. Health Perspect*. 103(7), 173-178.

Taquet A., Labarabe R. and Houssier C. (1998) Calorimetric investigations of ethidium and netropsin binding to chicken erythrocyte chromatin, *Biochemistry* 37, 9119-9126.

Tijssen P (1992) *Practice and theory of enzyme immunoassays*, Elsevier, Amsterdam.

Van der Meer B.W. (1999) Orientational aspects in pair energy transfer, *Resonance energy transfer*, John Wiley & Sons Ltd., Chichester.

Van der Meer B.W., Coker III G. and Chen S.-Y.S. (1994) *Resonance energy transfer*, VCH publishers, Inc., New York.

Van Oss C.J. (1995) Hydrophobic, hydrophilic and other interactions in epitope-paratope binding, *Molecular Immunology* 32(3), 199-211.

Van Regenmortel M.H.V. (1998) From absolute to exquisite specificity. Reflections on the fuzzy nature of species, specificity and antigenic sites, *Journal of Immunological Methods* 216, 37-48.

Velev O.D. (1997) Assembly of protein structures on liposomes by non-specific and specific interactions, *Adv. Biophys.*, 34139-34157.

Vigorito E., Robles A., Balter H., Nappa A. and Goni F. (1995) [^{125}I] IgM (KAU) human monoclonal cold agglutinin: labelling and studies on its biological activity, *Appl. Radiat. Isot.* 46(10), 975-979.

Wang W., Vincent D.L., Early R.J., Weems C.W. (1994) The quantification of phytoestrogens in fresh plant material by reversed-phase high performance liquid chromatography , *Yunnan Zhiwu Yanjiu* 16(4), 424-30.

Wells A.F., Miller C.E. and Nadel M.K. (1966) Rapid fluorescein and assays method for fluorescent-antibody conjugates, *Appl. Microbiol.* 14, 271-275.

Wild M.K., Huang M.C., Schulze-Horsel U. Van der Merve P.A and Vestweber D. (2001) Affinity, kinetics and thermodynamics of E-selectin binding to E-selecting ligand-1*, *Journal of Biomolecular Chemistry*, june 12, in press.

Witorsch R.J. (2000) Endocrine disruption: a critical review of environmental estrogens from mechanistic perspective, *Toxic Subst. Mech.* 19(1), 53-78.

Yamanaka S., Arizono K., Madsuda Y., Soyano K., Urushitani H., Iguchi T. (1998) *Biosci. Biotechnol. Biochem.* 62(6), 1196-1200.

Zammatteo N., Girardeaux C., Delforge D., Pireaux J.J. and Remacle J. (1996) Amination of polystyrene microwells: application to the covalent grafting of DNA probes for hybridization assays, *Analytical Biochemistry*, 236, 85-94.

Zeck A., Weller M.G. and Niessner R. (1999) Characterisation of a monoclonal TNT- antibody by measurement of the cross reactivities of nitroaromatic compounds, *Fresenius Journal of Analytical Chemistry* 364 (1-2), 113-120.

Zeder-Lutz G., Zuber E., Witz J. and Van Regenmortel M.H.V. (1997) Thermodynamic analysis of antigen – antibody binding using biosensor measurements at different temperatures, *Analytical Biochemistry*, 246, 123-132.

7. Appendix

7.1. ABBREVIATIONS

ABS	Acrylnitril butadiene styrol co-polymere
Alexa680	Alexa fluor 680 C_2 maleimide, inner salt
B8D8	Monoclonal anti-vitellogenin-IgG
BSA	Bovine Serum Albumin
DMF	Dimethylformamide
E1	Estrone
E1-17-CMO	Estrone-17-N-carboxymethyl oxime
E1-3-CME	Estrone-3-carboxymethyl ether
E2	Estradiol
E2-3-BA	Estradiol -3-O-butyric acid
E2-3-IBA	Estradiol -3-O-isobutyric acid
E2-3-MA	Estradiol -3-O-malonic acid
E2-17-Hg	Estradiol-17-O-hemiglutarate
EE2	Ethinylestradiol
FRET	Fluorescence Resonance Energy Transfer or Förster Resonance Energy Transfer
GOPTS	Glycidyloxypropyltrimethoxysilan
HBS	Hepes Buffer solution
LOD	Limit of detection
MTP	Microtiterplate
NTP	Nanotiterplate
OVA	Ovalbumin or chicken egg albumin
PBS	Phosphate buffer solution
PSFIA	Phase Separation Fluorescence Immuno-Assay
RIfS	Reflectometric Interference Spectroscopy

SPR	Surface Plasmon Resonance
TMP	Test mid point
WR	Working range
αE1	Anti-estrone-IgG
αE2	Anti-estradiol-IgG
αES	Anti-(estrone and estradiol)-IgG or anti-total-estrogens-IgG
15H11	Monoclonal anti-estradiol-IgG

7.2.   PUBLICATIONS

- Schobel U., Coille I., Brecht A., Steinwand M. and Gauglitz G. (accepted) Miniaturisation of a homogeneous fluorescence immunoassay based on energy transfer using nanotiterplates as high density sample carrier, *Anal. Chem.*

- Coille I, Reder S., Bucher S. and Gauglitz G (accepted) Comparison of two fluorescence immunomethods for the detection of endocrine disrupting chemicals in water, *Biomol. Engineering.*

- Coille I., Gauglitz G and Hoebeke J. (submitted) Characterisation of antibodies and analytes by surface plasmon resonance for the optimisation of a competitive immunoassay based on energy transfer, *Fresenius'J. Anal. Chem.*

- Coille I., Cuilleron C.J. and Hoebeke J. (in preparation) Characterisation of a monoclonal anti-estradiol antibody, *Eur. J. Biochem.*

7.3. <u>ACADEMIC TEACHERS</u>

E. Bayer, G. Gauglitz, W. Göpel[†], V. Hoffmann, G. Jung, B. Koppenhöffer, A. Kovar, D. Leipert, H.M. Liebich, H. Oberhammer, D. Oelkrug, V. Schurig, C. Ziegler

7.4.   CURRICULUM VITAE

Name: Ingrid Coille

Date of birth: 09/29/74, in Hénin-Beaumont, France

Nationality: French

Marital status: Single

Education

09/1991 – 06/1992: ″Baccalaureat C″ (′A′ Level), majoring in Maths and Physics, with honours (mention AB) at the ″lycée Condorcet″ (high school) of Lens, France.

09/1992 – 06/1994: ″D.U.T.″ (Diploma of a technical Institute) in chemistry, at the ″Institut Universitaire de Technologie″ of Béthune, France.

09/1994 – 06/1995: ″D.E.U.G. B ″ (2nd year study) with chemistry orientation, with honours, at the University of Rouen, France.

09/1995 – 06/1997: ″M.S.T.″ (Master's Degree) specialising in Chemical Control and Analysis, at the University of Dijon, France.

Mai 1997: Inscription at the University of Tübingen, Germany.

December 1997: Examination for the Master Thesis,

10/97 - 01/98: Master Thesis in the institute of Physical Chemistry in the group of the Prof. Dr. Gauglitz, at the University of Tübingen, Germany.

Theme: "Detection of pesticides in organic solutions with a fluoro-immunoassay".

02/98 - 09/01: PhD thesis under double supervision, at the institute of Physical Chemistry in the group of the Prof. Dr. Gauglitz, University of Tübingen, Germany and at the institute of molecular and cellular biology under the direction of the Dr. Hoebeke, University of Strasbourg, France.

Subject: Thermodynamic and kinetic characterisation of antibody/haptens pairs and optimisation of a immunoassay of fluorescence in homogeneous phase.

7.5.   FRENCH SUMMARY

Dans une première partie un anticorps monoclonal anti-oestradiol est complètement caractérisé par rapport à divers oestrogènes et dérivés par la méthode de résonance de plasmons de surface (SPR). La concentration active des anticorps est déterminée. Les constantes d´équilibres, les constantes cinétiques et les variables thermodynamiques sont mesurées pour comprendre le mode d´interaction avec les analytes.

Un caractérisation de l´activité, de l´affinité et de la cinétique de trois anticorps polyclonaux est également réalisée par SPR. La détermination des constantes d´affinité a été réalisée parallèlement par spectroscopie d´interférences réflectométriques (RIfS). Les anticorps polyclonaux utilisés sont anti-oestrone, anti-oestradiol et anti-oestrogènes. Les analytes sont divers oestrogènes naturels et synthétiques. Les interactions anticorps / haptène en surface ou en solution, ainsi que les deux méthodes de determination des constantes d´affinité sont comparées par des tests statistiques. Dans le but d´utiliser ces systèmes anticorps / analyte avec un immuno-essai de fluorescence, les constantes d´affinité et les concentrations actives sont déterminées avant et après marquage avec le fluorophore Cy5. L´influence du marquage est décrite.

Des simulations de l´immunoessai de fluorescence permettent de voir l´effet de paramètres importants dans un essai competitif : la concentration du dérivé en competition avec l´analyte, les constantes d´affinité du système et le rapport de ces constantes.

Ces systèmes anticorps / analytes étudiés par SPR sont transférés à un immuno-essai de transfert d´energie (ETIA) en solution. L´essai est développé en micro-plaque. A l´aide des constantes mesurées et de l´influence des constantes observées dans les simulations, les résultats obtenus sont comparés acvec les résultats attendus selon les simulations.

La mèthode est validée par des mesures d´oestrogènes dans une eau synthétique de station d´épuration. La dernière étape consiste en la miniaturisation de l´ETIA. Les difficultés de la réduction concernent principalement l´adsorption non spécifique sur les parois, la précision du pipetage et l´évaporation. L´essai peut être appliqué avec succès dans une nano-plaque, dont le volume d´une cavité est de 70 nl environs.

L´immunoessai de fluorescence en solution a été appliqué à un couple protéine / anticorps (vitellogenine / anticorps anti-vitellogine). Aucun transfert d´énergie n´a pu être observé. L´activité de l´anticorps et de la protéine marqués a été testée par un immunoessai de fluorescence en phase hétérogène. La protéine a été marquée avec un autre fluorophore, mais

l´immunoessai en phase homogène est resté infructueux. L´immunoessai de fluorescence en phase hétérogène a montré que la protèine marquée est reconnue par l´anticorps.

7.6.   GERMAN SUMMARY

Zuerst wurde ein monoklonaler Anti-Estradiol-Antikörper mit verschiedenen Östrogenen und Östrogenderivaten mit Hilfe der SPR (Oberflächenplasmonenresonanz) vollständig charakterisiert. Die aktive Konzentration des Antikörpers wurde bestimmt. Die Gleichgewichtskonstanten, die kinetischen Konstanten und die thermodynamischen Variablen wurden gemessen, um die Wechselwirkungen zwischen Antikörper und Analyte zu verstehen. Die Bestimmung der Aktivität, der Affinität und der Kinetik von drei polyklonalen Antikörpern wurde mit SPR durchgeführt. Die Affinitätskonstanten wurden parallel dazu mit RIfS (Reflektometrische Interferenzspektroskopie) bestimmt. Die verwendeten Antikörper waren Anti-Östron, Anti-Östradiol und Anti-Östrogen. Die Analyte waren natürliche und synthetische Östrogene. Die auf der Oberfläche und in der Lösung bestimmten Affinitätskonstanten sowie die mit den zwei Methoden bestimmten Affinitätskonstanten wurden mit statistischen Tests verglichen. Für den Einsatz dieser Antikörper/Hapten-Systeme in einem Fluoroimmunoassay wurden außerdem die aktiven Konzentrationen und die Affinitätskonstanten vor und nach dem Markieren mit dem Fluorophor Cy5 gemessen. Der Einfluss der Markierung ist beschrieben.

Simulierungen des Fluoroimmunoassays zeigten den Einfluss von wichtigen Parametern auf einen kompetitiven Immunoassay: Die Konzentration des Derivats in Konkurrenz mit dem Analyt, die Affinitätskonstanten des Systems und das Verhältnis der Konstanten.

Die mit SPR untersuchten Antikörper/Analyte-Systeme wurden in einem ETIA (Energietransfer Immunoassay) in Lösung eingesetzt. Der Assay wurde in Mikrotiterplatten entwickelt. Die gemessenen Kalibrierkurven wurden mit den gemessenen Affinitätskonstanten und den Simulationen verglichen.

Der ETIA wurde bei verschiedenen Messungen von Östrogenen in synthetischem Abwasser validiert. Der letzte Schritt bestand in der Miniaturisierung des ETIA. Die Schwierigkeiten der Miniaturisierung liegen hauptsächlich in der unspezifischen Adsorption auf der Oberfläche, die Genauigkeit des Pipettierens und die Kontrolle des Verdampfens. Der Assay wurde erfolgreich in einer Nanotiterplatte mit einem Wellsvolumen von 70 nl gemessen.

Der Fluoroimmunoassay wurde auf ein Antikörper/Protein-Paar (Vitellogenin/Anti-vitellogenin-Antikörper) angewendet. Dabei wurde kein Energietransfer beobachtet. Das Protein wurde mit einem neuen Fluorophor markiert, aber der Assay in Lösung war weiterhin nicht erfolgreich. Die Fähigkeit zur Bindung von markiertem Antikörper und Protein wurde mit einem Fluoroimmunoassay in heterogener Phase geprüft. Der heterogene

Fluoroimmunoassay zeigte, dass das neue markierte Protein den Antikörper trotzdem binden konnte.